

Aus dem Max-Planck-Institut für Biophysikalische Chemie in Göttingen

Abteilung Zelluläre Biochemie

Direktor: Prof. Dr. Reinhard Lührmann

**“Electron microscopic localization of tagged proteins in the yeast
S. cerevisiae spliceosomal U4/U6.U5 tri-snRNP”**

Dissertation

zur Erlangung des Doktorgrades

der Mathematisch-Naturwissenschaftlichen Fakultäten

der Georg-August-Universität zu Göttingen

vorgelegt von

Irina Häcker

aus Stuttgart

Göttingen 2008

D7

Referent: Prof. Dr. R. Ficner

Korreferent: Prof. Dr. E. A. Wimmer

Tag der mündlichen Prüfung: 02.07.2008

Meiner Familie
&
Marc

Table of contents

Abstract	11
Zusammenfassung	13
1 Introduction	15
1.1 Gene Structure and pre-mRNA processing.....	15
1.2 Pre-mRNA splicing.....	15
1.3 The chemistry of the splicing reaction	17
1.4 Spliceosome assembly in yeast	18
1.5 The spliceosomal U snRNPs.....	20
1.6 The U4/U6.U5 tri-snRNP	27
1.6.1 The tri-snRNP is a highly conserved component of the spliceosome	27
1.6.2 The tri-snRNP undergoes large structural rearrangements upon spliceosome activation.....	28
1.6.3 Involvement of tri-snRNP proteins in the catalytic activation of the spliceosome and spliceosome dynamics.....	31
1.7 <i>Saccharomyces cerevisiae</i> a model organism for pre-mRNA splicing	33
1.8 Electron microscopy as a means for structural studies of complex macromolecules	33
1.9 Aim of this study	37
2 Materials and methods	39
2.1 Materials.....	39
2.1.1 Chemicals and media	39
2.1.2 Enzymes and enzyme inhibitors	40
2.1.3 Antisera, monoclonal and polyclonal antibodies.....	40
2.1.4 Peptides	41
2.1.5 Nucleotides.....	41
2.1.6 Oligonucleotides.....	42
2.1.7 Bacterial and yeast strains.....	44
2.1.8 Plasmids	46
2.1.9 Cell culture.....	46
2.1.10 Common buffers	46
2.1.11 Commercial reaction sets (kits)	48
2.1.12 Machines	48
2.1.13 Working equipment.....	49
2.2 Methods	50
2.2.1 Protein-biochemistry standard methods.....	50
2.2.1.1 Protein quantification	50
2.2.1.2 Phenol-Chloroform-Isoamylalcohol extraction.....	50
2.2.1.3 Proteinase K digestion.....	50
2.2.1.4 Denaturing polyacrylamide gel electrophoresis	51
2.2.1.5 Western blot analysis.....	51
2.2.1.6 Silver staining of protein gels.....	51
2.2.2 Molecular biology	52
2.2.2.1 Concentration determination of nucleic acids	52

2.2.2.2	Agarose gel electrophoresis of nucleic acids.....	52
2.2.2.3	Denaturing polyacrylamide gel electrophoresis of RNA	53
2.2.2.4	Silver staining of RNA gels.....	53
2.2.2.5	Synthesis of radioactively labeled DNA-probes for Northern analysis.....	54
2.2.2.6	Northern blot analysis	54
2.2.2.7	Polymerase chain reaction.....	54
2.2.2.8	Transformation of haploid yeast cells.....	57
2.2.2.9	Transformant characterization by PCR analysis.....	57
2.2.2.10	Transformant characterization by western blot analysis	58
2.2.2.11	N-terminal TAP tagging of yeast strains	58
2.2.2.12	Transformation of HB101 cells	59
2.2.3	Cell culture methods.....	59
2.2.3.1	Growth and culture of bacteria.....	59
2.2.3.2	Yeast cell culture.....	59
2.2.3.3	Extract preparation from yeast cells for snRNP purification using a mortar grinder...60	
2.2.4	Special methods.....	61
2.2.4.1	Tandem affinity purification of yeast snRNPs	61
2.2.4.2	Glycerol gradient sedimentation of purified snRNP particles	62
2.2.4.3	Co-immunoprecipitation of tri-snRNP snRNAs	62
2.2.4.4	Immunolabeling of TAP-purified yeast tri-snRNPs.....	63
2.2.4.5	Enzyme-linked immunosorbent assay	63
2.2.4.6	Electron microscopy analysis of TAP purified snRNPs.....	64
2.2.4.7	Labeling of immunocomplexes with colloidal gold and preparation of EM specimens 64	
2.2.4.8	Mass spectrometry	65
3	Results	66
3.1.1.1	Structural characterization of the <i>Saccharomyces cerevisiae</i> U4/U6.U5 tri-snRNP	66
3.1.2	Isolation of tri-snRNPs using the tandem affinity purification method	66
3.1.2.1	C-terminal TAP tagging of tri-snRNP proteins	67
3.1.2.2	TAP purification of yeast tri-snRNPs.....	70
3.1.3	Electron microscopy of double affinity-purified yeast tri-snRNPs.....	73
3.1.4	Labeling strategies	76
3.1.4.1	Genetic labeling of tri-snRNP proteins.....	76
3.1.4.2	Immunolabeling of tri-snRNP proteins.....	81
3.1.5	Localization of the U5-specific proteins Brr2p, Prp8p and Snu114p.....	92
3.1.6	Localization of the U4/U6 portion of the tri-snRNP.....	96
3.1.7	Localization of Prp6p and Prp31p	98
3.1.8	N-terminal TAP tagging of tri-snRNP proteins for future labeling studies	100
3.2	Investigation of the yeast U5 snRNP	104
3.2.1	Isolation of yeast U5 snRNPs using the TAP purification method.....	104
3.2.2	Electron microscopy of TAP-purified yeast U5 snRNPs.....	106
4	Discussion	108
4.1	The native yeast tri-snRNP is a dynamic particle and shows structural differences to the human tri-snRNP	108
4.2	A two-fold labeling strategy allows for the clear localization of functionally important proteins within the yeast tri-snRNP	110
4.3	Structural model of the yeast tri-snRNP based on the labeling studies	112
4.4	Functional implications from the labeling studies.....	115
4.4.1	Snu114p might regulate the activity of downstream proteins by structural rearrangements 115	
4.4.2	How is the U4/U6 snRNA unwound in the tri-snRNP?.....	118

4.4.3	The interaction between the C-terminus of Prp4p and Prp3p might be important for tri-snRNP stability	119
4.5	The yeast U5 snRNP	120
4.5.1	Comparison of the yeast and human U5 snRNP.....	120
4.5.2	The U5 snRNP is too heterogeneous for labeling studies and 3D structure determination 121	
4.5.3	Possible reasons for heterogeneous appearance of the yeast U5 snRNP in the electron microscope.....	121
4.6	Comparison of the yeast U5 snRNP and the tri-snRNP	122
4.7	Perspectives.....	123
5	References	125
6	Appendix	134
	List of Abbreviations	134
	Publications	138
	Danksagung.....	139
	Erklärung/Affidavit.....	140
	Curriculum Vitae	141

Abstract

Pre-mRNA splicing is catalyzed by a macromolecular machine called ‘spliceosome’. The spliceosome is assembled in a stepwise manner from the small nuclear ribonucleoprotein particles (snRNPs), namely U1, U2, U5 and U4/U6, and numerous non-snRNP splicing factors. The snRNPs contain one RNA molecule (or two extensively base-paired RNAs in the case of U4/U6) and several protein components. Spliceosome assembly is initiated by the association of U1 and U2 with the 5′ splice site and the branch point, respectively, forming the pre-spliceosome (complex A). Then U5 and U4/U6 join the spliceosome as a preformed U4/U6.U5 tri-snRNP to form the fully assembled pre-catalytic spliceosome (complex B). The tri-snRNP is an important and evolutionarily highly conserved component of the spliceosome. In *S. cerevisiae* the tri-snRNP contains at least 28 proteins, several of which play important roles in pre-mRNA splicing. During catalytic activation of the spliceosome the intricate network of protein-protein, protein-RNA, and RNA-RNA interactions of the tri-snRNP is extensively remodeled. One crucial step of spliceosome activation is the U4/U6 snRNA unwinding, which sets free the U6 snRNA to interact with the 5′ splice site of the pre-mRNA as well as with the U2 snRNA to form part of the catalytic core of the spliceosome. It is well established that the U5-specific proteins Prp8p, the ATPase Brr2p, and the GTPase Snu114p are directly involved in the unwinding of the U4/U6 snRNA duplex and that this process has to be tightly controlled. However, little is known about the overall structure of the yeast tri-snRNP and its molecular organization. We therefore used electron microscopy to investigate the structural details of the yeast tri-snRNP and to locate a number of its functionally important U5-, U4/U6-, and tri-snRNP-specific proteins in two dimensions. To achieve this goal, we applied two independent labeling techniques: (i) immunolabeling and (ii) genetic labeling with a 54 kDa globular protein tag, which was directly visualized in the electron microscope. Together, these approaches allowed us to reliably localize the C-termini of seven targeted proteins within the triangular structure of the native yeast tri-snRNP and to identify the subunits of the particle. In the ‘head’-like structure of the tri-snRNP’s main body we localized Brr2p, while the C-termini of Prp8p and Snu114p are located in the central region of the main body, suggesting that the main body harbors the U5 snRNP. A smaller ‘arm’ domain is connected to the central region of the main body through a linker. The arm contains the U4/U6 proteins Prp3p and Lsm8p. We therefore conclude that the arm represents the U4/U6 di-snRNP. In the linker region we localized Prp6p and Prp31p, which have been suggested to function as bridging proteins between U5 and U4/U6. By combining *in vivo* tagging with electron microscopy we provide for the first time important insights into the detailed

structural organization of the yeast tri-snRNP. Moreover, the data have several implications for the interactions between tri-snRNP proteins which lead to the unwinding of U4/U6 snRNA.

Zusammenfassung

Das Spleißen der prä-mRNA wird von einer makromolekularen Maschine, dem Spleißosom katalysiert. Das Spleißosom wird schrittweise aus den kleinen nukleären Ribonukleoprotein-Partikeln, den sogenannten U1, U2, U5 und U4/U6 snRNPs sowie zahlreichen nicht-snRNP Spleißfaktoren assembliert. Die snRNPs bestehen aus einem RNA-Molekül (bzw. zwei weitgehend basengepaarten RNAs im Fall von U4/U6) und mehreren Proteinkomponenten. Die Assemblierung des Spleißosoms beginnt mit der Bildung des Prä-Spleißosoms (Komplex A) durch die Interaktion des U1 snRNPs mit der 5' Spleißstelle und des U2 snRNPs mit dem Verzweigungspunkt. Die Integration von U5 und U4/U6 in Form eines U4/U6.U5 tri-snRNPs schließt die Assemblierung des Spleißosoms ab (prä-katalytisches Spleißosom oder Komplex B). Der tri-snRNP ist ein wichtiger und evolutionär stark konservierter Baustein des Spleißosoms. Einige der mindestens 28 Proteine des tri-snRNPs aus der Hefe *S. cerevisiae* spielen eine wichtige Rolle beim Spleißen der prä-mRNA. Während der katalytischen Aktivierung des Spleißosoms wird das komplizierte Netzwerk der Protein-Protein-, Protein-RNA- und RNA-RNA-Interaktionen des tri-snRNPs stark verändert. Ein erster wichtiger Schritt der Aktivierung ist die Entwindung der U4/U6 snRNAs. Nur so kann dann die U6 snRNA mit der 5' Spleißstelle der prä-mRNA und mit der U2 snRNA interagieren, wodurch ein Teil des katalytischen Zentrums des Spleißosoms gebildet wird. Es konnte gezeigt werden, dass die U5-spezifischen Proteine Prp8p, die ATPase Brr2p und die GTPase Snu114p direkt an der Entwindung der U4/U6 snRNAs beteiligt sind, und dass dieser Prozess einer strengen Kontrolle unterliegen muss. Es ist jedoch nur wenig bekannt über die Struktur des Hefe tri-snRNPs und seinen molekularen Aufbau. Deshalb haben wir die strukturellen Details des Hefe tri-snRNPs mittels Elektronenmikroskopie untersucht und verschiedene funktionell wichtige U5-, U4/U6- und tri-snRNP-spezifische Proteine in ihrer zweidimensionalen Verteilung lokalisiert. Dazu verwendeten wir zwei verschiedene Markierungs-Methoden: (i) Antikörper-Markierung und (ii) genetische Markierung mit einem globulären Protein (54 kDa), das unter dem Elektronenmikroskop direkt sichtbar war. Mit Hilfe dieser beiden Methoden konnten wir die C-terminalen Bereiche von sieben Proteinen eindeutig innerhalb der nativen Struktur des tri-snRNPs lokalisieren und die Untereinheiten des Komplexes identifizieren. Brr2p wurde in der kopf-ähnlichen Struktur, die C-Termini von Prp8p und Snu114p wurden dagegen im zentralen Bereich des Hauptkörpers lokalisiert, welcher daher wahrscheinlich das U5 snRNP enthält. Eine kleinere Arm-Domäne ist über ein „Gelenk“ mit dem zentralen Teil des Hauptkörpers verbunden. In diesem Arm befinden sich die U4/U6 Proteine Prp3p und Lsm8p, woraus wir

schließen, dass der Arm das U4/U6 snRNP enthält. Im „Gelenk“ wurden Prp6p und Prp31p lokalisiert, die wahrscheinlich die Interaktion von U5 mit U4/U6 vermitteln. Durch die Kombination von *in vivo* Markierungs-Methoden und Elektronenmikroskopie ermöglichen wir erstmalig wichtige Einblicke in die detaillierte strukturelle Organisation des tri-snRNPs aus der Hefe. Darüber hinaus lassen diese Daten Schlüsse auf mögliche Interaktionen der tri-snRNP Proteine zu, die zur Entwindung der U4/U6 snRNA führen.

1 Introduction

1.1 Gene Structure and pre-mRNA processing

Gene expression comprises all steps involved in converting the genetic information contained in DNA sequences into primary amino acid sequences via transcription, RNA processing and translation. In eukaryotes, messenger RNA (mRNA) molecules are first transcribed as primary transcripts (pre-mRNA) by RNA polymerase II. These pre-mRNAs then undergo a multi-stage maturation process before the final mature mRNA molecule is exported into the cytoplasm to serve as a template for protein synthesis. The maturation of pre-mRNA starts with the co-transcriptional capping of its 5' end. A 7-methylguanosine is linked by an unusual 5'-5'-triphosphate bond to the ribose at the 5' end of the pre-mRNA (Shatkin, 1976). This 'cap' is involved in the mRNA export from the nucleus, in the initiation of protein synthesis and in stabilization of the mRNA (McCracken et al., 1997). In addition, the 3'-end of pre-mRNA is modified by a process called polyadenylation in which the growing transcript is cleaved at a specific site and a poly(A) tail (100 to 200 adenine residues) is added by a poly(A) polymerase (Colgan and Manley, 1997).

The most striking feature of eukaryotic genes is that the protein-coding sequences (exons) are interspersed with non-coding regions (introns). Prior to transport into the cytoplasm, where translation takes place, the introns must be spliced out of the pre-mRNA and exons must be ligated correctly to form the mature mRNA. The nuclear machine that accomplishes the intricate task of intron removal is called the spliceosome, a multi-mega Dalton ribonucleoprotein complex.

The very 5' and 3' ends of the mature mRNA, although they are exonic regions, are not translated into an amino acid sequence and therefore these segments are referred to as untranslated regions (UTRs). They usually contain regulatory sequences controlling stability and translational activity of the transcripts.

1.2 Pre-mRNA splicing

The sites at which the primary transcript is cleaved to splice out the intron(s) must be selected very precisely because an error of only one nucleotide would shift the reading frame of the message and result in the translation of a non-functional protein. Splice site selection is complicated by the highly variable intron sequences and lengths, and the low information content defining the exon-intron boundaries. Three short (2-7 nucleotides) consensus sequences – the 5'

splice site (5' SS), the branchpoint (BP) sequence and the 3' splice site (3' SS) – define each intron. These cis-acting elements are highly conserved in yeast (*Saccharomyces cerevisiae*; *S. cerevisiae*) but less so in human, which makes correct splice site selection even more difficult. The 5' SS defines the 5' end of the intron (Figure 1.1). In yeast it is composed of R/**GUAUGU** (Lopez and Séraphin, 1999) ('/' indicates the exon/intron boundary, 'R' is a purine, nucleotides in bold indicate 90 % or higher conservation in yeast introns). In human, the consensus sequence of the 5' SS is AG/**GURAG**. The highly conserved yeast BP sequence **UACUAAC** (Lopez and Séraphin, 1999) contains an adenosine residue (underlined), which is essential for catalysis of the first step of splicing (1.3). The BP adenosine is located 10 to 155 nucleotides upstream of the yeast 3' SS, with a mean of 39 nucleotides (Spingola et al., 1999). In human, the branch site is located within the less conserved YURAY sequence (Zhang, 1998).

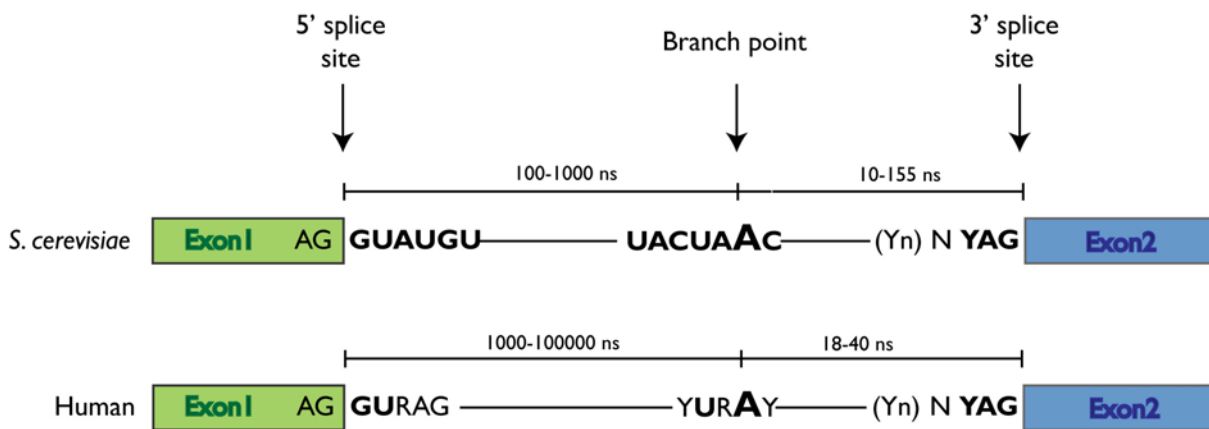


Figure 1.1 Comparison of conserved intronic consensus sequences of *S. cerevisiae* and human. Nucleotides with 90% or higher conservation are shown in bold. The BP adenosine is shown as big letter. The polypyrimidine tract is represented by (Yn); purines are shown with 'R'; ns = nucleotides. The scheme is not drawn to scale.

The 3' SS is found at the 3' end of the introns and consists of the YAG/ sequence, both in yeast and in human (Figure 1.1). In many yeast introns it is preceded by a pyrimidine-rich sequence of 8-12 nucleotides (polypyrimidine tract), that ends one nucleotide upstream of the 3' SS. However, the polypyrimidine tract is more important in human introns, possibly due to the less conserved branchpoint sequence.

The differences in sequence requirements for splicing in yeast and human may be a consequence of the way genes are organized and expressed in the two types of organisms. So far, in the yeast genome only 253 introns were identified in 248 of the 6000 yeast genes by bioinformatical and experimental methods, which accounts for only 3.8% of all genes (Lopez and Seraphin, 2000; Spingola et al., 1999). Interestingly, 27% of all yeast transcripts are spliced,

showing that intron containing genes in yeast are highly expressed. Yeast introns are rather short. The length distribution shows two peaks, one at around 100 and the other near 400 nucleotides. Only very few introns are up to 1000 nucleotides long (Spingola et al., 1999). In contrast, many human genes contain multiple introns of up to 100000 nucleotides, while exons are rather short. Moreover, some human exons are differentially spliced, creating a diversity of about 300000 proteins with only 30000 genes. This alternative splicing requires a complex regulation by various factors. Possibly, the reduced sequence conservation of the consensus sequences in mammals reflects the requirements of the quite different regulation of alternative splicing in these organisms.

1.3 The chemistry of the splicing reaction

Pre-mRNA splicing is catalyzed by a two-step mechanism (Moore et al., 1993; Moore and Sharp, 1993). As shown in Figure 1.2, in the first step, the 2' OH group of the conserved branchpoint adenosine (bold) attacks the phosphate at the 5' SS resulting in a free 5' exon containing a 3' terminal OH group and a branched lariat intermediate, which contains the intron and 3' exon. In the second step, the 3' OH of the 5' exon attacks the phosphate at the 3' SS, thereby ligating the 5' and 3' exons and releasing the intron in a lariat conformation. Subsequently, the lariat intron probably is debranched (Arenas and Hurwitz, 1987) and degraded whereas the mature mRNA is transported into the cytoplasm (Moore et al., 1993).

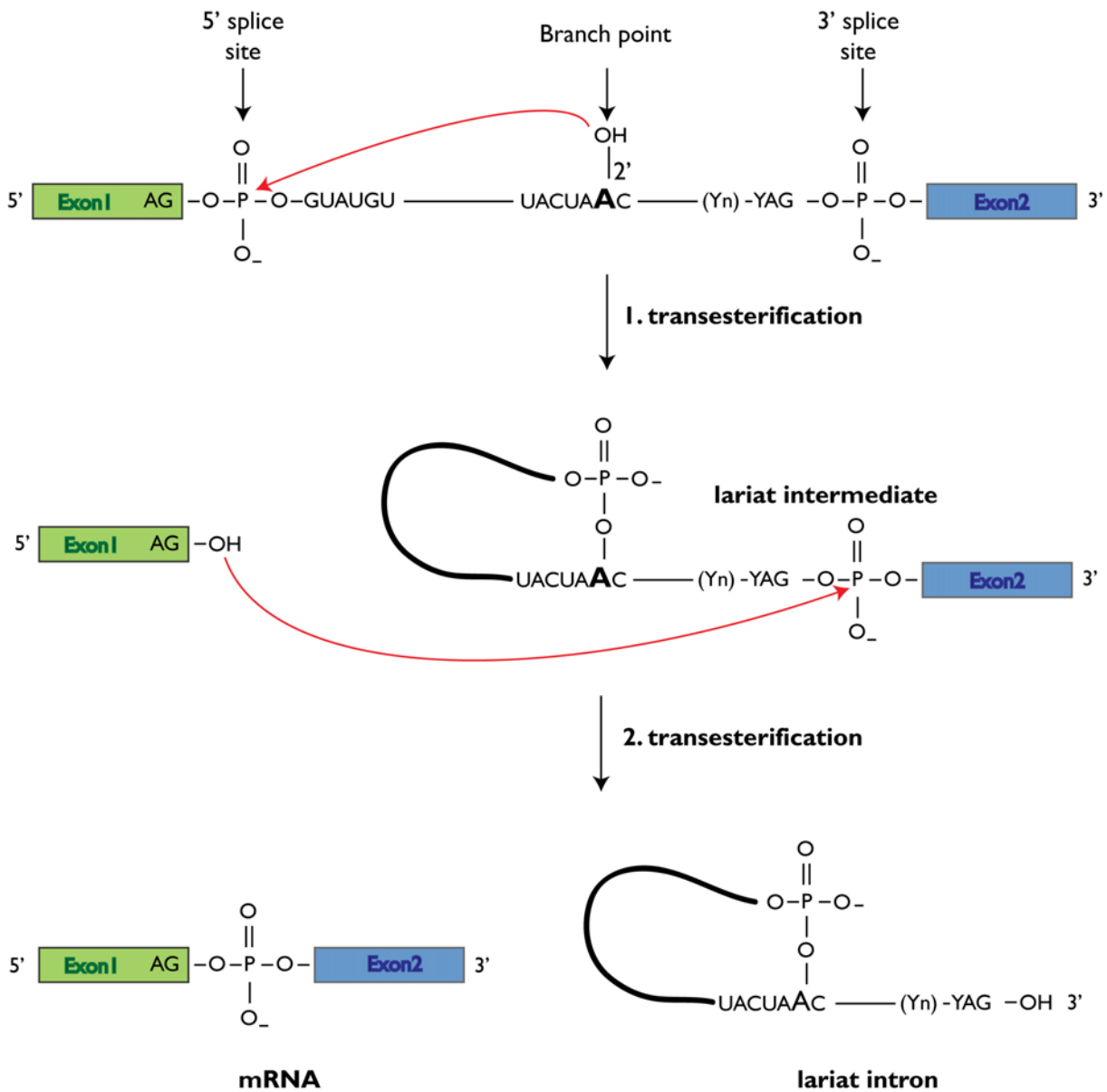


Figure 1.2 The chemistry of the splicing reaction. Two successive phosphoester transfer reactions lead to the excision of the (lariat) intron and the joining of the exons. For details see text. The branchpoint adenosine is drawn in bold; the polypyrimidine tract is represented by (Yn).

1.4 Spliceosome assembly in yeast

The splicing reaction is catalyzed by a complex macromolecular machine, the spliceosome. It consists of the U1, U2, U4/U6, and U5 small nuclear ribonucleoprotein particles (snRNPs; 1.5) and numerous non-snRNP splicing factors (Will and Lührmann, 2006). The spliceosome assembles in a step-wise manner on the pre-mRNA substrate. An overview of the splicing cycle is given in Figure 1.3. The spliceosomal complexes are designated by the more common human complex names; the yeast-specific names are shown in parentheses.

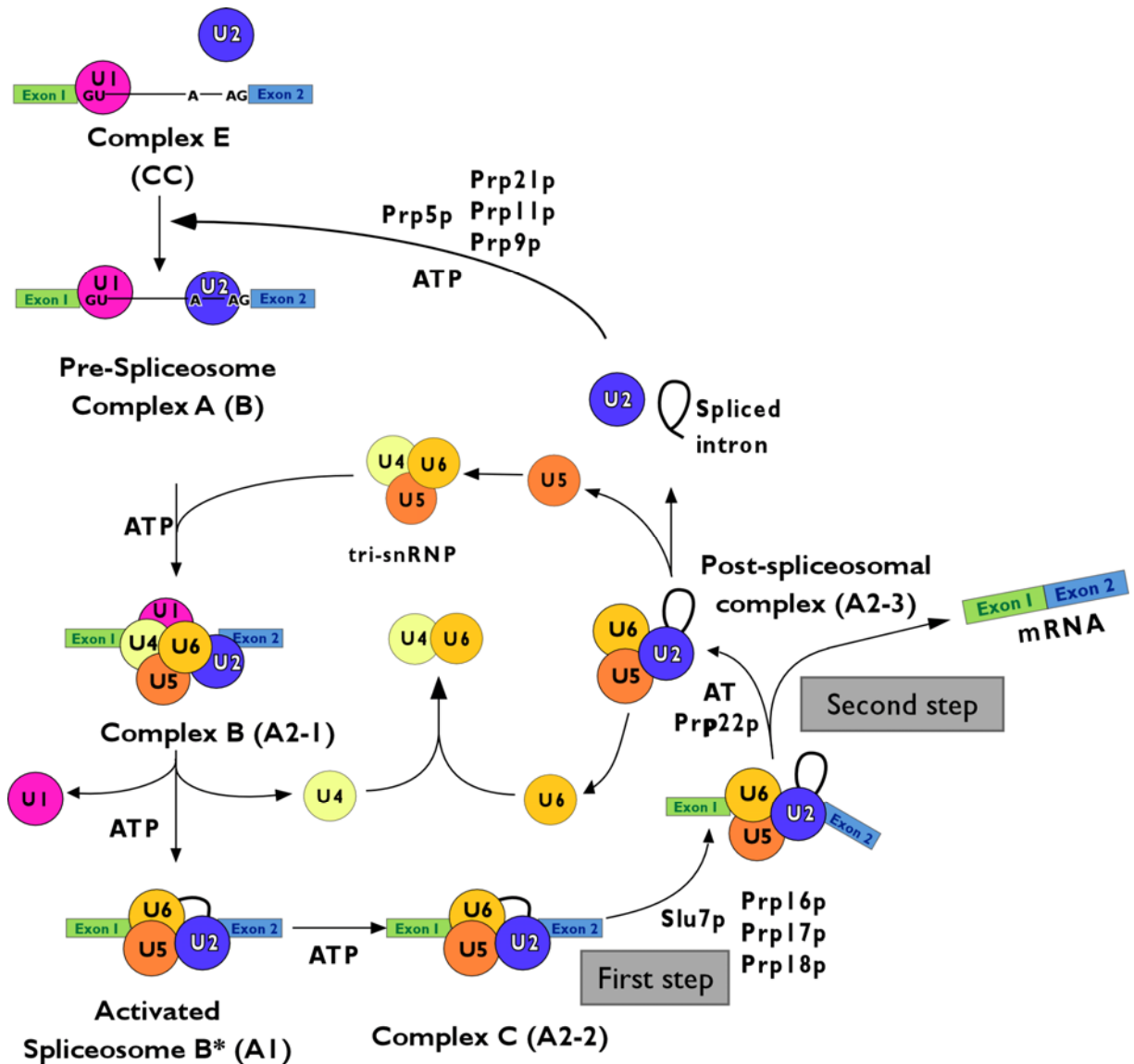


Figure 1.3 The spliceosomal cycle (for details see main text). The overall pathway of spliceosome assembly in lower and higher eukaryotes is highly conserved. However, the nomenclature is different in yeast and human. The spliceosomal complexes are designated by the more common human complex names; the yeast-specific names according to (Cheng and Abelson, 1987; Ruby and Abelson, 1991) are shown in parentheses. Moreover, the non-snRNP protein factors, which are important for the different steps of complex formation, are shown.

Spliceosome assembly is initiated by the ATP-independent interaction of the U1 snRNP with the conserved 5' SS of the pre-mRNA, mediated by a short stretch of RNA-RNA base pairing, forming the complex E (commitment complex, CC). At this stage, the human U2 snRNP has been shown to be already loosely associated with the pre-mRNA. This association is independent of the BP (Das et al., 2000). In the subsequent ATP-dependent formation of the complex A (pre-spliceosome, yeast complex B), the U2 snRNP stably interacts with the pre-

mRNA's branch site by Watson-Crick base pairing, leaving the BP adenosine unpaired to react as nucleophile in the first step of splicing (1.2). Next, the pre-formed U4/U6.U5 tri-snRNP particle interacts with complex A to form the pre-catalytic spliceosome or complex B (yeast A2-1), which contains a full set of U snRNAs. Previous studies showed that the human tri-snRNP can interact with the 5' SS and 5' exon independent of the U2 snRNP (Maroney et al., 2000), mediated by the U5 snRNP protein Prp8p. Thus, it has been hypothesized that the tri-snRNP in cooperation with U1 snRNP is involved in the 5' SS definition.

The transformation of the pre-catalytic spliceosome into the catalytically active complex B* (yeast A1) requires major structural rearrangements. During this process the U4/U6 snRNA duplex is unwound; U6 snRNA replaces U1 snRNA at the 5' SS, base pairs with U2 snRNA, and thereby forms a part of the catalytic core (1.6.2). Concomitantly, the U1 and U4 snRNPs dissociate from the spliceosome. Complex B* catalyzes the first step of splicing. By dissociation of first step factors and association of second step factors complex B* is transferred into the complex C (yeast A2-2), which catalyzes the second step of the splicing reaction. The mature mRNA is released, and the resulting post-spliceosomal complex (yeast A2-3), comprising the lariat intron, U2, U5, and U6 snRNA, disassembles. The lariat intron is degraded and the snRNPs are recycled for a new round of splicing (Brow, 2002; Will and Lührmann, 2006). snRNP recycling starts with the U4/U6 di-snRNP formation, in which the U4 and U6 snRNAs are again base paired. This process is mediated by Prp24p (Rader and Guthrie, 2002; Raghunathan and Guthrie, 1998b), which is transiently associated with the U6 snRNP and dissociates upon U4/U6 snRNP formation. Subsequently, U4/U6 is joined by the U5 snRNP to form the U4/U6.U5 tri-snRNP.

1.5 The spliceosomal U snRNPs

The major components of the spliceosome are the U1, U2, U5 and U4/U6 snRNPs, in which one uridine-rich small nuclear RNA (U snRNA) molecule (or two in case of U4/U6) is complexed with a common set of seven Sm proteins (Tan and Kunkel, 1966); only U6 snRNA is associated with seven Sm-like ('Like-Sm', Lsm) proteins (Mayes et al., 1999). Moreover, each snRNP contains several particle-specific proteins (Table 1.1).

Table 1.1 Protein components of the *S. cerevisiae* and the human snRNPs. See next page for legend

<i>S. cerevisiae</i> snRNPs							Human snRNPs					
proteins	U1	U2	U5	U4/U6	U4/U6.U5	sequence motif	proteins	U1	U2	U5	U4/U6	U4/U6.U5
SmB	●	●	●	●	●	Sm-motif	SmB/B'	●	●	●	●	●
SmD1	●	●	●	●	●		SmD1	●	●	●	●	●
SmD2	●	●	●	●	●		SmD2	●	●	●	●	●
SmD3	●	●	●	●	●		SmD3	●	●	●	●	●
SmE	●	●	●	●	●		SmE	●	●	●	●	●
SmF	●	●	●	●	●		SmF	●	●	●	●	●
SmG	●	●	●	●	●		SmG	●	●	●	●	●
Lsm2				○	○		Sm-motif	Lsm2				○
Lsm3				○	○	Lsm3					○	○
Lsm4				○	○	Lsm4					○	○
Lsm5				○	○	Lsm5					○	○
Lsm6				○	○	Lsm6					○	○
Lsm7				○	○	Lsm7					○	○
Lsm8				○	○	Lsm8					○	○
Snp1	●					RRM, RS 2 RRM C2H2 ZnF		70K	●			
Mud1	●						U1-A	●				
U1-C	●						U1-C	●				
Nam8	●						n.o.					
Prp39	●						n.o.					
Prp40	●						FBP11					
Prp42	●						n.o.					
Snu56	●						n.o.					
Snu71	●						n.o.					
Luc7	●						CGI-74					
Lea1		●				Leu-rich 2 RRM 2 SURP, UBQ C2H2 ZnF C2H2 ZnF HEAT repeats SAP, Pro-rich CPSF A 2 RRM RRM Cys-rich	U2-A		●			
Yb9		●					U2-B''		●			
Prp21		●					SF3a120		●			
Prp11		●					SF3a66		●			
Prp9		●					SF3a60		●			
Hsh155		●					SF3b155		●			
Cus1		●					SF3b145		●			
Rse1		●					SF3b130		●			
Hsh49		●					SF3b49		●			
Snu17		●					p14		●			
Rds3		●					SF3b14b		●			
Ysf3		●					SF3b10		●			
Prp5							DEAD RRM, SWAP SWAP, G-patch DExH G-patch, RRM DnaJ domain Tudor	hPrp5		●		
n.o.								SRI40		●		
n.o.						CHERP			●			
Prp43						hPrp43			●			
n.o.						SPF45			●			
n.o.						SPF31			●			
n.o.						SPF30		●				
Prp8			●		●	2 DExH, 2 SEC63 G-domain DEAD, RS GYF domain thioredoxin fold WD40	220K			●	●	
Brr2			●		●		200K			●	●	
Snu114			●		●		116K			●	●	
Prp28			●		●		100K			●	●	
Lin1			●		●		52K			●	●	
Dib1			●		●		15K			●	●	
n.o.			●		●		40K			●	●	
Prp3				●	●	PWI, DSRM WD40 RNA bdg. Motif PPIase	90K				●	
Prp4				●	●		60K				●	
Snu13				●	●		15.5K				●	
n.o.				●	●		CypH				●	
Prp6					●	TRP repeats Nop domain RS RS RS	102K			●	●	
Prp31					●		61K				●	
Prp38					●		FLJ-14936				●	
Snu23					●		FLJ-31121				●	
Snu66					●		110K				●	
Spp381					●		n.o.				●	
Sad1					●		65K				●	
n.o.					●	27K				●		

Notes to Table 1.1 (see previous page) snRNPs contain two different classes of proteins, the common proteins, which are associated with each snRNA (the Sm proteins with U1, U2, U4 and U5; the Lsm proteins with U6), and the particle-specific proteins, which are unique for each snRNP (Brow, 2002; Will and Lührmann, 2006). The yeast U1 snRNP contains more proteins than the human particle, whereas the human U2 snRNP contains a set of U2-related proteins (U2 proteins that are listed below the dotted line) that seems to be only loosely associated with the human U2 (Will et al., 2002) and, additionally, are not known in yeast as U2-specific proteins. n.o. = no confirmed ortholog known. Abbreviations: RRM, RNA recognition motif; RS, region rich in arg/ser dipeptides; ZnF, zinc finger; Ser-rich, serine rich; SURP, also known as SWAP, Suppressor-of-White-Apricot; UBQ, ubiquitin family; CPSF A, cleavage and polyadenylation specificity factor A; DnaJ, molecular chaperone dnaJ domain; HEAT; derived from Huntingtin protein, Elongation factor 3, the Alpha regulatory subunit of protein phosphatase 2A and the yeast PI3-kinase TOR1; SAP, after SAF-A/B, Acinus and PIAS motif; DEXH/DEAD, Asp- box of RNA helicase family; TPR, tetratricopeptide repeat; PWI, proline-tryptophan-isoleucine motif; PPIase, peptidyl-prolyl isomerase; HAT, histone acetyltransferase; DSRM, double-stranded RNA binding motif; bdg, binding.

The snRNPs are highly conserved in all eukaryotes. There are five different spliceosomal U snRNAs present in the cell nucleus, numbered in the order of their discovery: U1, U2, U4, U5, and U6 snRNA (Table 1.2; U3 snRNA instead is involved in ribosomal RNA processing). U4 and U6 snRNAs share extensive sequence complementarity and are mainly found base-paired in a U4/U6 di-snRNP (Guthrie and Patterson, 1988). In yeast, two isoforms of U5 snRNA exist, U5 long (U5L) and U5 short (U5S). They originate from the same primary transcript, which is differentially cleaved at its 3' stem-loop by RNase III, resulting in two different precursors, which are further processed into the long and short form of U5 snRNA, respectively (Chanfreau et al., 1997). Besides U5, also U1 and U2 snRNA precursors have 3' stem-loops, which are cleaved by RNase III during maturation of the snRNAs (Abou Elela and Ares, 1998; Seipelt et al., 1999) and are important for normal 3' end processing of the snRNAs.

Table 1.2 Lengths of U snRNAs in yeast and human.

U snRNAs in yeast		U snRNAs in human	
U snRNA	Length (ns)	U snRNA	Length (ns)
U1	568	U1	164
U2	1175	U2	187
U4	160	U4	145
U5L	214	U5	116*
U5S	179	(-)	(-)
U6	112	U6	106

Asterisk indicates that there are more than 10 isoforms of U5 snRNA in human, which are not shown explicitly in the table. ns = nucleotides

The spliceosomal snRNAs can be divided into two classes. The snRNAs of the first class, U1, U2, U4 and U5 snRNA are transcribed by RNA polymerase II and are capped at their 5'-end with an unusual hypermethylated 2,2,7-trimethylguanosine (m_3G) (Busch et al., 1982) during snRNP biogenesis (Will and Lührmann, 2001). In 1987 a monoclonal antibody, called 'H-20', was raised that recognizes the m_3G -cap structure of the snRNAs (Bochnig et al., 1987). This opened up the possibility to purify the snRNPs by immuno-affinity chromatography using this antibody (Kastner and Lührmann, 1999). In contrast, U6 snRNA is transcribed by RNA polymerase III and is modified at its 5' end with a γ -monomethylguanosine (Singh and Reddy, 1989).

A comparison of the U snRNAs of phylogenetically distant organisms by computational methods (Frank et al., 1994; Guthrie and Patterson, 1988) revealed that the snRNAs are highly conserved in short primary sequences (nearly 100% between the different organisms). These short sequence stretches are mainly located in the single stranded regions of the secondary structure models (Guthrie and Patterson, 1988), as shown for the human snRNAs in Figure 1.5 (inset). These regions are often involved in protein binding or in base-pairing interactions with the pre-mRNA or with other snRNAs within the spliceosome. In addition to the short primary sequences, also the secondary structure elements (stems and loops) of the snRNAs are highly conserved (Figure 1.4 and 1.5) (Guthrie and Patterson, 1988).

The U1, U2, U4 and U5 snRNAs share a common, single stranded U-rich consensus sequence, which is bound by a set of seven Sm proteins (named B, D1, D2, D3, E, F, and G). The Sm proteins form a doughnut shaped ring structure with a central hole through which the snRNA is threaded (Kambach et al., 1999). Homologues of these proteins are present in all organisms that have spliceosome-mediated pre-mRNA splicing. U6 snRNA does not contain a Sm binding site and consequently does not interact with the canonical Sm proteins. Instead, a set of seven Sm-like proteins (Lsm 2-8) binds to the U-rich 3' end of U6 snRNA (Vidal et al., 1999). The Lsm proteins form heteromeric complexes analogous to the Sm proteins (Achsel et al., 1999; Mayes et al., 1999; Salgado-Garrido et al., 1999) and most probably also form a seven-membered ring with a central nucleic acid binding pocket, as indicated by EM and X-ray crystallography (Achsel et al., 1999; Mura et al., 2001). Interestingly, the Lsm proteins 2-7 were found to be additionally involved in mRNA degradation in the cytoplasm, together with the Lsm1 protein (Bouveret et al., 2000; Fromont-Racine et al., 2000).

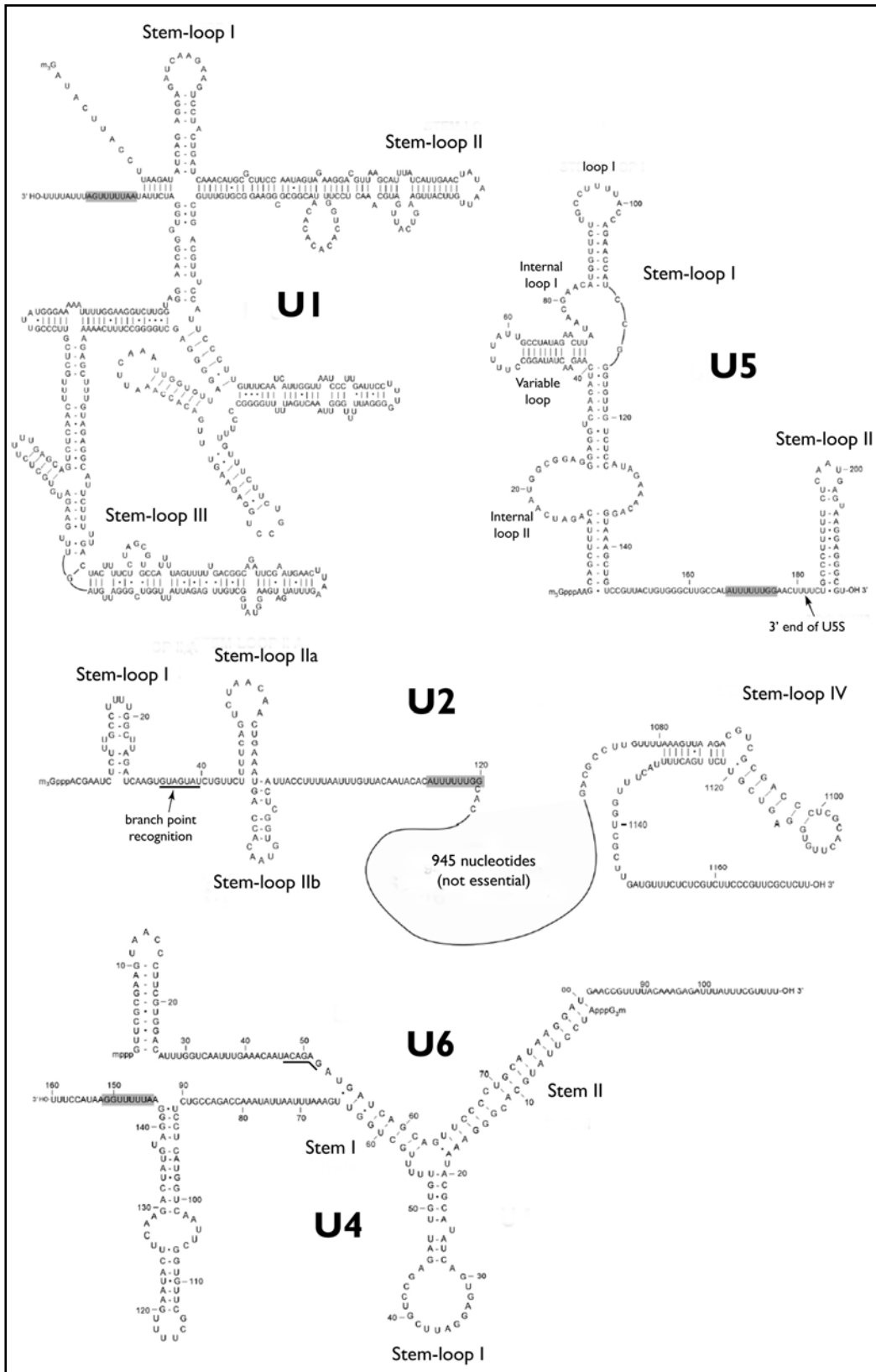


Figure 1.4 Primary sequences and proposed secondary structures of the yeast U snRNAs. The snRNAs assume conserved secondary structures with single stranded regions and stem-loops. The binding region of Sm proteins is shown with a grey bar. Adapted from (Kretzner et al., 1990) (U1); (Shuster and Guthrie, 1988) (U2); (Frank et al., 1994) (U5); (Brow and Guthrie, 1988) (U4/U6).

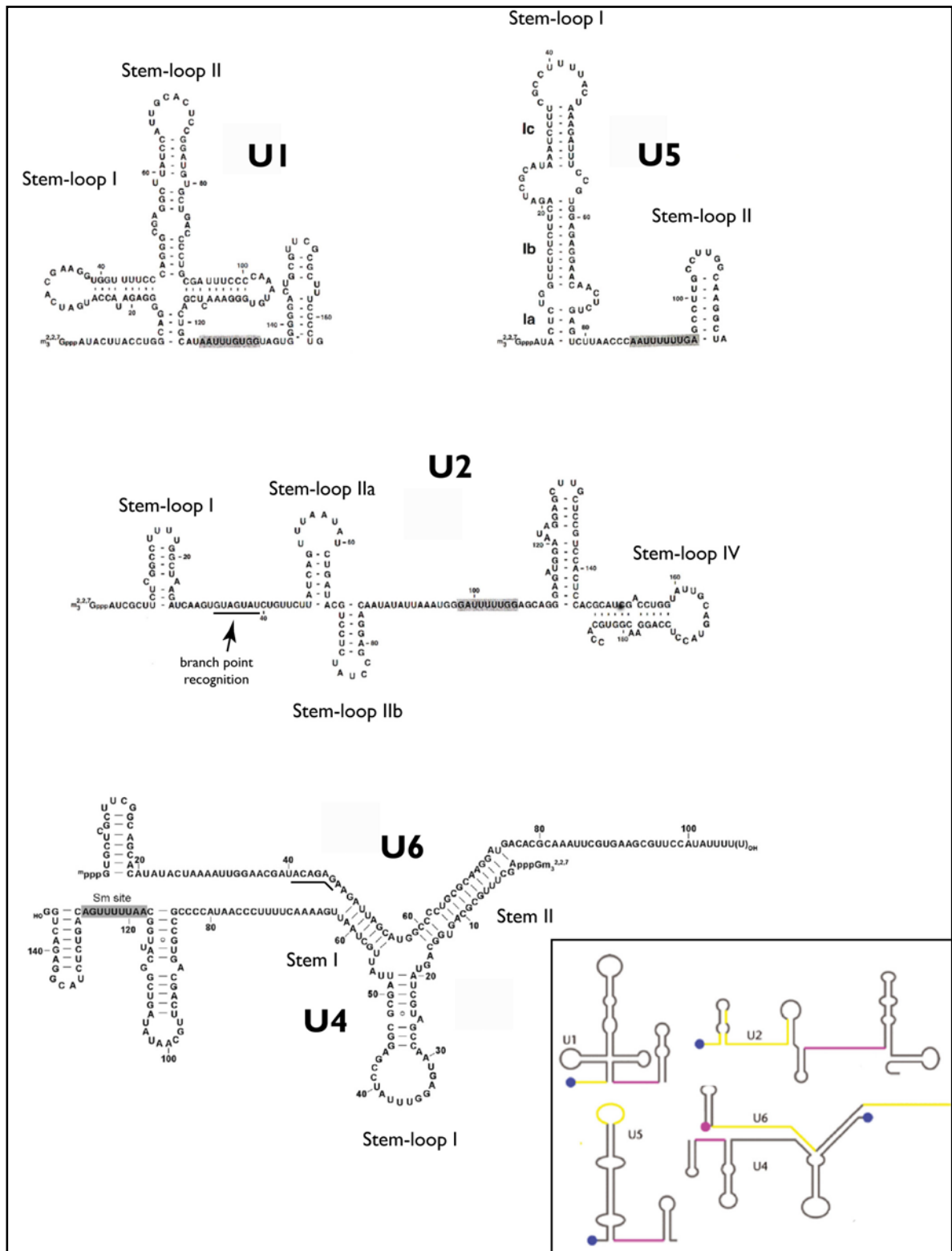


Figure 1.5 Primary sequences and proposed secondary structures of the human U snRNAs. The snRNAs assume conserved secondary structures with single stranded regions and stem-loops. The binding region of the Sm proteins is shown with a grey bar. Adapted from (Krol et al., 1990) (U1); (Lamond et al., 1989) (U2); (Krol et al., 1981) (U5); (Brow and Guthrie, 1988) (U4/U6). **Inset:** conserved regions involved in RNA-RNA interactions in the spliceosome are shown in yellow; the Sm binding site is shown in pink. The pink balls represent the γ -monomethylguanosin cap of the U6 snRNA, the blue balls represent the 2,2,7-trimethylguanosin cap. The figure was adapted from (Padgett, 2005).

The Sm/Lsm proteins together with the U snRNA form the snRNP core. In addition, each snRNP contains a set of particle-specific proteins (Table 1.1). In yeast, many of these proteins are named as 'Prp' proteins, implying their function in pre-mRNA processing. Like their RNA counterparts, both common and particle-specific snRNP proteins appear to be evolutionarily conserved, suggesting that they play an important role in snRNP function.

In yeast two different U5 snRNPs have been identified. One of them is the 18S U5 snRNP, which is incorporated into the tri-snRNP. It contains the U5-specific proteins Prp8p, Brr2p, Snu114p, Prp28p, Lin1p, and Dib1p (Table 1.1). A second U5 particle was co-purified with U1 snRNPs (Gottschalk et al., 2001) and has a quite different protein composition. This 16S particle comprises only Prp8p, Snu114p, and Aar2p. Recent studies suggested that the Aar2p-U5 snRNP is a cytoplasmic precursor in U5 snRNP maturation, which is transformed into the 18S U5 after transport into the cell nucleus (Boon et al., 2007).

As introduced in 1.4 the spliceosome additionally comprises numerous non-snRNP splicing factors, many of which are involved in the structural rearrangements prior and subsequent to the catalytic activation of the spliceosome. An important class of these factors is the family of DExD/H-box RNA helicases (Table 1.3) Two members of this family, Brr2p and Prp28p, are snRNP proteins. Some of these proteins are RNA-dependent NTPases and have been shown to unwind RNA duplexes *in vitro* (Schwer, 2001; Staley and Guthrie, 1998), for example Brr2p (Laggerbauer et al., 1998). Interestingly, recent findings suggest that the DExD/H-box proteins function by disrupting RNA-protein interactions that stabilize the base pairing interactions between the RNAs rather than by directly unwinding RNA duplexes (Fairman et al., 2004; Jankowsky et al., 2001). Prp28p for example is thought to displace U1 snRNA from the 5' SS by destabilizing the interaction between the U1-C protein and the 5' SS (Chen et al., 2001).

Altogether, mass spectrometry analysis of affinity purified human spliceosomal complexes revealed a total number of approximately 200 proteins that are constitutively or transiently associated with the spliceosome (Deckert et al., 2006; Hartmuth et al., 2002; Jurica et al., 2002; Makarov et al., 2002; Makarova et al., 2004; Rappsilber et al., 2002; Zhou et al., 2002). These proteins can be sorted into three different classes. In addition to the (1) snRNP proteins and non-snRNP splicing factors, proteins linked to (2) transcription, mRNA export and pre-mRNA processing events were identified as well as (3) proteins of unknown function or functions that are unrelated to the aforementioned processes.

Table 1.3 Yeast spliceosomal DExD/H-box proteins

DExD/H-box protein	Human homolog	Stage in splicing cycle
Sub2	UAP56	Pre-spliceosome
Prp5	hPrp5	Pre-spliceosome
Prp28	U5-100 kD	Early step I activation
Brr2 (Prp44)	U5-200 kD	Early step I activation
Prp2	hPrp2	Late step I activation
Prp16	hPrp16	Step II activation

1.6 The U4/U6.U5 tri-snRNP

1.6.1 The tri-snRNP is a highly conserved component of the spliceosome

One of the major components of the spliceosome is the U4/U6.U5 tri-snRNP. This particle is formed by association of the U5 snRNP with the U4/U6 di-snRNP. The purified yeast tri-snRNP is a particularly protein-rich particle (Table 1.1), in which one set of seven Sm proteins is associated with both the U4 and U5 snRNAs, while one set of the Lsm 2–8 proteins is bound to the 3' half of the U6 snRNA (Achsel et al., 1999; Vidal et al., 1999) (1.5). In addition, each snRNP contains several particle-specific proteins, which are evolutionarily highly conserved both in yeast and in human. In the yeast tri-snRNP the U5 snRNA is associated with the 15 kDa Dib1p and three high molecular weight proteins, namely Prp8p, the ATPase Brr2p, and the GTPase Snu114p, which are involved in the structural rearrangements during spliceosome activation (1.6.2; 1.6.3). Prp3p and Prp4p as well as the small Snu13p are stably bound to the U4/U6 snRNP. Yeast Prp3p and Prp4p directly interact with each other via the C-terminal propeller-like structure of the Prp4p, formed by seven Trp-Asp- (WD-) repeats, has been shown to be the interaction platform for Prp3p (Ayadi et al., 1998). In human, a biochemically stable, heteromeric complex of Prp4p, Prp3p, and the cyclophilin 'CypH' or '20K' (Horowitz et al., 1997; Teigelkamp et al., 1998) binds to the U4/U6 snRNA duplex via a direct contact of Prp3p with U6 snRNA in stem II (Nottrott et al., 2002). This interaction requires the presence of the human Snu13p ortholog, 15.5K (Nottrott et al., 2002) which binds to the 5' stem-loop of U4 snRNA (Nottrott et al., 1999). In yeast, association of Prp3p and Prp4p with U4/U6 snRNP requires the 5' portion of U4 snRNA. However, it is not known if the two proteins directly

contact the U4 snRNA or if the binding is mediated by other proteins (Anthony et al., 1997; Bordonne et al., 1990; Xu et al., 1990).

The yeast proteins Prp38p, Snu66p, Snu23p, Spp381p, Prp31p, and Prp6p associate more stably with the tri-snRNP than with individual U5 or U4/U6 snRNPs and are thus designated 'tri-snRNP-specific'. In contrast, the human homolog of Prp6p, the U5-102K, is stably associated with U5 snRNP, while the human Prp31p (U4/U6-61K) is a U4/U6 protein. The latter directly contacts the 5' stem-loop of U4 snRNA in native human tri-snRNPs (Nottrott et al., 2002). Prp6p is important for tri-snRNP integrity in yeast (Galissou and Legrain, 1993). Upon depletion, only low amounts of tri-snRNP are present in the extract, while U4/U6 levels are not decreased. Similarly, the human Prp31p is important for tri-snRNP formation (Makarova et al., 2002). Moreover, the human proteins have been shown to physically interact (Liu et al., 2006; Makarova et al., 2002; Schaffert et al., 2004). In combination, these data strongly indicate that Prp6p together with Prp31p functions as bridging protein in the tri-snRNP, connecting U5 to U4/U6.

The human tri-snRNP comprises three additional proteins, namely 20K and 40K, of which no confirmed yeast orthologs are known, and the human U5-100K, a DEAD-box RNA helicase. Its yeast homolog Prp28p has been shown to be involved in replacing the U1 snRNA at the 5' SS by U6 snRNA during spliceosome activation (Chen et al., 2001; Staley and Guthrie, 1999). Although Prp28p could not be identified by mass spectrometry in purified yeast tri-snRNPs (Gottschalk et al., 1999; Stevens and Abelson, 1999; Stevens et al., 2001), yeast tri-snRNPs can be isolated via TAP-tagged Prp28p (Small et al., 2006), showing that at least a sub-population of particles contains Prp28p.

1.6.2 The tri-snRNP undergoes large structural rearrangements upon spliceosome activation

During spliceosome assembly, a highly dynamic RNA-RNA, RNA-protein, and protein-protein network is formed (Nilsen, 1998; Will and Lührmann, 2006). Already in complex E the 5' SS, the BP region including the BP adenosine, and the 3' SS, are organized in close proximity (Kent and MacMillan, 2002; Kent et al., 2005). During the catalytic activation of the spliceosome, an ordered sequence of structural rearrangements leads to the formation of a U2/U6/pre-mRNA network (Figure 1.6), in which U2 and U6 snRNA are thought to form the catalytic core of the activated spliceosome. Thereby, the reactive groups of the pre-mRNA are brought into a favorable spatial position for the first and the second transesterification reaction.

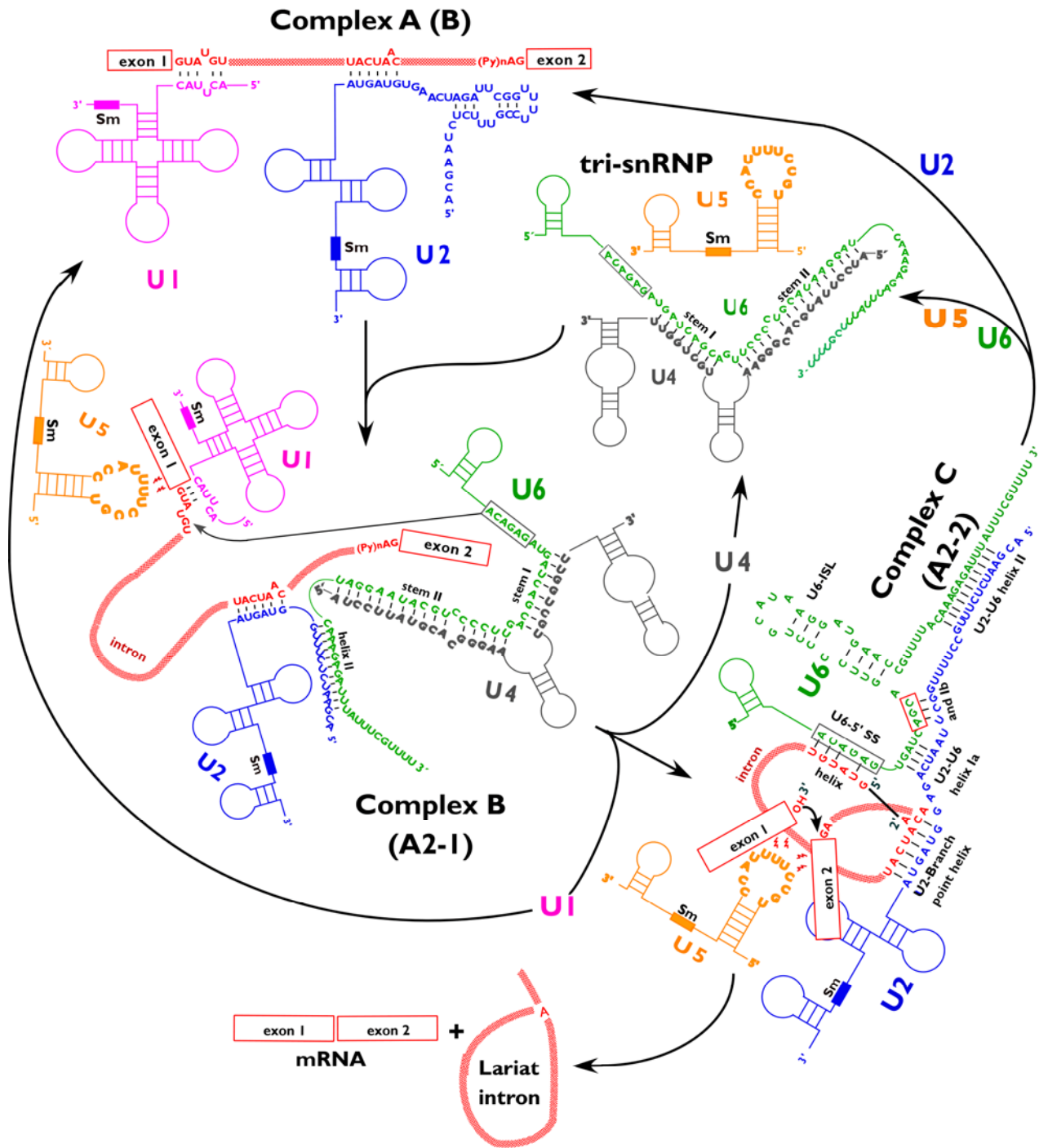


Figure 1.6 RNA-RNA rearrangements during spliceosome assembly. In complex A the U1 snRNA base pairs with the 5'-SS and the U2 snRNA with the BP sequence. Binding of the U4/U6.U5 tri-snRNP to complex A results in the formation of the fully assembled spliceosome (complex B) and initiates the RNA-RNA rearrangements that lead to the activation of the spliceosome. During these rearrangements, U1- and U4 snRNPs are released. The highly conserved ACAGAG sequence (grey box) of the U6 snRNA replaces U1 snRNA at the 5' SS. Stem I and the 3' terminal region of U6 snRNA form helices Ia/Ib and II with the U2 snRNA, respectively and helix II of U6 folds back on itself to form a new intramolecular stem-loop (U6-ISL). Thereby, the splice sites and the BP are positioned in close proximity for the first and second transesterification reaction (complex C). After the splicing reaction, the ligated exons and the lariat intron are released and the snRNPs are recycled for another round of splicing. Adapted from (Karaduman, 2006).

As part of the pre-catalytic spliceosome, the tri-snRNP is strongly affected by the structural rearrangements that occur during spliceosome activation. This is best understood on the RNA level. As in the U4/U6 di-snRNP, the U4 and U6 snRNAs are extensively base-paired within the tri-snRNP, and form the Y-shaped U4/U6 interaction domain, consisting of stems I and II separated by the 5' stem-loop of U4 snRNA (Figure 1.6). Upon spliceosome activation, the two intermolecular RNA helices of the U4/U6 snRNA duplex are unwound, followed by the dissociation of U4 snRNP from the spliceosome, while U6 snRNA undergoes several new base pairing interactions. The highly conserved ACAGAG-box of the U6 snRNA (Figure 1.6, grey box), which is single stranded in the tri-snRNP, base pairs with the 5' SS. It has been suggested that this base pairing interaction occurs even before U4/U6 snRNA unwinding (Li and Brow, 1996). Prior to or concomitant with this event, U1 snRNA must be released from the 5' SS (which results in dissociation of U1 snRNP). In yeast, the DExD/H box family member Prp28p (U5-100K in human) is involved in this process in an ATP-dependent manner (Staley and Guthrie, 1999). Different studies suggest that U1 snRNA displacement from and U6 snRNA pairing with the 5' SS is coupled (Chen et al., 2001; Kuhn et al., 1999; Kuhn et al., 2002; Lund and Kjems, 2002; Staley and Guthrie, 1999).

The region of U6 snRNA downstream of the ACAGAG-box (which contributes to U4/U6 stem I) is involved in the formation of the short U2/U6 helix Ia. A third U2/U6 snRNA base pairing interaction occurs between the 5' end of U2 and the 3' end of U6 snRNA (Figure 1.6, U2/U6 helix II) (Datta and Weiner, 1991). Moreover, the region of U6 snRNA constituting U4/U6 stem II forms a new intramolecular stem-loop (U6-ISL; Figure 1.6). Investigations of this U6-ISL suggested two different conformations. In one conformation the stem-loop is rather short and the invariant AGC triad at the base of U6-ISL (Figure 1.6, complex C, red box) is involved in the formation of U2/U6 helix Ib (Madhani and Guthrie, 1992), which was shown to be important for the second step of splicing (Hilliker and Staley, 2004). However, there is also evidence for an extended conformation that incorporates the AGC triad into the U6-ISL helix (Sashital et al., 2004; Sun and Manley, 1995). It was therefore proposed that the U6-ISL exists in both conformations and that a conformational switch occurs from the extended form in the first step of splicing to the helix Ib-containing structure in the second step of splicing (Cao and Chen, 2006; Sashital et al., 2004).

Furthermore, also the U5 snRNA interacts with the pre-mRNA via its highly conserved loop I sequence. Together with Prp8p it can be sequentially cross-linked to the 5' and 3' exon boundaries in the first and second step of splicing, respectively and is thought to be involved in the alignment of the exons for the second transesterification in cooperation with Prp8p (Grainger

and Beggs, 2005). However, U5 loop I is dispensable for the first step of splicing in yeast (O'Keefe and Newman, 1998) and even for both steps in human (Segault et al., 1999), indicating that not U5 loop I but Prp8p might be the principal factor that anchors the exons during the splicing reaction (Grainger and Beggs, 2005).

The rearrangements during spliceosome activation do not only occur on the RNA level, but also strongly affect the proteins. Regarding the yeast tri-snRNP, all U4/U6-specific proteins (Prp3p, Prp4p, and Snu13p), as well as the Lsm proteins, the U5 protein Dib1p and the tri-snRNP-specific proteins (Table 1.1) leave the spliceosome upon activation (P. Fabrizio, personal communication). Thus, of all tri-snRNP proteins only a core of U5-specific proteins, namely Prp8p, Brr2p, and Snu114p remains in the activated spliceosome. The important role of these proteins in pre-mRNA splicing will be explained (1.6.3). On the other hand, single protein factors as well as a protein complex, the Prp19-associated complex (Chen et al., 2002; Makarova et al., 2004) join the spliceosome during activation.

1.6.3 Involvement of tri-snRNP proteins in the catalytic activation of the spliceosome and spliceosome dynamics

The U5-specific proteins Brr2p, Snu114p and Prp8p remain associated with the spliceosome throughout the splicing cycle in yeast (Ohi et al., 2002; Stevens et al., 2002)(P. Fabrizio, unpublished data) as well as in human (Jurica and Moore, 2003; Will and Lührmann, 2006). They play important roles in the catalytic activation of the spliceosome, but also in splicing catalysis and spliceosome disassembly. There is strong evidence that the DExD/H-box ATPase Brr2p, which unwinds RNA duplexes *in vitro* (Laggerbauer et al., 1998), is the driving force behind the disruption of the U4/U6 snRNA helices during spliceosome activation (Kim and Rossi, 1999; Raghunathan and Guthrie, 1998a; Small et al., 2006). This conserved splicing factor contains two DExD/H-box domains, each followed by a SEC63 domain. U4/U6 snRNA unwinding requires both the first DExD/H-box domain and the first SEC63 domain (Raghunathan and Guthrie, 1998a; Small et al., 2006). Interestingly, recent studies showed that these domains of Brr2p are as well required for the disassembly of the spliceosome (Small et al., 2006). Thus, as an integral part of the spliceosome, the activity of Brr2p has to be tightly regulated throughout the splicing cycle.

There are two possible candidates for regulation of Brr2p activity: Snu114p and Prp8p. The GTPase Snu114p is a homolog of the ribosomal translation elongation factor EF-2/EF-G (Fabrizio et al., 1997), which drives translocation of tRNA and mRNA in the ribosome, indicating that also Snu114p might be involved in RNA rearrangements during splicing. It has

been shown that Snu114p, similar to Brr2p, plays a dual role in pre-mRNA splicing; deletions in the N-terminal (Bartels et al., 2002) and the C-terminal domain (Brenner and Guthrie, 2006) of Snu114p block U4/U6 snRNA unwinding and dissociation of U4 from the spliceosome. Moreover, different mutations in the G-domain of Snu114p (Bartels et al., 2003; Brenner and Guthrie, 2006) not only inhibited U4/U6 snRNA unwinding but also spliceosome disassembly, respectively (Small et al., 2006). These results suggest a cooperative function of Brr2p and Snu114p both in spliceosome activation and disassembly. Snu114p probably controls the activity of Brr2p by switching between a GTP- and a GDP-bound state, functioning as a regulatory G protein (Small et al., 2006). This regulation could occur directly, since the human orthologs of Brr2p and Snu114p have been shown to physically interact (Liu et al., 2006). Alternatively, the regulation might be mediated by Prp8p. All three proteins copurify from human U5 snRNPs as a very stable RNA-free complex (Achsel et al., 1998). Moreover, Prp8p and Brr2p directly interact with each other (van Nues and Beggs, 2001). Extensive studies with yeast *prp8* mutants showed that mutations in different regions of Prp8p can suppress *brr2-1* or *prp28-1* mutations, which block the unwinding of the U4/U6 RNA and U1 RNA/5' SS helices, respectively (Kuhn et al., 2002). It was therefore suggested that Prp8p might coordinate the activities of both helicases during spliceosome activation by allosteric interaction.

However, the exact mechanism of Brr2p regulation throughout the splicing cycle is still not known. Recent studies favor Snu114p as the central regulator of Brr2p (and Brr2p-dependent spliceosome dynamics) (Brenner and Guthrie, 2005; Small et al., 2006). Depending on the actual stage of the splicing cycle, Snu114p could up- or down-regulate Brr2p activity by switching between the GTP- and GDP-bound state (Small et al., 2006), which induces conformational changes that are relayed via Prp8p to Brr2p (Brenner and Guthrie, 2005). Prp8p has been assigned the part of a scaffold protein in the catalytic core of the spliceosome, where it can be cross-linked to all cis-acting elements of the pre-mRNA, namely the 5' SS, BP, and 3' SS (Grainger and Beggs, 2005) and is thought to tether the exons for the splicing reaction. Thus, Prp8p could be the factor that signals the status of the splicing substrate to Snu114p (Small et al., 2006). Interestingly, very recent data showed that Prp8p is ubiquitinated within the tri-snRNP. In its ubiquitinated state it represses U4/U6 snRNA unwinding in purified tri-snRNPs (Bellare et al., 2008), similar to Snu114p in its GDP-bound state (Small et al., 2006) indicating that the regulation of tri-snRNP disassembly might be partially redundant.

1.7 *Saccharomyces cerevisiae* a model organism for pre-mRNA splicing

The yeast *S. cerevisiae* for several reasons has always been an important organism to study pre-mRNA splicing. First of all, the easy handling, the presence of a large number of selectable markers, the existence of a haploid and a diploid state and the relative genetic stability have made yeast one of the favored model organisms of modern biology. Moreover, the efficiency and preciseness of homologous recombination in *S. cerevisiae* allows for the targeted integration or modification of yeast genes directly in the genome. This makes overexpression of the modified protein unnecessary, which otherwise can often lead to the formation of artificial protein complexes or aggregates. Moreover, the cells do not express a mixture of endogenous and modified protein. This enables large scale genomic and proteomic studies, but also detailed functional analysis of individual genes. Moreover, it provides a means for targeted labeling of proteins for structural studies.

Although much less abundant in yeast, the process of pre-mRNA splicing is highly conserved from yeast to human, not only in the general pathway, but also regarding the RNA and protein factors involved in this process (Burge et al., 1999). When, in 1996, the genome of *S. cerevisiae* was sequenced as the first eukaryotic organism (Goffeau et al., 1996), scientists were able to search for putative homologs of splicing factors by bioinformatical methods. By gene prediction algorithms it was also possible to detect introns present in yeast genes (Lopez and Séraphin, 1999; Spingola et al., 1999). Thus, while the higher abundance of spliceosomal components in mammalian cells favored biochemical investigations of pre-mRNA splicing in mammals, the genetic analysis progressed much faster in yeast due to its elegant and powerful genetic techniques. Due to the high conservation of pre-mRNA splicing between yeast and higher eukaryotes, the results obtained from the yeast system can help to learn more about splicing in humans.

1.8 Electron microscopy as a means for structural studies of complex macro-molecules

Single-particle electron microscopy (EM) to date represents the method of choice to investigate the structural organization of large macromolecular machines. EM offers an alternative to investigate the structures of proteins that are difficult to study by more traditional techniques, such as X-ray crystallography and nuclear magnetic resonance spectroscopy (NMR). Many proteins and complexes are too large for NMR, whereas in X-ray crystallography the need to obtain highly diffracting crystals can sometimes be an insurmountable obstacle on the way to the

structure of a protein. Complex protein assemblies, such as the spliceosome, pose additional problems because they may undergo rapid changes in composition and conformation. Moreover, each crystallization assay requires large amounts of material. In contrast, single-particle EM requires extremely small amounts of material, typically only a few picomoles. Using EM, one can visualize individual protein molecules with a molecular weight larger than 200 kDa or complex macromolecules with molecular weights up to many mega-Dalton. Depending on the investigated particle, sample preparation technique, and instrumentation, a resolution higher than 6 Å can be obtained. Very recently, the structure of a virus capsid has been determined at a resolution of 4.5 Å (Jiang et al., 2008). Although the complexity and dynamic nature of spliceosomes posed quite a challenge for the determination of a three-dimensional (3D) spliceosomal structure, it was possible to obtain 3D structures of the human spliceosomal B Δ U1 (Boehringer et al., 2004) and C complexes (Jurica et al., 2004) at a resolution of 30-40 Å using single-particle cryo-EM. Moreover, the 3D structure of the human tri-snRNP was determined at a resolution of 19-24 Å (Sander, 2006).

To obtain meaningful structural information from biological samples, image processing and classification is performed (Thuman-Commike, 2001; van Heel and Frank, 1981). For this, many thousands of single particles are selected from the electron micrograph either manually or semi-automated using computer programs (the latter requires verification by the user to remove selected areas that do not correspond to particles). In a rotational and translational alignment of the single images the particles are repositioned such that key structural features appear in the same position. The alignment is done iteratively either in a reference-free (Dube et al., 1993) or in a multi-reference (van Heel and Stofferl-Meilicke, 1985) alignment procedure. Image classification then identifies common features in the aligned images, which are then sorted into classes according to their similarities. Multivariate statistical analysis (MSA) is used in this step to compress the large quantities of image data into a set of 'eigen images' that sufficiently describe the overall variance of the data set (Frank and van Heel, 1982; van Heel and Frank, 1981). After classification, the images in each class are averaged, which results in images displaying a significantly improved signal-to-noise ratio (SNR), revealing fine structural details of the particle. Next, the relative orientation of the particles in the different classes has to be determined. Explaining the different methods that can be used at this step is beyond the scope of this introduction. Once the relative orientation of all particles is known, the 3D reconstruction can be computed.

Biological samples often have a heterogeneous appearance when viewed by EM, even if they might have appeared to be homogeneous after purification. The main reasons for

heterogeneous appearance are (1) different orientations of the particles on the carbon film, (2) the fragmentation of the sample (during purification or sample preparation for EM), and (3) different conformational states of the particle. Before a 3D structure can be calculated the reason for the heterogeneity has to be determined, because a reliable 3D structure reconstruction is only possible, if all images of the particle originate from the same structure. This is only the case when the heterogeneity is due to different orientations of the particle on the carbon film.

Single particle EM offers the possibility to localize subunits of complexes by targeted labeling and visualization of the label in the electron microscope. For a 3D structure determination of a labeled particle the same requirements are applied on the label as on the particle: it has to be structurally absolutely stable. If this is the case then the accuracy with which the label position can be determined depends on the size of the label (the smaller the better) and on the resolution. If a 3D structure determination is not possible because the particle is dynamic and/or the label is flexible, the localization of the label can be performed by two-dimensional (2D) image analysis, i.e. on the level of single images and/or class averages. Particles with a preferential orientation on the carbon film are best suited for 2D labeling studies, because the resulting characteristic view facilitates the alignment of the particles and thereby the identification of the label position. 2D labeling studies are usually performed in negative stain (the EM specimen is embedded in a layer of dried heavy metal solution, often uranyl acetate and formate), which significantly increases the specimen contrast. A label is well visible as an additional density in 2D images if it is located at the border of the particle in the x-y-plane (image plane; Figure 1.7 A, B; label position 1). However, although the label can be localized in the x-y-plane, an uncertainty about the label position in z-direction (which is the direction of the electron beam) remains. If, in contrast, the label protrudes in direction of the z-axis it is not visible as a new protuberance but merely results in a shift of the grey values in the image due to the increased density of the particle at that position (Figure 1.7 A, B; label positions 2 and 3). The larger the diameter of the particle at the label position the less is the relative change in electron density and the more difficult is the detection.

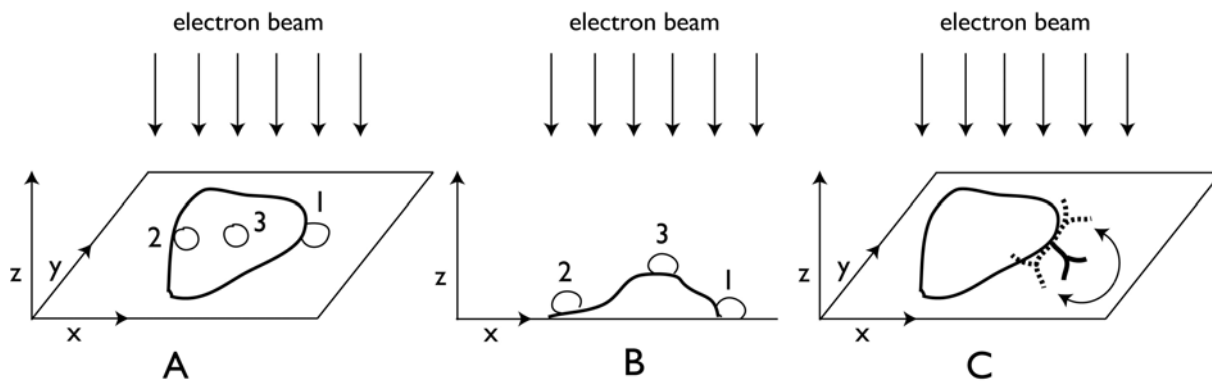


Figure 1.7 Difficulties arising from different label positions for localization in 2D EM images (for details see main text)

An additional uncertainty in the localization is caused by a flexibility of the label, which complicates the determination of the binding site of the label (Figure. 1.7 C). A very common labeling method that deals with this difficulty is immunolabeling. The flexibility can be an intrinsic property of the label, but also depends on the length of the linker between the particle and the label. In contrast to a structurally rigid label that appear as a well defined protuberance also after class averaging, a flexible label might be visible protruding from the border of the particle only in single particle images. Upon image processing the tag is easily averaged out. The same is true if a tag is located at a structurally flexible position of the labeled particle. In both cases image processing can confer statistical significance to the label and thereby corroborate the label position. However, this requires a very careful particle selection, alignment and classification, especially in the most difficult case when both label and particle are dynamic. In total, the accuracy of the localization in 2D depends on the size, position and flexibility of the label as well as on the dynamic of the labeled particle.

1.9 Aim of this study

The aim of this study was to shed light on the structural organization of an evolutionarily highly conserved component of the spliceosome, the U4/U6.U5 tri-snRNP. It is well established that several tri-snRNP proteins, namely Prp8p, Brr2p and Snu114p cooperate in the crucial process of the U4/U6 snRNA unwinding during the catalytic activation of the spliceosome. However, the mechanism of U4/U6 snRNA unwinding is still not fully understood. Moreover, not much is known about the molecular architecture of the tri-snRNP. To better understand how the functionally important proteins cooperate to fulfill their tasks that lead to spliceosome activation, it is important to understand their structural organization within the tri-snRNP.

Therefore, the aim of this work was (1) to learn how the U5-specific proteins that cooperate in the catalytic activation of the spliceosome, Prp8p, Brr2p, and Snu114p, are arranged relative to each other in the native yeast tri-snRNP. (2) Moreover, we wanted to understand, how Prp8p, Brr2p, and Snu114p are located relative to the U4/U6 snRNA. Therefore, it was important to localize the position of the U4/U6 snRNAs within the tri-snRNP via proteins that are known to directly interact with the snRNAs, such as Prp3p and Lsm8p. (3) The localization of U5-specific (Prp8p, Brr2p, Snu114p) and U4/U6-specific (Prp3p, Prp4p) proteins should allow to identify the position of the U5 snRNP and the U4/U6 snRNP within the tri-snRNP. (4) To learn more about the connection between the tri-snRNP's subunits in the native particle the position of Prp6p and Prp31p, which have been suggested to bridge U5 and U4/U6, should be mapped. (5) Additionally, Prp8p, Brr2p, and Snu114p should be localized in the U5 snRNP and their positions should be compared to that in the tri-snRNP. This should provide information about possible rearrangements of these proteins upon tri-snRNP formation.

To answer these questions, the U5 snRNP and the tri-snRNP were purified to homogeneity from yeast *S. cerevisiae* total cell extract under mild conditions using the tandem affinity purification (TAP) method and C-terminally TAP-tagged proteins. The purified particles were investigated by negative stain EM in cooperation with members of Dr. Holger Stark's cryo-EM group (Max Planck Institute for Biophysical Chemistry, Göttingen) to gain information about the native tri-snRNP structure. Tri-snRNPs were purified via different TAP-tagged proteins to investigate the influence of the tag on the native structure of the particles. To localize the functionally important proteins within the U5 snRNP and the tri-snRNP, the C-termini of the proteins were specifically labeled to directly visualize their position in the electron microscope. Therefore, two independent labeling techniques were established. First, the genetic labeling of the proteins with a 54 kDa globular protein tag, tDimer2, which was directly visible in the electron microscope, and second, the immunolabeling using C-terminal tags and tag-specific

antibodies. Antibodies against a variety tags were tested for their binding efficiency and specificity. These data provided important information about the structural organization of the yeast tri-snRNP and helped to improve our understanding of the processes involved in U4/U6 snRNA unwinding, not only in yeast, but since pre-mRNA splicing is evolutionarily highly conserved, also in human.

2 Materials and methods

2.1 Materials

2.1.1 Chemicals and media

Agarose, electrophoresis grade	Invitrogen, Netherlands
Ammoniumperoxodisulfate (APS)	Merck, Germany
Bacto agar	BD, USA
Bacto yeast extract	BD, USA
Bacto peptone	BD, USA
Bovine Serum Albumin (BSA)	Sigma-Aldrich, Germany
Brilliant Blue G-Colloidal concentrate	Sigma-Aldrich, Germany
Bromophenol blue	Merck, Germany
Calmodulin affinity resin	Stratagene, USA
Complete supplement mixture (CSM)	Bio 101 Inc., USA
D(+)-glucose monohydrate	Merck, Germany
D(+)-galactose monohydrate	Sigma-Aldrich, Germany
D(+)-raffinose pentahydrate	Sigma-Aldrich, Germany
DMSO (Dimethylsulfoxide)	Roth, Germany
DNA-molecular weight marker	Gibco, New Zealand
DOBA-powder (dextrose/galactose)	Bio 101 Inc., USA
DTT (Dithiothreitol)	Roth, Germany
EDTA (Disodium salt dihydrate)	Roth, Germany
Fish sperm DNA (10mg/ml)	Roche, Germany
Glycoblue	Ambion, USA
Glycogen	Roche, Germany
Glycine	Merck, Germany
HEPES (N-2-Hydroxyethylpiperazin- N-2-ethansulfonic acid)	Calbiochem, USA
IgG-sepharose	GE Healthcare, UK
Imidazole	Merck, Germany
2-Mercaptoethanol	Roth, Germany
Milk powder, dry, instant	Heirler, Germany
Paraformaldehyde	Merck, Germany
Ponceau S	Serva, Germany

Protein A-sepharose CL-4B	GE Healthcare, UK
Roti-Phenol-Chloroform-Isoamyl alcohol (PCI)	Roth, Germany
Rotiphorese Gel 30 solution	Roth, Germany
Rotiphorese Gel 40 solution	Roth, Germany
Sodiumdodecylsulfate (SDS)	Serva, Germany
Standard proteins for electrophoresis	Bio-Rad, Germany
Sucrose (for biochemistry)	Merck, Germany
TEMED (N, N, N', N'-Tetramethylethylenediamine)	Sigma-Aldrich, Germany
Tris-(hydroxymethyl)aminomethane (Tris)	Roth, Germany
Triton X-100	Sigma-Aldrich, Germany
tRNA <i>E. coli</i>	Boehringer, Germany
Tween 20	Sigma-Aldrich, Germany
Urea	Merck, Germany
Xylene cyanol	Fluka, Switzerland

2.1.2 Enzymes and enzyme inhibitors

Aprotinin	Serva, Germany
Benzamidine	Serva, Germany
Chymostatin	Serva, Germany
Complete TM protease inhibitor tablets, EDTA-free	Roche, Germany
Leupeptin	Serva, Germany
Pepstatin A	Serva, Germany
Phenylmethylsulfonylfluoride (PMSF)	Merck, Germany
Proteinase K	Sigma-Aldrich, Germany
Go-Taq DNA polymerase	Promega, USA
TEV Protease, recombinant (10 U/ μ l)	Invitrogen, Netherlands
Trypsin	Invitrogen, Netherlands

2.1.3 Antisera, monoclonal and polyclonal antibodies

Anti-Snu114p rabbit antiserum ('Camillo')	Dep. Lührmann; Dr. P. Fabrizio
Anti-Snu114p rabbit antiserum ('Peppone')	Dep. Lührmann; Dr. P. Fabrizio
Anti-Snu114 affinity purified	Dep. Lührmann; Dr. P. Fabrizio

Anti-Aar2 rabbit-antiserum ('Harry')	Dep. Lührmann; A. Gottschalk
Anti-Prp8p rabbit antiserum (region 8.6)	Dr. J. D. Beggs, Scotland
Anti-Prp3 rabbit-antiserum	Dr. J. L. Woolford, USA
Anti-Prp31 rabbit-antiserum	Dr. J. L. Woolford, USA
Anti-Prp4 rabbit-antiserum	Dr. J. Banroques, France
Peroxidase-antiperoxidase complex (PAP)	Sigma, Germany
HA-Tag polyclonal antibody	BD, USA
Living Colors YFP monoclonal antibody	BD, USA
Anti-GFP antibody (RGFP-45A-Z)	Immunology Consultants Laboratory, Inc., USA
Monoclonal anti-m3G antibody 'H-20'	Dep. Lührmann, Germany
Polyclonal anti-m3G antibody 'R1131'	Dep. Lührmann, Germany
Anti-TAP antibody ('anti-CBP')	Biocat, Germany
Goat anti rabbit/anti mouse antibodies, (Horseradish peroxidase coupled)	Jackson ImmunoResearch, USA

2.1.4 Peptides

Anti-TAP ('anti-CBP') immunizing peptide H ₂ N-CSSGALDYDIPTTASENLYFG-COOH	Dr. Krause, Marburg
---	---------------------

2.1.5 Nucleotides

Nucleoside-5'-triphosphate (100 mM): (ATP, CTP, GTP, UTP)	Pharmacia, Germany
Deoxynucleoside-5'-triphosphate (100 mM): (dATP, dCTP, dGTP, dTTP)	Pharmacia, Germany
Radionucleotides: [α - ³² P] dATP	Pharmacia, Germany

2.1.6 Oligonucleotides

DNA oligonucleotides for C-terminal TAP-tagging

Primers are displayed in 5' → 3' orientation. The complementary region to the plasmid is shown in lowercase letters, the complementary region to the yeast genome in UPPERCASE letters.

	Sequence
Brr2-C-TAP	
Oligo.For.Brr2	TCATATCTTGACGCAGATAAAGAGTTGTCCTTTGAAATAAATGTGAAAtccatggaaaagagaag
Oligo.Rev.Brr2	ATGTTATATATTGAAATCCATTTCGATTATCCAGGACTAAACAATGATTtacgactcactataggg
Check.For.Brr2	CGTAGTGGTTGATATCCTTTTCAGC
Check.Rev.Brr2	CACAATTAGATTAAATAGCCGC
Prp3-C-TAP	
Oligo.For.Prp3	CTGGGTCAGTTTGATTCAGAGCATTTTTATTACCTGTTCAAACGtccatggaaaagagaag
Oligo.Rev.Prp3	AATATTTAATATGAAACAAAGCGTATCATTTTGTAGACACCGATAtacgactcactataggg
Check.For.Prp3	CCTAAGCCTGAACCGAAAG
Prp6-C-TAP	
Oligo.For.Prp6	TACTGCACACCTAGAGAGATTTTATTGCGCTTGATGAATGACAAAAtccatggaaaagagaag
Oligo.Rev.Prp6	ATATACGCGCAGGCTAAGTAGAAAACAACGCAAGATAGAATTACTtacgactcactataggg
Check.For.PRP6	GCGGAGTTACTCGTCACACAGG
Prp31-C-TAP	
Oligo.For.Prp31	CATACTAACCAGAGAAGAAGAGACCAATTGGTTTTCCGGTCATGGTtccatggaaaagagaag
Oligo.Rev.Prp31	ACTATATAATATCTTTTTAAATATATCAAGTATGTAGAAGAGCctacgactcactataggg
Check.For.PRP31	TGTGCAAAAGTATCACTAGCCGCAAGAG
Universal C-TAP	
Check.Rev.TAP.U	atcatttagcttttttagcttctgc

DNA oligonucleotides for C-terminal tDimer2-tagging

Primers are displayed in 5' → 3' orientation. The complementary region to the plasmid is shown in lowercase letters, the complementary region to the yeast genome in UPPERCASE letters.

	Sequence
Brr2-tDimer2	
Oligo.F5.Brr2	CATATCTTGACGCAGATAAAGAGTTGTCCTGAAATAAATGTGAAAggtgacggtgctggttta
Oligo.R3.Brr2	TGTTATATATTGAAATCCATTTCGATTATCCAGGACTAAACAATGATTtcogatgaattcgagctcg
Check.For.Brr2	TCCTTTCAGCAAACGGGTAT
Check.Rev.Brr2	CAAAGAAGGAGAACAGGATGAAG
Dib1-tDimer2	
Oligo.F5.Dib1	AAGGGCTGGTGGTCTCTCCATACGATTATAATCATAAGCGTGTTCAggtgacggtgctggttta
Oligo.R3.Dib1	CTGAATTGTTAAGACATCGTGCGCCCTAGCCTACATAGTTATTATGAAAtcgatgaattcgagctcg
Check.For.Dib1	GTGGATCAGGCTATTGTTACCG
Check.Rev.Dib1	CACTGAATTGTTAAGACATCGTGC

Prp3-tDimer2	
Oligo.F5.Prp3	CGCTGGGTCAGTTTGATTGATTGAGCATTTCATTTTACCTGTTCAAACGggtgacggtgctggttta
Oligo.R3.Prp3	ATAATATTTAATATGAAACAAAGCGTATCATTTTGTAGACACCGATAtcgatgaattcgagctcg
Check.For.Prp3	CCTAAGCCTGAACCGAAAG
Check.Rev.Prp3	GCGTATCATTTTGTAGACACCG
Prp4-tDimer2	
Oligo.F5.Prp4	ATTTTTTAGTGAGCGCGGATGGGATAGGTCTATCAAGCTCTGGAATggtgacggtgctggttta
Oligo.R3.Prp4	TAATAAACGTTAGTTTCAAAAATACTAAATACATTTCTTTACACAAtcgatgaattcgagctcg
Check.For.Prp4	GGAGACTTTGGGATGCGTCA
Check.Rev.Prp4	CCAGGGCAAAAAACCAGGAAATG
Prp6-tDimer2	
Oligo.F5.Prp6	AATACTGCACACCTAGAGAGATTTTATTGCGCTTGATGAATGACAAAggtgacggtgctggttta
Oligo.R3.Prp6	AAATATACGCGCAGGCTAAGTAGAAAACAACGCAAGATAGAATTACTtcgatgaattcgagctcg
Check.For.Prp6	GCGGAGTTACTCGTCACACAGG
Check.Rev.Prp6	CGCAGGCTAAGTAGAAAACAACGC
Prp8-tDimer2	
Oligo.F5.Prp8	TGGCGGGGACGAAGAGTTAGAGGCCGAACAAATCGATGTATTTAGCggtgacggtgctggttta
Oligo.R3.Prp8	CATATATATCTATGAAATAACAGATTCCAGTTTATTGGGGAATATATtcgatgaattcgagctcg
Check.For.Prp8	AACATTTATGTTTCGGCTGATG
Check.Rev.Prp8	TAGTGCGGAAAGCGTAGCTT
Prp31-tDimer2	
Oligo.F5.Prp31	CATACTAACCCAGAAGAAGAGACCAATTGGTTTCCGGTCATGGTGGTGACGGTGCTGGTTTA
Oligo.R3.Prp31	ACTATATAATATCTTTTTAAATATATCAAGTATGTAGAAGAGCCTCGATGAATTCGAGCTCG
Check.For.Prp31	TGTGCAAAAGTATCACTAGCCGCAAGAG
Check.Rev.Prp31	ATCTGGGTTGCAGCGTGTGGTGTTTGGC
Snu66-tDimer2	
Oligo.F5.Snu66	GGAAAAATACCCCTGAAAATGGTAGTTTGTTTGAATTTGATGACAAAggtgacggtgctggttta
Oligo.R3.Snu66	AGATATTGAATATTTAAAGCTGGGGCTAGTAGAATTTGCTGATTAGGtcgatgaattcgagctcg
Check.For.Snu66	ACGAGGGAGATGCTGAAAATGC
Check.Rev.Snu66	CAATGGCTTGAGATTCAGGCACA
Snu114-tDimer2	
Oligo.F5.Snu114	TAAGCGCTGAATTATACGCTCAATTAAGAGAAAATGGCTTAGTACCGggtgacggtgctggttta
Oligo.R3.Snu114	ATAAAAATATTGTGGACATATTGCTTAATTCCTATGCGCCAAGATTTtcgatgaattcgagctcg
Check.For.Snu114	ATTGTTGGAGGTTTCGTGGAC
Check.Rev.Snu114	CAACTAACTGTGCTTTGTTACCG
Universal tDimer2	
Check.Rev.tD2.U	tggtgtagtcctcgttggtg
Universal yECitrine	
Check.Rev.yEC.U	tggagtatTTTgTTgataatggtc

DNA oligonucleotides for N-terminal TAP-tagging

Primers are displayed in 5' → 3' orientation. The complementary region to the plasmid is shown in lowercase letters, the complementary region to the yeast genome in UPPERCASE letters.

	Sequence
Brr2-N-TAP	
Oligo.N.For.Brr2	TATAAGTAATTGCTTTGGAAGATTACCGTGAGCCTTCGTTATTAAGaacaaaagctggagctcat
Oligo.N.Rev.Brr2	AATTTCTCTAATTTTTTGGCCTTATCCTTCGTTTCATGCTCAGTCATccttatcgatcatcaagtg
Check.N.Rev.Brr2	CCAGTAGCGTTGGAGCAGAA
Prp8-N-TAP	
Oligo.N.For.Prp8	CTTGTGCGATTGAACTTCCTTCCAAAAAATAAGCGTCAAAGAAAGaacaaaagctggagctca
Oligo.N.Rev.Prp8	GTCGCTGTCTCTTCAAACCAGGAGGTGGGGCGGTAGTCCACTCATccttatcgatcatcaagtg
Check.N.Rev.Prp8	GACGAACCACCTCTGTTCATATG
Prp4-N-TAP	
Oligo.N.For.Prp4	GAGCCTGAGGGAAATGACTAGTACTATTACCTTGTGAACGGAAAGaacaaaagctggagctcat
Oligo.N.Rev.Prp4	TTGCAAATCTACCGGAAGATTTTCAAGTGCAATATATTTACTCATccttatcgatcatcaagtg
Check.N.Rev.Prp4	TGGGAGATCTTGTGGGACATG
Universal N-TAP	
Check.For.TAP.U	ctttcggcgcctgagcatc

2.1.7 Bacterial and yeast strains

Name	Genotype	Description
HB101	<i>supE44, hsdS20 (rB- mB-)recA13, ara-14, proA2, lacY1, galK2, rpsL20, xyl-5, mtl-1, leuB6, thi-1</i>	a general host for plasmids that does not contain α -complementation
TR2a	<i>MATa; trp1-Δ1; his3-Δ; ura3-52; lys2-801; ade2-101</i>	haploid <i>MATa</i> , dissected from TR1 a/ α (Sikorski and Hieter, 1989)
YPH499	<i>MATa; trp1-Δ63; his3-Δ200; ura3-52; lys2-801; ade2-101; leu2-Δ1</i>	haploid <i>MATa</i> , (Sikorski und Hieter, 1989) (Sikorski and Hieter, 1989)
YCB3	<i>MATa; trp1-Δ1; his3-Δ; ura3-52; lys2-801; ade2-101; SNU114::TAP Tag-TRP1, C-terminus; PRP4::protein A C-terminus</i>	haploid yeast strain like TR2a, in which TAP tag was inserted at the C-terminus of <i>Snu114</i> using plasmid pBS1479, and protein A tag at the C-terminus of <i>PRP4</i> (Cornelia Bartels, Göttingen)
YEK2	<i>MATa; trp1-Δ1; his3-Δ; ura3-52; lys2-801; ade2-101; BRR2::TAP Tag-TRP1 C-terminus</i>	haploid yeast strain like TR2a, in which TAP tag was inserted at the C-terminus of <i>BRR2</i> using plasmid pBS1479 (Karagöz, 2006)
YEK3	<i>MATa; trp1-Δ1; his3-Δ; ura3-52; lys2-801; ade2-101; BRR2::TAP tag-TRP1 C-terminus; PRP4::tDimer2 tag-SpHIS5 C-terminus</i>	haploid yeast strain like YEK2, in which tDimer2 tag was inserted at the C-terminus of <i>PRP4</i> using plasmid pKT146 (Karagöz, 2006)
YEK5	<i>MATa; trp1-Δ1; his3-Δ; ura3-52; lys2-801; ade2-101; BRR2::TAP tag-TRP1 C-terminus; PRP6::tDimer2 tag-SpHIS5 C-terminus</i>	haploid yeast strain like YEK2, in which tDimer2 tag was inserted at the C-terminus of <i>PRP6</i> using plasmid pKT146 (Karagöz, 2006)

YEK6	<i>MATa; trp1-Δ1; his3-Δ; ura3-52; lys2-801; ade2-101; BRR2::TAP tag-TRP1 C-terminus; SNU114::tDimer2 tag-CaURA3 C-terminus</i>	haploid yeast strain like YEK2, in which tDimer2 tag was inserted at the C-terminus of <i>SNU114</i> using plasmid pKT176 (Karagöz, 2006)
YIH2	<i>MATa; trp1-Δ1; his3-Δ; ura3-52; lys2-801; ade2-101; BRR2::TAP tag-TRP1 C-terminus; DIB1::tDimer2 tag-SpHIS5 C-terminus</i>	haploid yeast strain like YEK2, in which tDimer2 tag was inserted at the C-terminus of <i>DIB1</i> using plasmid pKT146 (this study)
YIH3	<i>MATa; trp1-Δ1; his3-Δ; ura3-52; lys2-801; ade2-101; BRR2::TAP tag-TRP1 C-terminus; PRP3::tDimer2 tag-SpHIS5 C-terminus</i>	haploid yeast strain like YEK2, in which tDimer2 tag was inserted at the C-terminus of <i>PRP3</i> using plasmid pKT146 (this study)
YIH4	<i>MATa; trp1-Δ1; his3-Δ; ura3-52; lys2-801; ade2-101; BRR2::TAP tag-TRP1 C-terminus; PRP8::tDimer2 tag-SpHIS5 C-terminus</i>	haploid yeast strain like YEK2, in which tDimer2 tag was inserted at the C-terminus of <i>PRP8</i> using plasmid pKT146 (this study)
YIH8	<i>MATa; trp1-Δ1; his3-Δ; ura3-52; lys2-801; ade2-101; BRR2::TAP tag-TRP1 C-terminus; PRP31::tDimer2 tag-SpHIS5 C-terminus</i>	haploid yeast strain like YEK2, in which tDimer2 tag was inserted at the C-terminus of <i>PRP31</i> using plasmid pKT146 (this study)
YIH10	<i>MATa; trp1-Δ1; his3-Δ; ura3-52; lys2-801; ade2-101; SNU114::TAP tag-TRP1 C-terminus; BRR2::tDimer2 tag-SpHIS5 C-terminus</i>	haploid yeast strain like YRK1, in which tDimer2 tag was inserted at the C-terminus of <i>BRR2</i> using plasmid pKT146 (this study)
YIH15	<i>MATa; trp1-Δ1; his3-Δ; ura3-52; lys2-801; ade2-101; PRP3::TAP tag-TRP1 C-terminus</i>	haploid yeast strain like TR2a, in which TAP tag was inserted at the C-terminus of <i>PRP3</i> using plasmid pBS1479 (this study)
YIH16	<i>MATa; trp1-Δ1; his3-Δ; ura3-52; lys2-801; ade2-101; PRP6::TAP tag-TRP1 C-terminus</i>	haploid yeast strain like TR2a, in which TAP tag was inserted at the C-terminus of <i>PRP6</i> using plasmid pBS1479 (this study)
YIH17	<i>MATa; trp1-Δ1; his3-Δ; ura3-52; lys2-801; ade2-101; PRP31::TAP tag-TRP1 C-terminus</i>	haploid yeast strain like TR2a, in which TAP tag was inserted at the C-terminus of <i>PRP31</i> using plasmid pBS1479 (this study)
YIH18	<i>MATa; trp1-Δ63; his3-Δ200; ura3-52; lys2-801; ade2-101; leu2-Δ1; PRP8::TAP Tag N-terminus</i>	haploid yeast strain like YPH499, in which TAP tag was inserted at the N-terminus of <i>PRP8</i> using plasmid pBS1761 (this study)
YIH19	<i>MATa; trp1-Δ63; his3-Δ200; ura3-52; lys2-801; ade2-101; leu2-Δ1; BRR2::TAP Tag N-terminus</i>	haploid yeast strain like YPH499, in which TAP tag was inserted at the N-terminus of <i>BRR2</i> using plasmid pBS1761 (this study)
YIH20	<i>MATa; trp1-Δ63; his3-Δ200; ura3-52; lys2-801; ade2-101; leu2-Δ1; SNU114::TAP Tag N-terminus</i>	haploid yeast strain like YPH499, in which TAP tag was inserted at the N-terminus of <i>SNU114</i> using plasmid pBS1761 (this study)
YRK1	<i>MATa; trp1-Δ1; his3-Δ; ura3-52; lys2-801; ade2-101; SNU114::TAP Tag-TRP1, C-terminus</i>	haploid yeast strain like TR2a, in which TAP tag was inserted at the C-terminus of <i>SNU114</i> using plasmid pBS1479 (R. Karaduman, Göttingen)
YRK2	<i>MATa; trp1-Δ1; his3-Δ; ura3-52; lys2-801; ade2-101; PRP4::TAP Tag-TRP1, C-terminus</i>	haploid yeast strain like TR2a, in which TAP tag was inserted at the C-terminus of <i>PRP4</i> using plasmid pBS1479 (R. Karaduman, Göttingen)
YRK4	<i>MATa; trp1-Δ1; his3-Δ; ura3-52; lys2-801; ade2-101; SNU23::TAP Tag-TRP1, C-terminus</i>	haploid yeast strain like TR2a, in which TAP tag was inserted at the C-terminus of <i>SNU23</i> using plasmid pBS1479 (R. Karaduman, Göttingen)

YRK5	<i>MATa; trp1-Δ1; his3-Δ; ura3-52; lys2-801; ade2-101; PRP8::TAP Tag-TRP1, C-terminus</i>	haploid yeast strain like TR2a, in which TAP tag was inserted at the C-terminus of <i>PRP8</i> using plasmid pBS1479 (R. Karaduman, Göttingen)
------	---	--

2.1.8 Plasmids

Plasmid	Description
pBS1479	Shuttle vector containing C-TAP tag; ARS, CEN; Amp ^R , <i>K.lactis TRP1</i> (Puig et al., 2001)
pBS1761	Shuttle vector containing N-TAP tag; ARS, CEN; Amp ^R , <i>K.lactis TRP1</i> (Puig et al., 2001)
pRS313	Shuttle vector containing ARS, CEN; Amp ^R , <i>S.pombe HIS5</i> (Sikorski and Hieter, 1989)
pRS314	Shuttle vector containing ARS, CEN; Amp ^R , <i>K.lactis TRP1</i> (Sikorski and Hieter, 1989)
pRS316	Shuttle vector containing ARS, CEN; Amp ^R , <i>C.albicans URA3</i> (Sikorski and Hieter, 1989)
pKT239	Shuttle vector, pFA6a, containing yECitrine-3HA tag; ARS, CEN; Amp ^R , <i>S.pombe HIS5</i> (Sheff and Thorn, 2004)
pKT146	Shuttle vector, pFA6a, containing tDimer2 tag, ARS, CEN; Amp ^R , <i>S.pombe HIS5</i> (Sheff and Thorn, 2004)
pKT176	Shuttle vector, pFA6a, containing tDimer2 tag, ARS, CEN; Amp ^R , <i>C.albicans URA3</i> (Sheff and Thorn, 2004)
pSH62	Shuttle vector, containing Cre recombinase, ARS, CEN; Amp ^R , <i>S.pombe HIS5</i> (Güldener et al., 1996)

2.1.9 Cell culture

Yeast and bacterial media were prepared as described (Sambrook et al., 1989) using deionized water from a Millipore apparatus and were autoclaved at 121°C and 1 bar for 15 min. For preparation of plates the sugars contained in the yeast media were added before autoclaving, for preparation of liquid medium the sugars were prepared as sterile filtrated solutions and were added to the medium after autoclaving.

2.1.10 Common buffers

Commonly used media, buffers and solutions were essentially prepared as described (Sambrook, 1989; Sambrook et al., 1989). Deionized water was from a Millipore apparatus. Solutions were autoclaved if necessary (121°C, 20 min, 1 bar). Thermolabile components were filter-sterilized (0.22 μm). The pH was adjusted using HCl or NaOH if not stated otherwise.

1 M Na-PO₄

1 M Na₂HPO₄
1 M NaH₂PO₄
pH 6.5

1x Protein loading dye	75 mM Tris-HCl, pH 6.8 1.25 mM EDTA, pH 8.0 20% (v/v) glycerol 2.5% (w/v) SDS 0.125% (w/v) bromophenol blue 50 mM DTT
1x Running buffer SDS-PAGE	25 mM Tris-HCl, pH 6.8 192 mM glycine 1% (w/v) SDS
1x Western blotting buffer	1.5 L Slab4 Buffer 0.6 L methanol 0.9 L ddH ₂ O
4x Separating gel buffer	1.5 M Tris 0.4% (w/v) SDS adjust to pH 8.8
4x Stacking gel buffer	0.5 M Tris 0.4% (w/v) SDS adjust pH to 6.8
5x DNA loading dye	30% glycerol 5 mM EDTA, pH 8.0 0.25% (w/v) bromophenol blue 0.25% (w/v) xylene cyanol
10x PBS buffer	1.3 M NaCl 188 mM K ₂ HPO ₄ 12 mM KH ₂ PO ₄ pH 8.0
10x TBE	0.89 M Tris 0.89 M boric acid 25 mM EDTA pH 8.0
10x TBS	200 mM Tris 1.37 M NaCl adjust to pH 7.6
10x TE	100 mM Tris-HCl, pH 8.0 10 mM EDTA, pH 8.0
20x SSC	3M NaCl 0.3 M NaCitrate
RNA loading dye	80% formamide 1 mM EDTA pH 8.0 0.05% (w/v) bromophenol blue 0.05% (w/v) xylene cyanol

Slab 4 Buffer	50 mM Tris 105 mM glycine 0.1% (w/v) SDS
---------------	--

2.1.11 Commercial reaction sets (kits)

BCA protein assay kit	Thermo Fisher Scientific Inc., USA
ECL Western Blot Detection Kit	GE Healthcare, UK
ECL Western Blot Detection Kit	Thermo Fisher Scientific Inc., USA
Expand Long Template PCR Mix	Roche, Germany
Prime It II Random Primer Labeling Kit	Stratagene, USA
Brilliant Blue G-Colloidal Concentrate	Sigma, Germany

2.1.12 Machines

Autoclaves	H+P Labortechnik, Germany
Biofuge fresco	Kendro, USA
Biofuge pico	Kendro, USA
DNA Thermal Cycler	Hybaid Omni Gene, UK
Gel documentation unit	Bio-Rad, USA
Gelelectrophoresis apparatus	in-house
Geldryer Model 583	Bio-Rad, USA
Gradient Master	BioComp Instruments, Canada
'head-over-tail' Rotor	Cole-Parmer, USA
Heating blocks	Eppendorf, Germany
Hybridization oven	Hybaid Biometra, UK
Megafuge 1.0R	Kendro, USA
Milli-Q-water supply apparatus	Millipore, USA
Mortar Grinder RM100	Retsch, Germany
pH-Meter	Mettler Toledo, Switzerland
Phosphorimager Typhoon 8600	Amersham Pharmacia, Germany
Power supply EPS 2A 2000	Hoefler Pharmacia Biotech, USA
Power supply EPS 3501/XL	Amersham Pharmacia, Germany
Liquid Scintillation Analyzer Tri-Carb 2100 T	Packard, USA
Sorvall SLC-6000 rotor	Kendro, USA

Sorvall SS-34 Rotor	Kendro, USA
Sorvall TH660 Rotor	Kendro, USA
Sorvall T865 Rotor	Kendro, USA
Sorvall T647.5 Rotor	Kendro, USA
Speed Vac Concentrator 5301	Eppendorf, Germany
Spectrophotometer Ultrospec 3000 pro	Amersham Pharmacia, Germany
Tabletop centrifuges	Heraeus, Germany
Trans-Blot Cell	Bio-Rad, USA
Ultracentrifuge Evolution	Kendro, USA
Vortex	Janke & Kunkel, Germany
X-ray film developer X-Omat 2000	Kodak, USA
Liquid scintillation analyzer	Packard, USA

2.1.13 Working equipment

Cassettes for film exposure	Kodak, USA
Dialyses membranes MWCO 6000-8000 Da	SpektraPor, USA
Nylon membrane Hybond XL	Amersham Pharmacia, Germany
Parafilm	Roth, Germany
ProbeQuant™ G-50 micro columns	GE Healthcare, UK
Protran Nitrocellulose membrane	Schleicher & Schüll, Germany
Reacti-Bind secondary antibody coated plates (goat anti-rabbit, goat anti-mouse)	Thermo Fisher Scientific Inc., USA
Siliconized object slide	ICN Biomedicals, USA
Sterile filters 0.2 µm or 0.45 µm	Millipore, USA
Surgical blades	Martin, Germany
Whatman 3MM Paper	Whatman Paper, U.K.
X-ray films BioMax MR	Kodak, USA
0.8 x 4-cm Poly-Prep columns	Bio-Rad, USA

2.2 Methods

2.2.1 Protein-biochemistry standard methods

2.2.1.1 Protein quantification

To quantitatively determine the concentration of proteins, the BCA Protein Assay Kit from Pierce was used according to the manufacturer's instructions. This assay is a detergent-compatible formulation based on bicinchoninic acid (BCA) for the colorimetric detection and quantification of total protein. Cu^{2+} is reduced to Cu^{1+} by protein in an alkaline medium (Biuret Reaction). The BCA chelates Cu^{1+} ions forming purple-colored complexes with an absorption maximum at 562 nm (Smith et al., 1985).

2.2.1.2 Phenol-Chloroform-Isoamylalcohol extraction

The Phenol-Chloroform-Isoamylalcohol extraction (PCI-extraction) was used for separating proteins from nucleic acids. The solution was extracted with the same volume of PCI-solution and thoroughly mixed. To separate the aqueous and organic phases, the suspension was centrifuged for 5 min at room temperature and 13000 rpm. The nucleic acids in the upper aqueous phase were precipitated by addition of 1/10 vol. 3 M NaOAc pH 5.2 and 2.5 vol. 100% ethanol (p.a.). To improve precipitation of RNAs, 15-30 μg of glycoblue were added. The proteins in the lower organic phase were precipitated with 5 vol. of cold acetone (p.a.). Nucleic acids or proteins were precipitated overnight at -20°C or one hour at -80°C . Subsequently, they were pelleted for 20 min at 4°C and 13000 rpm. The pellet was washed with 70% (v/v) cold ethanol and pelleted again. The pellet was finally dried 2-3 min under vacuum and resuspended in an appropriate buffer.

2.2.1.3 Proteinase K digestion

To obtain protein-free RNA, proteinase K digestion of the proteins was performed. For co-immunoprecipitations (2.2.4.3) 2 μl of the stock solution (proteinase K mix) were added to the protein-A-Sepharose beads (typically 20-30 μl). The stock solution contained 1% (w/v) SDS, 7.5 mM EDTA, and 1 $\mu\text{g}/\mu\text{l}$ proteinase K. If proteinase K digestions were done in solution these concentrations were the final concentrations in the assay. All reactions were incubated for 30 min at 37°C . RNA was extracted by PCI-extraction and precipitated.

2.2.1.4 Denaturing polyacrylamide gel electrophoresis

Proteins were separated by denaturing polyacrylamide gel electrophoresis (SDS-PAGE) adapted from (Laemmli, 1970). Protein samples were dissolved in 1x SDS loading dye and proteins were denatured for 5 min at 95°C and loaded onto a high TEMED (0.33% (v/v)) polyacrylamide gel (PAA) (acrylamide (AA):bisacrylamide (BAA) = 37.5:1). 0.033% (w/v) APS was used for polymerization. The separating gel was a 12% or a 8% to 12% PAA step gel. The stacking gel was 5% PAA. Gels were run vertically in 1x SDS-PAGE running buffer until the bromophenol blue dye reached the bottom of the gel. The protein bands were visualized either by Coomassie or by silver staining.

2.2.1.5 Western blot analysis

After performing high-TEMED SDS-PAGE, proteins were transferred to a nitrocellulose membrane by wet-blotting adapted from Burnette et al. (Burnette, 1981). The transfer was carried out at least for 2 h at 70 V and 4°C in 1x western blotting buffer (2.1.10). For proteins bigger than 250 kDa, the time was prolonged up to 4 h or the gels were blotted overnight at 20 V. Membranes were washed shortly with ddH₂O, (stained with 'Ponceau S' if desired) and blocked for 2 hrs at room temperature (RT) or overnight at 4°C in 1x TBS, 0.1% (v/v) Tween-20, 5% (w/v) milk powder. Immunoblotting was performed 1-2 hr at RT or overnight at 4°C with antibodies specified in the figure legends according to standard protocols. Horseradish peroxidase (HRP)-conjugated anti-rabbit or anti-mouse antibodies were used as the secondary antibody (1 hr at RT, dilution 1:50000) and proteins were detected by enhanced chemiluminescence using an ECL kit according to the manufacturer's instructions. When the Peroxidase-antiperoxidase complex (PAP) was used to detect the Protein A of the TAP tag no secondary antibody was needed.

2.2.1.6 Silver staining of protein gels

Silver staining of protein gels was performed adapted from Blum et al. (Blum et al., 1987). During the procedure, all the solutions were 10 times the gel volume and all steps were performed on a shaker. The protein gel was first fixed in a solution of 40% methanol, 10% acetic acid at least for 30 min or overnight while gently shaking. After fixation, the gel was washed twice with 50% ethanol and once with 30% ethanol for 20 min each. The gel was then treated with 0.8 mM Na₂S₂O₃ for exactly 60 seconds, and washed three times shortly with ddH₂O to remove the thiosulfate from the surface. After that, the gel was incubated with 0.012 M AgNO₃, 0.026%

formaldehyde solution for 30-40 min. The stained gel was washed three times shortly with ddH₂O before applying the developing solution containing 0.56 M Na₂CO₃, 0.0185% formaldehyde, 16 μM Na₂S₂O₃. Developing was stopped with a solution of 40% methanol, 10% acetic acid. The gel was transferred to a Whatman paper and dried under vacuum at 80°C for 1 hr.

2.2.2 Molecular biology

2.2.2.1 Concentration determination of nucleic acids

To determine the concentration of nucleic acids, the extinction in an aqueous solution was measured at wavelengths 260 nm and 280 nm in comparison to the corresponding buffer without nucleic acids. The concentration was then calculated using pre-determined absorption values at 260 nm as described (Sambrook et al., 1989). The ratio of OD₂₆₀/OD₂₈₀ determined the purity of the nucleic acid solution, which was 2.0 for pure RNA or oligonucleotides, and 1.8 for pure DNA. Lower ratios show protein contamination, which has to be removed by PCI-extraction.

1 OD₂₆₀ = 50 μg/ml double-stranded DNA

1 OD₂₆₀ = 33 μg/ml single-stranded DNA

1 OD₂₆₀ = 40 μg/ml single-stranded RNA

2.2.2.2 Agarose gel electrophoresis of nucleic acids

To analyze polymerase chain reactions (PCR), agarose gel electrophoresis of nucleic acids was performed as described (Sambrook et al., 1989). Depending on the length of PCR products, gels contained 1 - 2% (w/v) agarose and 0.4 μg/ml ethidiumbromide in 1x TBE buffer. Samples were supplemented with DNA loading dye. The nucleic acids were separated horizontally at 100-120 V in 1x TBE buffer. The bands were visualized with UV-light at 254 nm.

Migration rates of the marker dyes through agarose gels		
% agarose (w/v)	xylene cyanol	bromophenol blue
0.7-1-7	4000 bp	300 bp
2.5-3.0	800 bp	100 bp

2.2.2.3 Denaturing polyacrylamide gel electrophoresis of RNA

To separate RNA fragments up to 2000 nts, denaturing polyacrylamide gel-electrophoreses was used. The gels contained 8 M urea, 0.5x TBE and, depending on the size of the RNA fragments, the concentration of polyacrylamide varied between 5% and 20% (Sambrook et al., 1989). The gels were polymerized with 50 μ l 10% (w/v) APS and 5 μ l TEMED per 10 ml gel solution. RNA samples were resuspended in 10 μ l of RNA loading buffer and denatured for 3 min at 95°C and immediately put on ice. The electrophoresis was performed in 0.5x TBE buffer until the xylene cyanol reached the bottom of the gel. The RNA fragments on the gel were visualized by silver staining. In the case of radioactively labeled samples, RNA molecules were detected by autoradiography.

Migration rates of marker dyes in denaturing polyacrylamide gels		
polyacrylamide (%)	xylene cyanol	bromophenol blue
5.0	130 bases	35 bases
6.0	106 bases	29 bases
8.0	76 bases	26 bases
10.0	55 bases	12 bases
20.0	28 bases	8 bases

2.2.2.4 Silver staining of RNA gels

Silver staining of RNA gels was performed adapted from Merril et al. (Merril et al., 1981). During the procedure, at least a 10-fold volume of the gel volume was required for all solutions and all steps were performed on a shaker. First, the gel was fixed in a solution of 40% methanol, 10% acetic acid for at least 30 min or overnight. After fixation, the gel was washed twice with a solution of 10% ethanol, 5% acetic acid for 15 min in order to dissolve and remove interfering substances. After that, the gel was washed shortly with ddH₂O and subsequently stained in 12 mM AgNO₃ solution for 30 min. The stained gel was washed twice shortly with ddH₂O. Then, it was treated shortly with the developing solution (0.28 M Na₂CO₃, 0.0185% formaldehyde) to remove excess silver from the surface of the gel. The solution was discarded and the gel was developed in new developing solution. Developing was stopped by adding 5% acetic acid solution. The gel was transferred to a Whatman paper and dried under vacuum at 80°C for 1 hr.

2.2.2.5 Synthesis of radioactively labeled DNA-probes for Northern analysis

To detect spliceosomal RNAs in a Northern blot analysis, radioactively labeled DNA probes were synthesized from their corresponding DNA templates using the 'Prime It II Random Primer Labeling Kit' (Stratagene). Plasmids containing the DNA templates were digested with restriction enzymes and were purified from an agarose gel using 'QIAquick Gel Extraction Kit' (Qiagen). For synthesis of the DNA probes, 25 - 50 ng of DNA template, 23 μ l ddH₂O and 10 μ l of random ninemer primers were denatured at 95°C for 5 min and subsequently cooled down at room temperature by short centrifugation in order to allow hybridization. In the following, 10 μ l of dATP primer buffer, 5 μ l of [α -³²P] dATP (3000 Ci/mmol) and five units of Klenow enzyme were added to the reaction and incubated for 10 min at 40°C. The reaction was stopped by adding 2 μ l of 0.5 mM EDTA solution. The DNA-probes were purified from free radioactive dATP by 'ProbeQuant™ G-50' columns. For Northern blot analysis, 10-20x 10⁶ cpm of the labeled DNA-probes were used.

2.2.2.6 Northern blot analysis

To detect a specific RNA in a sample, northern blot analysis was performed. For this, the RNAs were separated on a denaturing polyacrylamide gel (2.2.2.3) and transferred to a nylon membrane by wet-blotting overnight in 25 mM NaPO₄ at 16 - 18V and 4°C. The nylon membrane was blocked with pre-hybridization buffer (25 mM NaPO₄ pH 6.5; 6x SSC; 5x Deinhardt's solution [0.1% (w/v) polyvinylpyrrolidone, 0.1% (w/v) BSA, 0.1% (w/v) Ficoll 400]; 0.5% (w/v) SDS; 50% (v/v) deionized formamide; 0.1 mg/ml denatured salmon sperm DNA) for 1-2 h at 42°C to prevent unspecific binding. Subsequently, the radioactively labeled DNA-probes (2.2.2.5) were added (10-20 x 10⁶ cpm/probe) to the pre-hybridization buffer and the nylon membrane was hybridized for 24-48 h. After hybridization, the nylon membrane was washed twice 1 min with wash buffer 1 (2x SSC, 0.5% (w/v) SDS) at room temperature, twice 1 min with wash buffer 2 (2x SSC, 0.1% (w/v) SDS) at room temperature, and once 30 min with wash buffer 2 at 50°C. After washing, the hybridized probes were visualized by autoradiography.

2.2.2.7 Polymerase chain reaction

In polymerase chain reactions (PCR), either plasmid DNA or yeast chromosomal DNA was used as templates. The reactions were performed in a DNA thermocycler using Taq-polymerase or the 'Expand long template PCR mix'-kit (Roche). PCR conditions were different depending on

template and kind of DNA-polymerase. The PCR products were purified from the reaction by PCI-extraction and precipitation of the DNA.

PCR for the amplification of TAP marker cassette

To TAP-tag the C-terminus or N-terminus of selected tri-snRNP proteins, the TAP-marker cassette was amplified from the plasmids pBS1479 (*Kluveromyces lactis* (*K. lactis*) TRP1) and pBS1761 (*K. lactis* TRP1), respectively. A typical PCR reaction contained:

Plasmid DNA (pBS1479)	0.05-0.1 µg
10x Taq buffer	10 µl
dNTP mix (2.5 mM dATP, dGTP, dCTP, and dTTP)	150 µM
Primer forward (20 µM)	200 nM
Primer reverse (20 µM)	200 nM
Go-Taq-polymerase (5 U/µl)	1 µl
with ddH ₂ O up to 100 µl	

<u>PCR program</u>		<u>Cycle</u>
5 min	94°C	1 x
30 s	94°C	
30 s	50-55°C	30 x
1 min/kb	72°C	
5 min	72°C	1 x

PCR for the amplification of the fluorescent protein marker cassette

To introduce fluorescent protein tags at the C-terminus of selected tri-snRNP proteins, tDimer2 and yECitrine-3HA tag sequences were amplified by PCR from the plasmids pKT146 (*Schizosaccharomyces pombe* (*S. pombe*) HIS5) or pKT176 (*Candida albicans* (*C. albicans*) URA3) and pKT239 (*S. pombe* HIS5), respectively. A typical PCR reaction contained:

Plasmid DNA (pKT146, pKT176 or pKT239)	0.05 µg
10x Buffer 1(kit)	10 µl
Primer forward (20 µM)	300 nM

Primer reverse (20 μ M)	300 nM
dNTP mix (2.5 mM dATP, dGTP, dCTP, and dTTP)	350 μ M
Expand long template PCR mix (5 U/ μ l) with ddH ₂ O up to 100 μ l	1.5 μ l

<u>PCR program</u>		<u>Cycle</u>
2 min	94°C	1 x
30 s	94°C	
30 s	50°C	30 x
1 min/kb	68°C	
7 min	68°C	1 x

PCR for characterization of transformants

To analyze whether a tag was correctly integrated into the genome, chromosomal DNA was isolated from transformant yeast cells and PCR analysis was performed using check oligonucleotide primers. A typical PCR reaction contained:

Chromosomal yeast DNA	0.5 μ l
10x Taq buffer	2 μ l
dNTP mix (2.5 mM dATP, dGTP, dCTP, and dTTP)	1.2 μ l
Primer forward (20 μ M)	200 nM
Primer reverse (20 μ M)	200 nM
Go-Taq DNA polymerase (5u / μ l) with ddH ₂ O up to 20 μ l	0.1 μ l

<u>PCR program</u>		<u>Cycle</u>
1 min	94°C	1 x
30 s	94°C	
30 s	55°C	30 x
1 min/kb	72°C	
5 min	72°C	1 x

2.2.2.8 Transformation of haploid yeast cells

To construct yeast strains expressing the TAP-tag or a fluorescent protein tag at the C-terminus of selected proteins, 10 to 30 µg of the PCR-amplified tag-sequences (2.2.2.7) were transformed into the haploid yeast strain TR2a using the lithium acetate method. 50 ml of yeast culture were grown overnight to 1 OD₆₀₀/ml. The cells were washed with 25 ml of 10 mM Tris/HCl pH 7.5. Subsequently, yeast cells were resuspended in 25 ml of LiT solution (10 mM Tris/HCl pH 7.5, 100 mM LiOAc, sterile filtered) with 10 mM DTT and incubated for 40 min at room temperature with very gentle shaking. After centrifugation, the cells were resuspended in 750 µl of LiT solution (with 10 mM DTT). For the following transformation reactions, 100 µl of the yeast cells were mixed with 50 µl of LiT, 5 µl of denatured Salmon sperm DNA (10 µg/µl), and different amounts of PCR product (10 µg - 30 µg). A positive control with 200 ng of the plasmids pRS313 (*S. pombe HIS5*), pRS314 (*K. lactis TRP1*) or pRS316 (*C. albicans URA3*), respectively and a negative control without DNA were included. After incubation of the mixtures for 10 min at room temperature, 300 µl of PEG solution (2 g PEG 3350, 2 ml LiT solution, dissolved at 50°C, sterile filtered) were added and incubated further for 10 min at RT. Heat-shock was performed for 15 min at 42°C. After the heat-shock, the cells were centrifuged briefly. The cell pellet was resuspended carefully in 1 ml of YPD-medium and incubated for 1 h at 30°C for recovery of the cells. After recovery, the cells were pelleted again and resuspended carefully in 100 µl of 10 mM Tris/HCl pH 7.5. 50 - 100 µl of the cell suspension were plated on a glucose containing selection medium (2.2.3.2) (SC-TRP, SC-HIS, SC-URA) and incubated for 2-4 days at 30°C. To confirm the ability to grow on selection medium, transformant colonies were streaked out on fresh selection medium and incubated again for 2-3 days at 30°C.

2.2.2.9 Transformant characterization by PCR analysis

The correct integration of either the TAP cassette or the fluorescent protein cassette into yeast genomic DNA was verified by PCR analysis. Single transformant colonies were picked from the selection medium and cultured in 1 ml YPD-medium for 17-18 h at 30°C. Cells were centrifuged briefly, resuspended in 100 µl TE/SDS (10 mM Tris/HCl pH 7.5, 1 mM EDTA, 3% (w/v) SDS), and vortexed for 15 min at room temperature. Subsequently, 500 µl of 1x TE (10 mM Tris/HCl pH 7.5, 1 mM EDTA) buffer were added and nucleic acids were extracted with 600 µl PCI. The upper phase containing chromosomal DNA was precipitated with 0.7 vol. of isopropanol by centrifugation for 30 min at 4°C and 13000 rpm. The DNA pellet was dried under vacuum for 2-3 min, resuspended in 20 µl of ddH₂O and the integration was checked by PCR analysis (2.2.2.7).

2.2.2.10 Transformant characterization by western blot analysis

Western blot analysis was used to check whether the integrated TAP cassette or fluorescent protein cassette was expressed correctly in the yeast cells. Single colonies were picked and inoculated in 1.5 ml of YPD-medium for 17-18 hrs. The cells were centrifuged briefly and washed with 1 ml cold water. Cells were then resuspended in 100 μ l AGK buffer (2.2.3.3) containing 4 μ l of complete protease inhibitor mix (Roche, prepared according to manufacturer's instructions), 0.5 mM PMSF, and 0.5 mM DTT. Cells were disrupted with acid washed glass beads (about 30 μ l of beads were used) by vortexing 5 times for 30 seconds. Cells were kept on ice between the vortexing steps. After disruption, 100 μ l protein loading dye were added and the cells were boiled for 5 min at 95°C, followed by centrifugation for 2 min at RT. 30 - 50 μ l of the supernatant were loaded on a 12% high-TEMED SDS-polyacrylamide gel. Subsequently, the proteins were blotted on a nitrocellulose membrane and incubated with primary antibody (2.2.1.5). For the TAP-tag, the membrane was incubated with PAP antibody in 1:2000-dilution. For the yECitrine-3HA-tag, anti-YFP antibody (1:2000 dilution) or anti-HA antibody (2.1.3) (1:1000 dilution) was used as primary antibody and anti-rabbit or anti-mouse-coupled peroxidase (2.1.3) (1:50000) as secondary antibody. For the tDimer2-tag no antibody was available. Correct expression was therefore checked by the shift of molecular weight of the tagged proteins in SDS-PAGE gels followed by silver staining.

2.2.2.11 N-terminal TAP tagging of yeast strains

For N-terminal TAP-tagging 10 and 13 μ g of the PCR-amplified tagging cassette from plasmid pBS1761 (2.2.2.7) (Puig et al., 2001) was transformed into the strain YPH499 (Sikorski and Hieter, 1989) as described (2.2.2.8). The transformed cells were streaked out on selection medium, SC-TRP, containing 2% (w/v) galactose, 2% (w/v) sucrose, 2% (w/v) raffinose and 0.05% (w/v) glucose and incubated at 30°C for 3-5 days. Transformant colonies were streaked out on fresh selection medium and grown again for 2-3 days at 30°C. The correct integration and expression of the tag was tested by PCR analysis (2.2.2.9) and Western blot analysis (2.2.2.10). The transformants now contain an N-terminally TAP-tagged gene under the control of a *GAL1* promoter (Puig, 2001). To remove the *GAL1* promoter, the positively tested transformants were transformed with the plasmid pHS62 (Hegemann, 1996) containing a Cre recombinase and streaked out on selection medium (2.2.3.2), SC-HIS, containing 2% (w/v) galactose, 2% (w/v) sucrose, 2% (w/v) raffinose, and 0.05% (w/v) glucose. To test for the loss of the marker associated with the *GAL1* promoter and for the loss of Cre-expressing plasmid, the transformant

colonies were then grown on YPD medium. The resulting strains were kept as glycerol stocks (2.2.3.2).

2.2.2.12 Transformation of HB101 cells

For preparation of competent cells according to the CaCl_2 method a pre-culture of HB101 was inoculated in 5 ml Luria Bertani (LB)-medium and incubated at 37°C overnight. The pre-culture was used to inoculate a 50 ml LB culture. The culture was incubated at 37°C until it reached 0.3 to 0.5 OD/ml, transferred into a 50 ml Falcon tube, and centrifuged for 10 min at 2000 rpm. Cells were resuspended in 25 ml cold 50 mM CaCl_2 and centrifuged again. After resuspension in 3 ml of cold 50 mM CaCl_2 , sterile glycerol was added to 10%, and the cells were kept at -80°C in 300 µl aliquots. Transformation was performed as described (Sambrook et al., 1989). 10-50 ng of the plasmid DNA were mixed with 50 µl of competent cells and incubated on ice for 30 min. Heat-shock was performed for 1 min at 42°C and cells were immediately chilled on ice for 1 min. Subsequently, 800 µl of LB-medium were added and incubated for 1 hr at 37°C. Cells were centrifuged briefly and the cell pellet was resuspended in 50 µl of 10 mM Tris/HCl pH 7.5. Cells were plated on the selection media (LB-Kan^R or LB-Amp^R) and incubated overnight at 37°C. The isolation of the plasmid DNA from the transformed strain was carried out using QIAfilter mini- and maxi-prep kits according to manufacturer's instruction.

2.2.3 Cell culture methods

2.2.3.1 Growth and culture of bacteria

E. coli cells were grown in LB-medium or on LB-plates (Sambrook et al., 1989). Depending on the transformed plasmid, which contains genes for antibiotic resistance, LB medium contained 100 µg/ml Ampicillin, 30 µg/µl Kanamycin, or 30 µg/µl Chloramphenicol, respectively. For longer storage, 500 µl of bacteria cell suspension was mixed with 250 µl of 50 % sterile glycerol and kept at -80 °C.

2.2.3.2 Yeast cell culture

S. cerevisiae cells were cultivated according to standard methods (Sambrook et al., 1989). To select transformants after transformation of a plasmid or a piece of DNA, synthetic defined (SD)-medium was used. This mixture contained all the essential amino acids except for the amino acid used for selection.

Cell culture on plates: To prepare plates, the medium (YPD, YPG or SC) was autoclaved for 15 min at 121°C and cooled down to 50°C. Subsequently, sterile 50% D(+)-glucose or 25% D(+)-galactose was added to the YP medium to a final concentration of 2%. The medium was poured into Petri dishes and cooled down at RT until the agar polymerized. The plates were stored at room temperature. Yeast cells from a glycerol stock (see below) or after transformation were streaked on the plates and incubated 2-4 days at 23°C, 25°C or 30°C, depending on the phenotype of the cells. For a long time storage of the cells, the plates were sealed with a parafilm and kept at 4°C up to 3 months.

Cell culture in liquid medium: For the liquid cultures of yeast cells, usually 5-20 ml of pre-culture in YPD medium were prepared and incubated overnight at the optimal temperature. The OD₆₀₀ of the cells in pre-culture was measured and usually 15 OD of cells were inoculated into 2 liters of YPD or YPG culture in a 5 L Erlenmeyer flask. After 16-17 hr the cells reached OD₆₀₀ of 3-5/ml.

Glycerol stocks: For long time storage, 800 µl of a fresh yeast pre-culture in YPD or YPG medium were mixed with 400 µl of sterile 50% glycerol and kept at -80°C.

2.2.3.3 Extract preparation from yeast cells for snRNP purification using a mortar grinder

Total extract preparation from yeast cells for U5 snRNP and U4/U6.U5 tri-snRNP purification was performed as described (Gottschalk, 1999). Yeast cells from corresponding yeast strains were grown overnight at 30°C up to OD₆₀₀ of 3.5-4.5/ml. Cells were pelleted for 10 min at 5000 rpm using an SLC-6000 rotor. The cell pellet from 2 L yeast culture was washed with 200 ml of cold ddH₂O and with 50 ml AGK buffer (20 mM Hepes/KOH pH 7.9, 200 mM KCl, 1.5 mM MgCl₂, 8% (v/v) glycerol). The cells were resuspended in 10 ml of AGK buffer (additionally containing 0.5 mM DTT, 0.5 mM PMSF, 2 mM benzamidine, 1 µM leupeptin, 2 µM pepstatin A, 4 µM chymostatin, 2.6 µM aprotinin) per 2 L culture and transferred into a 50 ml Falcon tube. KCl was adjusted to 200 mM and the cell suspension was dropped into liquid nitrogen, using either a glass pipette or a dropping funnel. The cell beads were stored at -80°C or broken using a mortar grinder (Retsch). In one round of grinding, beads from 8 L culture were ground for 15 min at the highest pressure. The resulting cell powder was either stored at -80°C or thawed slowly at 28°C. The cell lysate was centrifuged for 30 min at 17000 rpm (25000 g) using a SS-34 rotor to remove cell debris. The supernatant was transferred into a new tube and further centrifuged for 1 h at 37000 rpm (100000 g) using a T-865 rotor. Alternatively, for large amounts of cells a T647.5 rotor was used for 50 min at 42000 rpm (100000 g). After this centrifugation step, the cell lysate

separates into three different phases: the uppermost white layer included lipids and liposomes; the middle yellow phase contained total cell extract and the pellet comprises ribosomes, fine cell debris, and genomic DNA. The middle phase was recovered with a pipette and dialyzed twice for 1.5 h against Buffer D (20 mM Hepes/KOH pH 7.9, 50 mM KCl, 0.2 mM EDTA, 0.4 mM MgCl₂, 20% (v/v) glycerol, 0.5 mM DTT, 0.5 mM PMSF, 2 mM benzamidine). The dialyzed extract was shock-frozen in liquid nitrogen and stored at -80°C.

2.2.4 Special methods

2.2.4.1 Tandem affinity purification of yeast snRNPs

The tandem affinity purification (TAP) is a two-step affinity purification employing first an IgG matrix and then a calmodulin affinity resin (Puig et al., 2001). Yeast strains expressing TAP-tagged snRNP proteins were constructed as described (2.2.2.8). Frozen yeast extract from these strains was thawed in a 28°C water bath. Subsequently, the buffer composition of the extract was adjusted to 10 mM Tris/HCl pH 8.0, 100 mM NaCl (in addition to the 50 mM KCl resulting from dialysis), and 0.1% NP-40. IgG-sepharose beads (100 µl beads for extract from 4 L of yeast culture) were washed with 10 ml of IPP 150 buffer (10 mM Tris/HCl pH 8.0, 150 mM NaCl, 0.1% NP-40) and incubated with yeast extract in a 50 ml Falcon tube for 2 h at 4°C by using a head-over-tail rotor. After binding to the IgG-sepharose beads, the extract was transferred into 10 ml (0.8 x 4 cm) BioRad Poly-Prep columns such that each column contained 100 µl of IgG beads. The columns were drained by gravity flow. The beads were washed three times with 10 ml of IPP 150 buffer followed by washing once with 10 ml TEV cleavage buffer (10 mM Tris/HCl pH 8.0, 150 mM NaCl, 0.1% NP-40, 0.5 mM EDTA, 1 mM DTT). Then the TAP tag was cleaved with 100 units TEV protease per 4 L culture in 1 ml of TEV cleavage buffer for 2 h at 16°C, rotating head-over-tail. The TEV cleavage eluate of two IgG-sepharose columns was combined and transferred into a new Biorad Poly-Prep column containing 100 µl of the calmodulin affinity resin, which had been washed with 10 ml of calmodulin binding buffer (10 mM Tris/HCl pH 8.0, 150 mM NaCl, 0.1% mM NP-40, 1 mM Mg(OAc)₂, 1 mM imidazole, 2 mM CaCl₂, 10 mM β-mercaptoethanol). The IgG-sepharose beads were eluted by washing with 3.5 ml of calmodulin binding buffer. Then, the CaCl₂ concentration was adjusted to 2 mM and the calmodulin affinity beads were incubated rotating head-over-tail for 1-2 h at 4°C. After incubation the column was drained by gravity flow and washed three times with 10 ml of calmodulin binding buffer. To elute the particles, the calmodulin resin was incubated twice with 300 µl elution buffer (= calmodulin binding buffer with the exchange of 0.1% NP-40 for 0.02%

NP-40 and 2 mM CaCl₂ for 2 mM EGTA) for 20 min. The beads were resuspended every 5 min. Finally, the eluate was collected by gravity flow.

2.2.4.2 Glycerol gradient sedimentation of purified snRNP particles

After TAP-purification yeast snRNP particles were further purified for electron microscopy analysis and mass spectrometry by glycerol gradient centrifugation. The particles were layered on a linear 10-30% glycerol gradient. 100 ml of the gradient solutions contained 10 or 30% (v/v) glycerol, 20 mM Hepes/KOH pH 7.9, 200 mM KCl 1.5 mM MgCl₂, 0.2 mM EDTA, 0.5 mM PMSF, 0.5 mM DTT. The gradient solutions were filtered before use. When particles were fixed during the gradient centrifugation for EM, glutaraldehyde was added to a final concentration of 0.04 or 0.1% (w/v) to the 30% glycerol gradient solution. Gradients (TH660) were mixed for 75 s at a speed of 20 rpm and an angle of 83° using a gradient master. U5 snRNP particles were sedimented for 15 h at 23700 rpm and tri-snRNP particles for 12 h at 33000 rpm at 4°C using a Sorvall TH660 rotor. Centrifugation time for particles of different size was adapted accordingly. After centrifugation, 24 fractions of 175 µl were collected. Collection was done from the bottom of the gradient tube by using a bottom-fraction-collector (in case of EM analysis) or from the top using a pipette.

2.2.4.3 Co-immunoprecipitation of tri-snRNP snRNAs

To test the binding efficiency of antibodies directed against snRNP specific proteins, the snRNA-cap or tags (TAP-tag, yECitrine-tag, tDimer2-tag, 3HA-tag), co-immunoprecipitations were performed. Reactions were performed in Eppendorf tubes. 20-30 µl of protein A-sepharose beads were equilibrated by washing three times with 500 µl NET-2 150 buffer (40 mM Tris/HCl, pH 7.4, 150 mM NaCl, 0.04% NP-40). The antibody was coupled to the beads in 500 µl NET-2 150 buffer for 1-2 h at 4°C using a head-over-tail rotor. The amount of antibody used per assay varied between 2 µl and 10 µl, depending on the quality and/or concentration of the antibody. After coupling, the beads were washed three times with 500 µl of NET-2 150 buffer. Subsequently, 15-30 µl yeast total cell extract in 500 µl NET-2 150 buffer were added and incubated 2 h at 4°C by head-over-tail rotation. After binding, beads were washed four times with NET-2 150 buffer. Then, the samples were digested with 2 µl proteinase K mix (2.2.1.3) in the residual 20-30 µl NET-2 150 buffer, which remain after removing the supernatant of the last wash. The reaction was incubated for 30 min at 37°C. 200 µl of stop splicing buffer (for 20 ml: 50 mM NaOAc, pH 5.2, 0.3 mM EDTA, 0.1% SDS, 300 µg *E.coli* tRNA), 200 µl of ddH₂O, and

200 μ l of PCI were added and the RNA was extracted, precipitated with ethanol, and resuspended in RNA loading buffer.

2.2.4.4 Immunolabeling of TAP-purified yeast tri-snRNPs

To localize the position of tri-snRNP proteins by EM, different antibodies were tested in immunolabeling reactions. For this, the tri-snRNPs were purified using the TAP method (2.2.4.1). The eluate of the calmodulin column was incubated with the antibody for 90 min at 4°C, rotating slowly end over end. The reaction was loaded on a 10-30% linear glycerol gradient (2.2.4.2) and sedimented for 15 hr at 29000 rpm and 4°C using a TH660 rotor (Sorvall). If required, 0.04-0.1% glutaraldehyde was added to the 30% gradient solution. Gradients were fractionated from the bottom in case of EM analysis (2.2.4.6); otherwise fractionation was performed from the top. An aliquot of each fraction was analyzed by ELISA (2.2.4.5) to detect the antibody in the gradient fractions. If the gradient fractions contained glutaraldehyde, the excess of glutaraldehyde was removed immediately after gradient fractionation by adding 1 M glycine, pH 7.0 (10 μ l/120 μ l gradient solution) and incubation for 30 min at 4°C.

2.2.4.5 Enzyme-linked immunosorbent assay

To detect the antibody in gradient fractions, an enzyme-linked immunosorbent assay (ELISA) was performed using secondary antibody (goat anti-rabbit; goat anti-mouse) coated 96-well plates (Thermo Fisher Scientific Inc., USA) according to the manufacturer's instructions. If the gradient fractions contained glutaraldehyde, the excess of glutaraldehyde was removed immediately after gradient fractionation by adding 1 M glycine, pH 7.0 (10 μ l/120 μ l gradient solution) and incubation for 30 min at 4°C. Initially, the wells were washed three times with 200 μ l 1x wash buffer (20 mM PBS pH 8.0, 0.5% (w/v) Tween-20). Then, depending on the amount of TAP-purified tri-snRNPs and antibody used for the immunolabeling reaction, 90-98 μ l of 1x blocking buffer (1x wash buffer, 3% (w/v) BSA) was added into the wells and filled up to 100 μ l by adding 2 to 10 μ l of the gradient fractions. The reaction was incubated for 2 hr at RT or overnight at 4°C. The wells were again washed three times with 200 μ l 1x wash buffer. Then, the secondary antibody, HRP-conjugated anti-rabbit or anti-mouse antibody (dilution 1:50000 – 1:75000) was added in 100 μ l 1x blocking buffer and incubated at 37°C for 1 hr or overnight at 4°C. After washing three times with 200 μ l 1x wash buffer, the assay was developed by incubation with 50-100 μ l 1-step TMB (3,3',5,5'-tetramethylbenzidine) solution (Thermo Fisher Scientific Inc., USA), which develops a blue color upon oxidization catalyzed by HRP. The development was

stopped by adding 50-100 μ l 2 M sulfuric acid, changing the color from blue to yellow, with a maximum absorbance at 450 nm. The absorbance in the wells was then measured at 450 nm.

2.2.4.6 Electron microscopy analysis of TAP purified snRNPs

Image acquisition was performed in a transmission electron microscope operated at 160 kV and equipped with a field emission gun (CM200 FEG, FEI, Eindhoven, The Netherlands). A 4kx4k CCD camera (TemCam-F415, TVIPS, Gauting, Germany) was used with 2-fold binning of the pixels and a magnification of 122000. The specimens were prepared as described (Golas et al., 2003) and imaged at room temperature. Briefly, a carbon film was floated on the surface of the particle solution allowing adsorption over 15 min. The carbon film was then transferred to a second well filled with 2% uranyl formate solution and incubated for 2 min. Subsequently, the carbon film with adsorbed particles was attached to a 200 mesh copper grid on which a carbon film containing holes of \sim 1–2 μ m diameter had previously been mounted. Finally, another carbon film floated onto a second solution of uranyl formate was used to form a sandwich. The grids were stored under dry conditions until image acquisition. Of each sample, a few hundred up to a few thousand particle images were manually selected. Class averages were computed by three to five rounds of reference-free alignment (Dube et al., 1993) using exhaustive alignment via polar coordinates (Sander et al., 2003) and multivariate statistical analysis followed by hierarchical ascendant classification with moving elements refinement as implemented in the IMAGIC-5 software (van Heel et al., 1996).

2.2.4.7 Labeling of immunocomplexes with colloidal gold and preparation of EM specimens

Fractions of the gradient containing antibody-labeled tri-snRNPs (or unlabeled complexes as control) were pooled and incubated with Protein A coated colloidal gold (G. Posthuma, Cell Microscopy Center, University Medical Center Utrecht). In each experiment the amount of colloidal gold was optimized by visual inspection, depending on the particle concentration in the sample and the colloid concentration in the colloidal gold-solution. Approximately 0.1 μ l of colloidal gold solution was mixed with 100 μ l of the sample containing the immunocomplexes. This mixture was incubated at 4°C for 90 min and then used directly for EM-grid preparation, which was performed as described previously (Golas et al., 2003), but with a prolonged particle-adsorption period of 2 hours. Images were obtained at room temperature at a magnification of 55000 on a calibrated CM120 electron microscope (FEI, Eindhoven, The Netherlands) in eucentric height at a defocus of approximately 2 μ m. The microscope was equipped with a

TemCam F224A digital camera (TVIPS, Gauting, Germany). Particles were analyzed and grouped into similarity classes by visual inspection, and the position of the gold label was verified with respect to the particle's orientation.

2.2.4.8 Mass spectrometry

For analysis of tri-snRNP proteins by mass spectrometry (MS), putative gradient fractions containing tri-snRNPs were pooled and concentrated in a vacuum concentrator. The proteins were then directly separated with the NuPAGE® Novex® gel system from Invitrogen (1 mm, 4-12% Bis-Tris gel) according to the manufacturer's instructions. Coomassie staining of proteins was performed with Brilliant Blue G-Colloidal concentrate (Sigma), following the manufacturer's instructions except for the incubation with the staining suspension, which was done overnight. The gel was scanned and analyzed by MS in collaboration with Dr. H. Urlaub, Bioanalytical Mass Spectrometry, Göttingen. An entire lane of the Coomassie blue-stained gel was cut into 40-50 slices, and proteins were digested in gel with trypsin and extracted as described (Shevchenko et al., 1996). The extracted peptides were analyzed in a liquid chromatography-coupled electrospray ionization quadrupole time of flight (Q-ToF Ultima; Waters) mass spectrometer under standard conditions. Proteins were identified by searching fragment spectra of sequenced peptides against the NCBI non-redundant database (nr) using Mascot as search engine.

3 Results

3.1.1.1 Structural characterization of the *Saccharomyces cerevisiae* U4/U6.U5 tri-snRNP

3.1.2 Isolation of tri-snRNPs using the tandem affinity purification method

To purify tri-snRNPs from *S. cerevisiae* whole cell extract we used the well-established tandem affinity purification (TAP) method (Puig et al., 2001) (Figure 3.1), which employs genetically tagged fusion proteins. The TAP tag consists of two IgG binding domains originating from the *Staphylococcus aureus* protein A (ProtA) and a calmodulin-binding peptide (CBP) separated by a

tobacco etch virus (TEV) protease cleavage site.

This TAP tag was genetically fused to the C-terminus of the *S. cerevisiae* tri-snRNP proteins and thereby allowed for the purification of the particles at their low natural expression levels without the need for overexpression of the tagged protein that might lead to the formation of artificial protein complexes. In the following, the term ‘yeast’ will refer to *S. cerevisiae*.

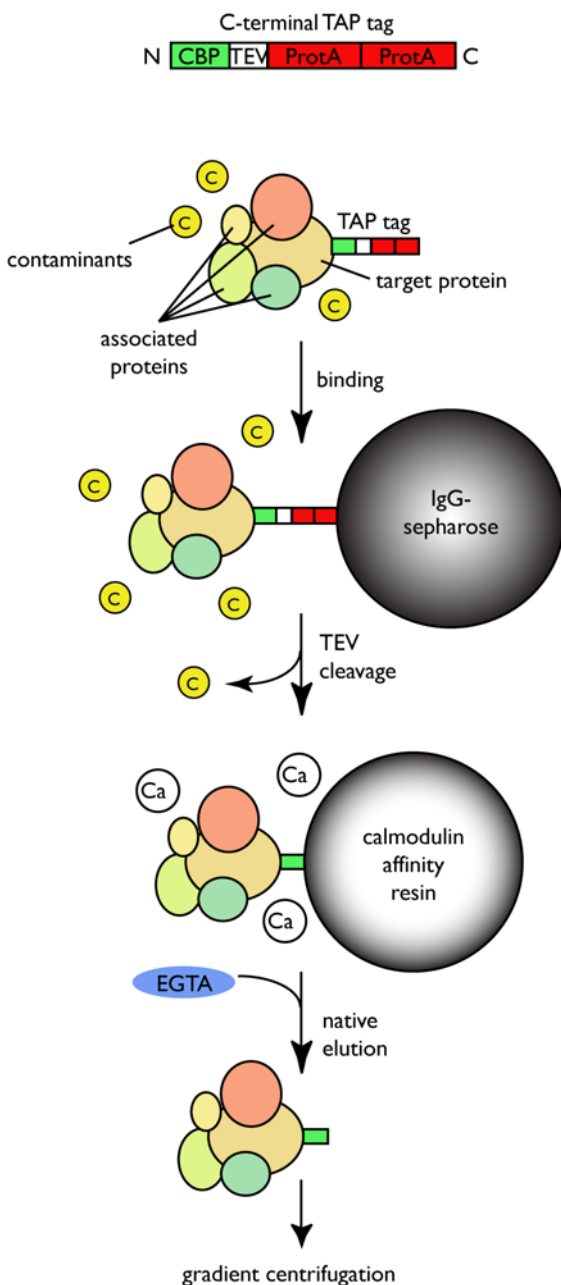


Figure 3.1 Overview of the TAP purification strategy. In the first affinity purification step, complexes containing the TAP-tagged proteins are tightly bound to IgG-sepharose. Washing removes contaminating proteins, subsequent elution under native conditions requires the cleavage of the TAP tag by the TEV protease at the cleavage site located between the CBP and ProtA. In the second purification step the TEV eluate is incubated with calmodulin coated beads in the presence of calcium ions (Ca²⁺). Washing removes the TEV protease and remaining contaminants prior to elution of the bound complexes under gentle conditions with EGTA, which chelates the Ca²⁺. Subsequent gradient ultracentrifugation separates the target complex from other possibly co-purified complexes containing the same TAP-tagged protein. C = contaminants, Ca = Ca²⁺

3.1.2.1 C-terminal TAP tagging of tri-snRNP proteins

The C-terminal TAP tagging was performed with four different tri-snRNP proteins (Brp2p, Prp6p, Prp31p, and Prp3p) according to standard protocols (Puig et al., 2001). The sequence of the TAP tag was encoded on plasmid pBS1479 (Figure 3.2 A1) which additionally contained the auxotrophic *TRP1* gene from *K. lactis* as selection marker (Puig et al., 2001). Typically, the auxotrophic genes used as selection markers originate from other yeast species or genera and share little or no sequence homology to the *S. cerevisiae* auxotrophic genes to prevent homologous recombination of the selection markers at endogenous genomic sites in the yeast genome.

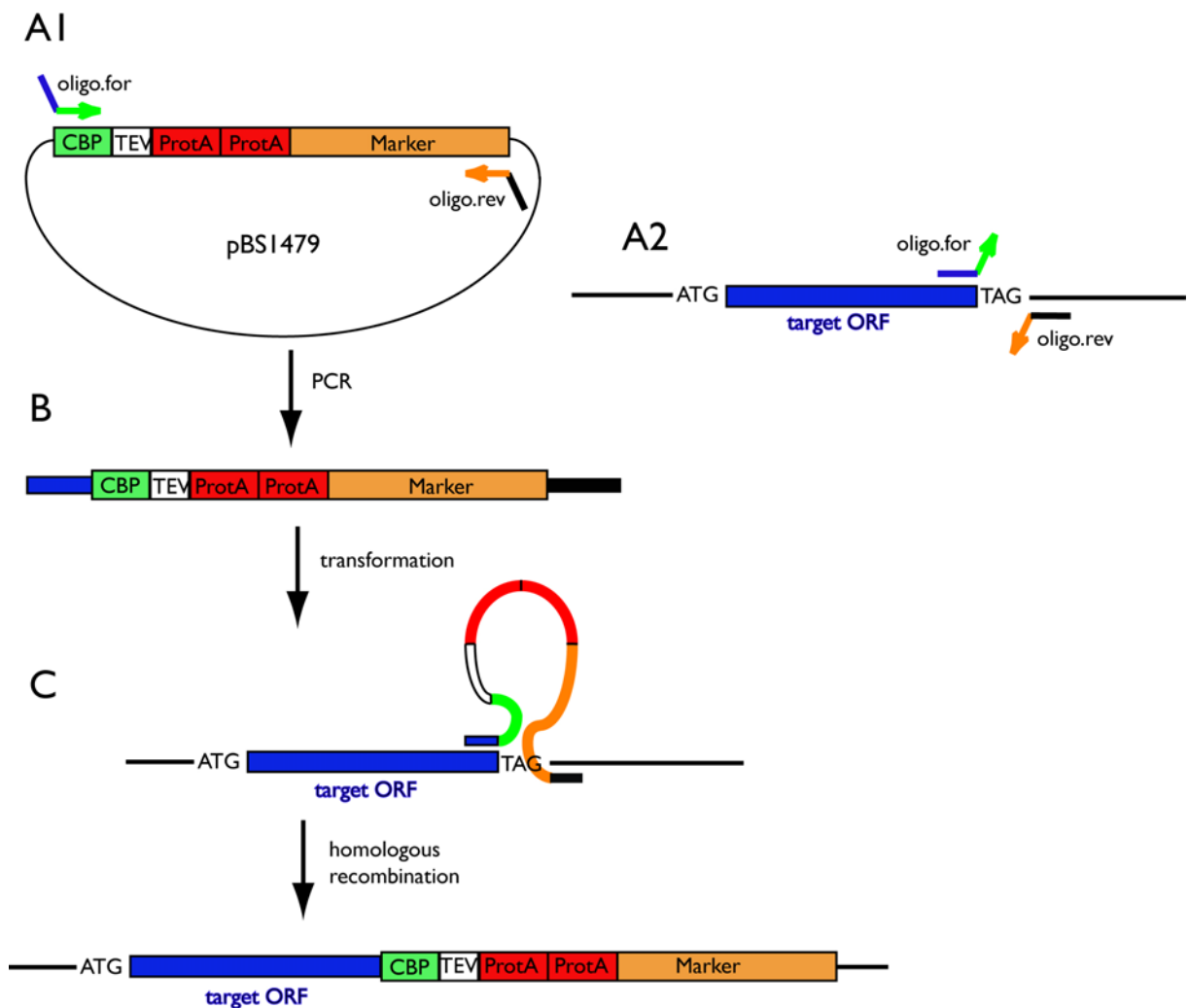


Figure 3.2 C-terminal TAP tagging strategy. The tagging cassette containing the TAP tag and the selection marker is amplified from plasmid pBS1478 using primers that contain regions of homology to the target gene up- and downstream of the stop codon. Yeast cells are transformed with the PCR product, which integrates into the genome by homologous recombination, thereby replacing the stop codon of the target gene by the TAP tag.

The cassette for C-terminal TAP tagging was amplified by PCR. Each primer used for PCR amplification consisted of a 3' complementary sequence to the plasmid and of a 5' complementary sequence to the yeast genome (Figure 3.2 A2). The forward primer (*oligo.for*, see 2.1.6) hybridized to the 5' end of the CBP coding sequence in the plasmid pBS1479 and to the 40-50 nucleotide region starting one base upstream of the target gene stop codon in the yeast genome. The reverse primer (*oligo.rev*, see 2.1.6) hybridized downstream of the selection marker in the plasmid and in the genome downstream of the stop codon. Thus, the PCR-amplified tagging cassette was flanked by sequences complementary to the sequences up- and downstream of the stop codon of the target gene (Figure 3.2 B). The purified PCR product (analyzed on a 1% agarose gel, not shown) was then used for the transformation of the haploid yeast strain TR2a (see 2.1.7), which has a deletion in the TRP gene (Sikorski and Hieter, 1989). Due to the primer design the tagging cassette could integrate into the genome in frame with the target gene by homologous recombination (Figure 3.2 C).

The transformants were incubated 2-3 days on tryptophane deficient synthetic dextrose (SC-TRP) plates at 30°C. Transformants grew like TR2a parent cells without any detectable growth defect at 30°C. Single transformant colonies were picked and streaked out on fresh SC-TRP plates to confirm their ability to grow on TRP-deficient medium. After further incubation at 30°C the transformants were screened by PCR and by western blot analysis for the correct integration and expression of the TAP tag. The testing of the transformants is described below for the tri-snRNP protein Prp6p. The colonies obtained from the transformation with the tagging cassettes for TAP tagging of Brr2p, Prp31p, and Prp3p, respectively were checked accordingly (not shown).

To verify the correct integration of the tag at the 3' end of the target gene, chromosomal DNA was isolated from transformant colonies and PCR analysis was performed, using a forward primer (*check.for.Prp6*; see 2.1.6) that anneals in the 3' region of the target gene and a universal reverse primer (*check.rev.TAP.U*; see 2.1.6) that binds to the two ProtA sequences of the TAP tag (Figure 3.3 A). Therefore, two PCR products were obtained when the TAP tag was integrated at the 3' end of the target gene (Figure 3.3 B, lane 2 and 3), whereas PCR did not work when the tag was not integrated (Figure 3.3 B, lane 1). To prove that the absence of a PCR product in fact results from a failed integration of the tagging cassette a control PCR was performed using the *check.for.Prp6* forward primer and a reverse primer that anneals to a sequence downstream of the stop codon of the *PRP6* gene (*check.rev.Prp6*; see 2.1.6). In the case of failed integration of the

TAP cassette this primer led to a short PCR product of 473 bp (Figure 3.3 C, lane 4). Upon correct integration a PCR product of 2070 bp would have been expected.

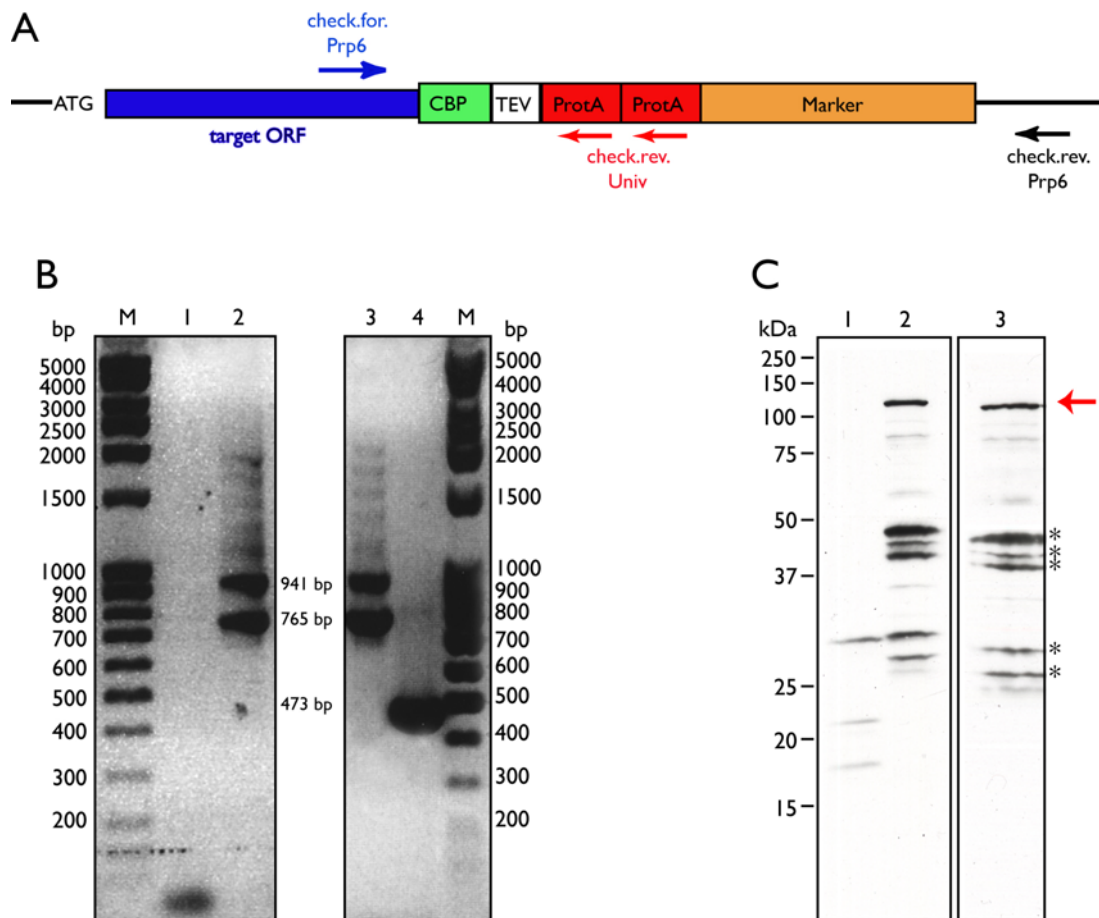


Figure 3.3 Verification of the correct integration and expression of the C-terminal TAP tag. The procedure for the verification of the integration and expression of the C-terminal TAP tag is explained for the tri-snRNP protein Prp6p. **A:** Chromosomal DNA was isolated from transformant colonies and was checked for correct integration of the TAP tag by PCR analysis using a forward primer complementary to a sequence in the C-terminal region of the target gene (*check.for.Prp6*) and two different reverse primers, *check.rev.TAP.U* and *check.rev.Prp6*, respectively (used in separate PCR reactions). *check.rev.TAP.U* bound to the ProtA sequence of the TAP tag, *check.rev.Prp6* to a sequence downstream of the *PRP6* stop codon. **B:** The PCR products were analyzed on a 1% agarose gel. In case of a correct TAP tag integration event the *check.rev.TAP.U* primer had two recognition sites (**A**) and thus produced two PCR products of 765 and 941 bp in combination with the *check.for.Prp6* primer (**B**, lane 2 and 3). If the tag was not integrated no PCR product was obtained (**B**, lane 1). A 473 bp fragment was obtained using the *check.rev.Prp6* primer in combination with the *check.for.Prp6* primer when the tag was not integrated (**B**, lane 4). M = marker (lengths (bp) of the DNA fragments are indicated) **C:** Correct expression of the Prp6p-TAP tag fusion protein was analyzed by western blot using the PAP (peroxidase-antiperoxidase complex) antibody, which detected the ProtA part of the TAP tag (lane 2 and 3; red arrow). No band was detected with the clone where PCR analysis had shown a failed integration (lane 1) as expected from the PCR results. Asterisks indicate ProtA containing degradation products of Prp6p-TAP tag.

Transformant clones were then analyzed for the expression of the TAP-tagged protein by western blot (Figure 3.3 C). The western blot was developed with a peroxidase-antiperoxidase complex (PAP), which interacts with the ProtA of the TAP tag. (The parent strain TR2a does not contain endogenous ProtA.) With the clones that showed a correct integration of the TAP cassette by PCR analysis, we detected a band at ~ 125 kDa in the western blot. This corresponds to the size of the fusion protein of Prp6p (104 kDa) and the TAP tag (20 kDa) (Figure 3.3C, lane 2 and 3). In contrast, with the clone that showed a failed integration by PCR analysis we could not detect a band in the western blot (Figure 3.3 C, lane 1).

Positive transformants with a correct integration and expression of the TAP tag were also identified for Brr2p, Prp31p, and Prp3p, respectively (not shown). To test if the TAP tags fused to Prp6p, Brr2p, Prp31p, and Prp3p, respectively were accessible for TAP purification, one positive clone of each TAP-tagged protein was selected for a small scale TAP purification (from 2 L yeast culture). The eluate of the calmodulin column was analyzed for the protein and RNA content by SDS-PAGE and denaturing PAGE, respectively, followed by staining with silver (not shown). If a purification of tri-snRNPs was possible the clone was selected as a new recombinant strain to purify native yeast tri-snRNPs at their natural expression level. Tri-snRNPs could be purified at comparable yields with all four TAP-tagged proteins constructed in this work (Brr2p, Prp31p, Prp6p, and Prp3p) as well as with TAP-tagged Snu114p, Prp8p, and Prp4p (received from Ramazan Karaduman, Cellular Biochemistry, Max Planck Institute for Biophysical Chemistry, Göttingen) and with TAP-tagged Lsm8p (Euroscarf, Frankfurt).

3.1.2.2 TAP purification of yeast tri-snRNPs

To obtain highly pure particles for mass spectrometry (MS) and electron microscopy (EM) analysis, tri-snRNPs were TAP-purified and subjected to gradient centrifugation. Gradients were fractionated from bottom to top to avoid contamination of the particle fractions with low molecular weight material (e.g. detergents) from the top of the gradient, and analyzed for their protein and RNA content. The initial TAP purification was performed via TAP-tagged Brr2p. The analysis of the snRNAs contained in the gradient fractions (Figure 3.4 A) showed that under chosen gradient conditions (see 2.2.4.2) the four tri-snRNP-specific snRNAs (U5L, U5S, U4, and U6) co-migrated in fractions 17-20. The proteins detected in the corresponding lanes of the SDS-PAGE gel (Figure 3.4 B) showed the typical lengths of the proteins contained in the yeast tri-snRNP as known from previous tri-snRNP purifications (Gottschalk et al., 1999; Stevens and Abelson, 1999; Stevens et al., 2001). This strongly indicated that the tri-snRNPs sedimented in

fractions 17-20 of the gradient. In fractions 13-15 more U5L and U5S snRNAs were present than U4 and U6 snRNAs (Figure 3.4 A). Together with the protein pattern in these fractions this indicates that fractions 13-15 predominantly contained U5 snRNPs as determined from comparison with previous purifications (Stevens et al., 2001). The TAP-tagged Brr2p seemed to peak in fractions 7-9 (Figure 3.4 B).

To verify that the particles migrating in fractions 17-20 indeed represent complete tri-snRNPs, their protein content was analyzed by MS (Fig 3.4 C) in collaboration with Dr. Henning Urlaub from the Bioanalytic Mass Spectrometry group (Max Planck Institute for Biophysical Chemistry, Göttingen). MS analysis confirmed the presence of all known tri-snRNP proteins.

Importantly, the analysis of the tri-snRNPs purified via the other seven TAP-tagged proteins (Prp8p, Snu114p, Prp6p, Prp31p, Lsm8p, Prp3p, and Prp4p) showed that, independent of the protein used for TAP purification, purified tri-snRNPs display the typical RNA and protein content of the yeast tri-snRNP (not shown). Moreover, also the purification efficiency of tri-snRNPs via the different TAP-tagged proteins was comparable.

Interestingly, in the top fractions of the gradient (Figure 3.4 A and B, fractions 1-3) a complete set of tri-snRNP proteins and RNAs was detected. This was only observed when the gradients were fractionated from the bottom. In case of fractionation from the top, the top fractions were essentially free of proteins and RNAs (not shown). This can be explained as follows: during gradient fractionation from the bottom, the top fractions of the gradient are moving top down into the gradient tube and wash off the proteins that stick to the wall of the tube. Thus, the uppermost fractions contain all proteins that were attached to the wall along the full length of the tube.

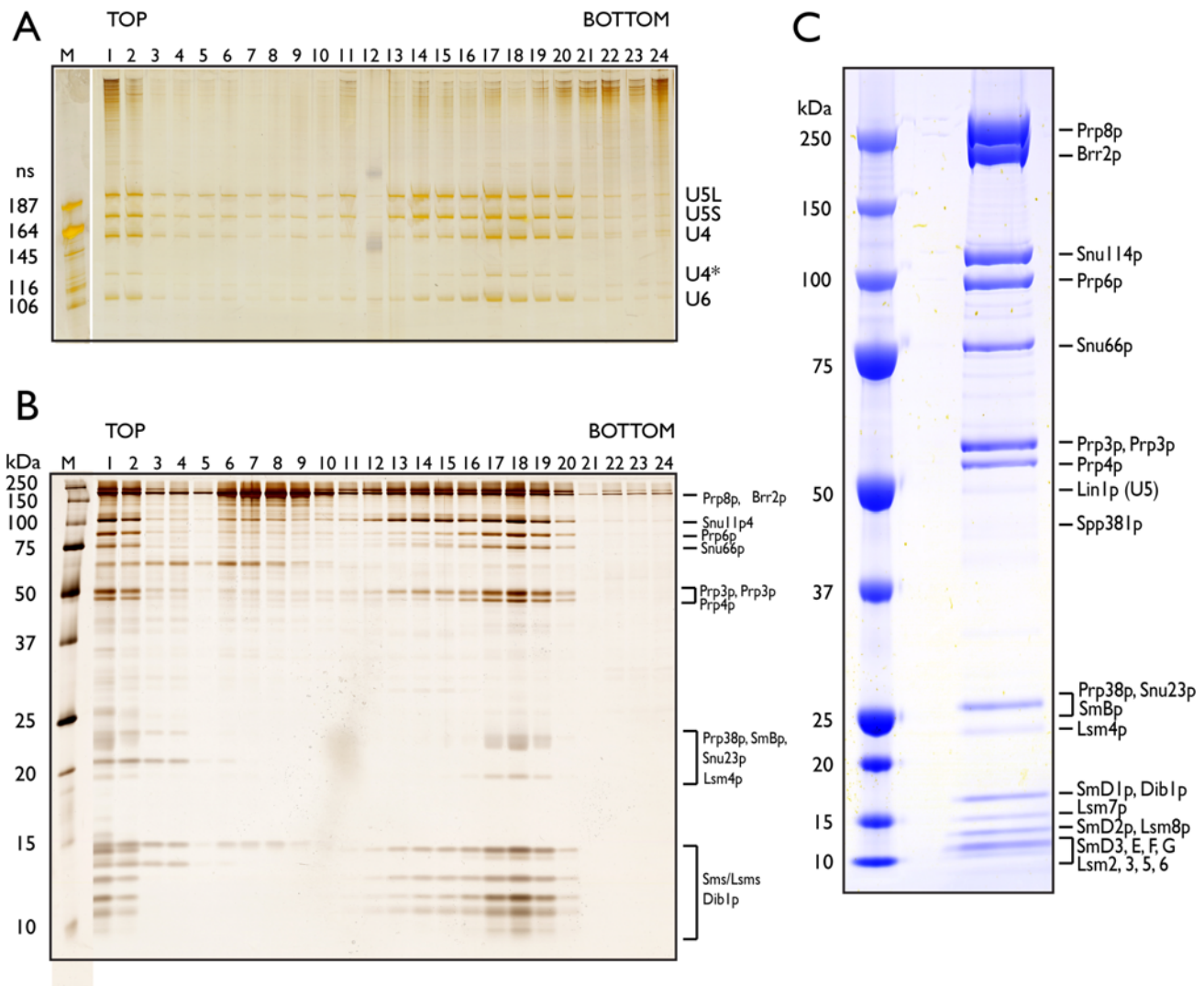


Figure 3.4 Characterization of TAP-purified *S. cerevisiae* U4/U6.U5 tri-snRNPs. Tri-snRNPs, TAP-tagged at Brr2p, were TAP-purified from whole cell extract and sedimented on a glycerol gradient. The gradient was fractionated from bottom to top. A: RNAs were extracted from the gradient fractions, ethanol precipitated, separated on a denaturing polyacrylamide gel and visualized by staining with silver. The positions of the yeast snRNAs are shown on the right. U4* is a fragment of U4 snRNA lacking the 3' end (Anthony et al., 1997). The lengths (ns) of the human snRNAs used as a marker ('M') are indicated on the left. B: Proteins were extracted from the gradient fractions, acetone precipitated, separated by 12% SDS-PAGE and visualized by staining with silver. The positions of the proteins are shown on the right as determined by comparison with previous purifications (Gottschalk et al., 1999; Stevens and Abelson, 1999; Stevens et al., 2001). The molecular weights (kDa) of protein standards are indicated on the left. C: For MS analysis tri-snRNP fractions were pooled, concentrated in a vacuum concentrator and separated on a 1 mm thick pre-cast 4-12% NuPAGE Bis-Tris gel. The gel was subsequently stained with Colloidal Coomassie. The tri-snRNP proteins identified by mass spectrometry are indicated on the right. Lin1p is a contaminant from the co-purified U5 snRNP.

3.1.3 Electron microscopy of double affinity-purified yeast tri-snRNPs

To gain first insight into the structure of the yeast tri-snRNP, TAP-purified particles were analyzed by single-particle EM in collaboration with Monika M. Golas and Björn Sander from the Cryo-EM group (Max Planck Institute for Biophysical Chemistry, Göttingen). For EM analysis the particles were fixed during gradient centrifugation following the ‘GraFix’ protocol (Kastner et al., 2008). This method combines the sedimentation of particles in a density gradient with a mild chemical fixation (Figure 3.5). The fixation stabilizes the particles and protects them against unspecific aggregation, disruption or deformation caused by the various forces acting on the particles during sample preparation for EM (Kastner et al., 2008). Commonly used fixatives in EM are aldehydes. The aldehyde groups react with the amino groups of the proteins by forming a Schiff base and thereby intra- and intermolecularly cross-linking the proteins in a complex. The strength of the fixation reagent depends on the number of aldehyde groups. For GraFix the di-aldehyde glutaraldehyde is used. The cross-linked complexes can be directly used for negative stain and cryo negative stain EM or even for unstained cryo-EM.

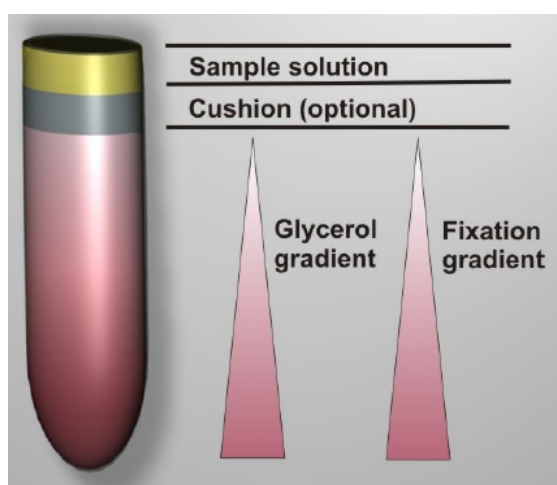


Figure 3.5 ‘GraFix’. The particles migrate into a gradient of increasing glutaraldehyde concentration prepared by adding the fixation reagent to the denser gradient solution. A cushion prepared of the lighter gradient solution can be used for buffer exchange during the initial period of gradient centrifugation, because sample buffers often contain primary amines, which are incompatible with aldehyde cross-linking (Kastner et al., 2008).

For fixation of the yeast tri-snRNP glutaraldehyde was used with a maximum concentration of 0.1% at the bottom of the gradient. Ultracentrifugation conditions were chosen such that tri-snRNPs sedimented in the lower third of the gradient, which corresponded to a glutaraldehyde concentration of approximately 0.075%. EM specimens were prepared from the tri-snRNP fractions of the gradient according to standard protocols (see 2.2.4.6). The tri-snRNP particles were visualized by negative stain EM using 2% uranyl formate and the double carbon film method (Kastner et al., 1990). Comparison of samples before and after ‘GraFix’ by negative-stain EM showed that ‘GraFix’ significantly improved the image contrast. Moreover, we observed

less degradation artifacts in the background. Both findings are an essential prerequisite for reliable detection of labeled proteins by EM. Additionally, 'GraFix' enhanced the binding of the particles to the carbon film, thereby reducing the sample quantity necessary for each experiment.

EM images revealed a monodisperse population of elongated, triangular particles with a maximum dimension of 30-34 nm (Figure 3.6 A, TAP tag at Brr2p). To improve the signal-to-noise ratio (SNR), particle images were iteratively aligned and classified following the 'reference-free alignment' protocol (Dube et al., 1993). The predominant view of the particle (Figure 3.6 B, TAP tag at Brr2p) comprises two building blocks including a slim main body with a pointed lower end ('foot') and a broader 'head' structure. A smaller 'arm' domain of about 2/3 of the head diameter is connected to the main body at a central linker region. The smaller arm domain is well distinguishable from the head in the class averages (Figure 3.6 C).

Comparison of the class averages shows that head and arm adopt two predominant positions relative to each other. In an 'open state' the head is bent to the left while the arm points away from the main body to the right so that head and arm domain are well separated from each other (Figure 3.6 C, e.g. sixth column). In a 'closed state' they extend in parallel directions and are positioned in close proximity (Figure 3.6 C, e.g. first column). Besides these two predominant views all other possible combinations of head and arm positions can be detected to a minor extent (Figure 3.6 C and data not shown). The closed and open states were found in comparable frequencies in all purification runs, regardless of which protein contained the TAP tag for purification. Importantly, the addition of the TAP tag to each of the seven proteins investigated in this study (i.e. Prp8p, Snu114p, Prp6p, Prp31p, Prp3p, and Lsm8p, respectively) did not alter the appearance of the particles in the electron microscope as exemplified for Brr2p, Snu114p, and Prp3p (Figure 3.6 C). Thus, the TAP tag had no influence on the structure of the tri-snRNP.

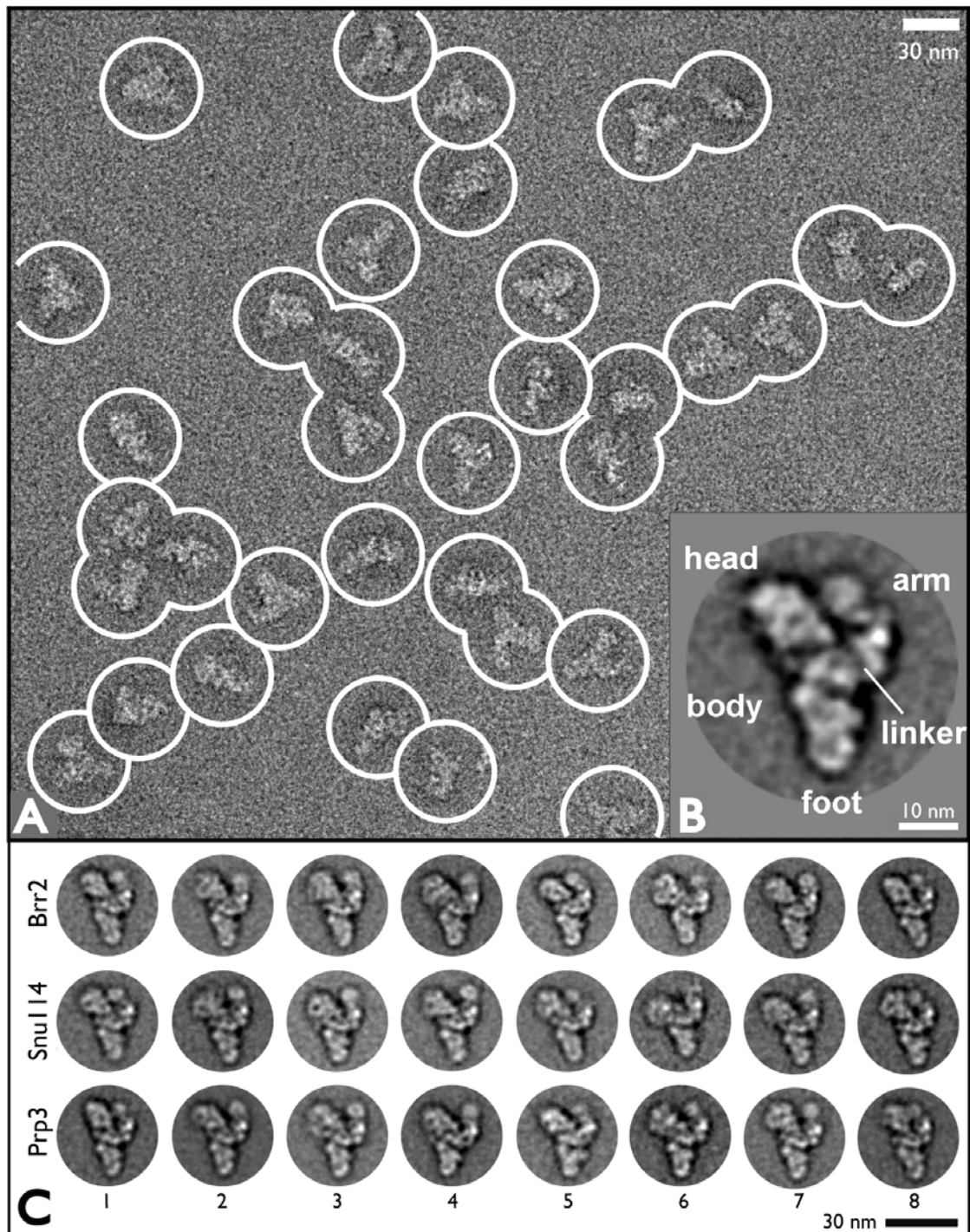


Figure 3.6 EM of TAP-purified yeast tri-snRNPs. TAP-purified tri-snRNPs were sedimented on a glycerol gradient. The gradient was fractionated from bottom to top; the tri-snRNP particles were absorbed to a carbon film, negative stained, and the carbon film was attached to a copper grid for EM analysis. A: Representative EM overview image of negatively stained tri-snRNP (TAP-tagged at Brr2p) showing a monodisperse population of triangular complexes. B: A representative class average reveals the tri-snRNP's domain architecture at a high SNR comprising an elongated main body with an upper head and a lower foot domain, and a small arm, which is connected to the central portion of the main body by a linker domain. C: Representative set of tri-snRNP class averages obtained from TAP-tagged particles upon tagging of Brr2p (upper row), Snu114p (central row), and Prp3p (lower row). This figure was kindly provided by B. Sander and M. Golas (Cryo-Electron Microscopy, Max Planck Institute for Biophysical Chemistry, Göttingen)

To investigate if the closed and open states are the result of different conformations or of different orientations of the particles on the carbon film, we tilted the specimens in the electron microscope. This did not change the open or closed appearance of individual particles, which – together with the very similar appearance of fine structural details in the foot domain in the open and close forms – indicates that this difference is indeed due to changes in conformation. Besides the complete particles, a subpopulation of particles lacks either the arm and the linker domain or only the arm domain (not shown). It could not be determined if these particles have been damaged during sample preparation or if they represented stable sub-complexes of the tri-snRNP that were co-purified and could not be separated from complete tri-snRNP particles by the applied purification strategy.

3.1.4 Labeling strategies

3.1.4.1 Genetic labeling of tri-snRNP proteins

To localize the functionally important proteins within the structure of the yeast tri-snRNP we genetically fused a protein tag to the C-terminus of the proteins that could be directly visualized in the electron microscope. For tagging we chose the 27 kDa protein yECitrine and the 54 kDa protein tDimer2 because their globular structure is well suited for visualization by EM. Both proteins are fluorescent proteins and are available as tagging cassettes constructed for genetic labeling of yeast proteins (Sheff and Thorn, 2004). However, their fluorescent nature could not be used for the localization studies because it is not possible to combine fluorescence detection with EM. yECitrine is a fluorescence-optimized variant of the yellow fluorescent protein (YFP), which on his part is a yellow variant of the *Aequorea* green fluorescent protein (GFP) (Cormack et al., 1997; Sheff and Thorn, 2004). This tag has already been successfully used to identify the positions of the different Lsm proteins within the Lsm-ring of yeast U6 snRNP by EM (Ramazan Karaduman, personal communication). tDimer2 is a fluorescence-optimized dimer of the red fluorescent protein DsRed from *Discosoma* (Campbell et al., 2002). Both proteins have a compact β -barrel structure (built by 11 β -strands, Figure 3.7 A), which is highly conserved although the amino acid sequence identity of GFP and DsRed is only about 23% (Yarbrough et al., 2001). A short linker of 12 residues links the two DsRed subunits of tDimer2 (Campbell et al., 2002), which are positioned perpendicular to each other (Figure 3.7 B).

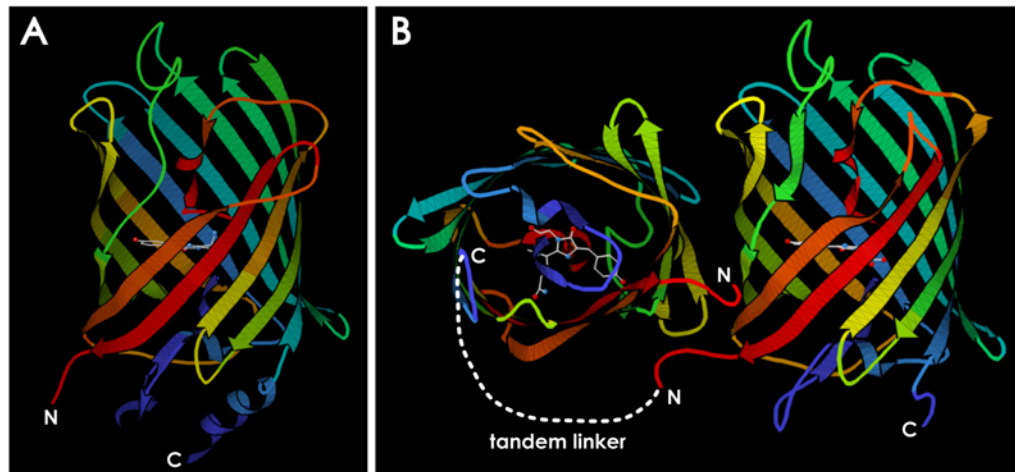


Figure 3.7 Crystall structures of Citrine and tDimer2. A: Crystal structure of the yellow GFP variant Citrine (PDB identification: 1huy (Griesbeck et al., 2001)). B: Crystal structure of tDimer2 based on the crystal structure of the DsRed tetramer (PDB identification: 1g7k (Yarbrough et al., 2001)) and adapted as described (Campbell et al., 2002). The DsRed monomers are positioned perpendicular to each other. The 12-residue linker between the monomers is indicated by a white dotted line.

The yECitrine or tDimer2 tag was fused to the C-terminus of selected tri-snRNP proteins by homologous recombination in the strain TR2a (as described for C-terminal TAP tagging, 3.1.1.1, Figure 3.2) using tagging cassettes that encode the fluorescent protein and a selection marker. The yECitrine cassette additionally contains a 3HA epitope tag fused onto the fluorescent tag, which can be used for purification. The cassettes were amplified by PCR from the tagging vectors pKT239 (yECitrine) and pKT146 or pKT176 (tDimer2) (Sheff and Thorn, 2004) such that the amplified cassette is flanked by sequences complementary to the regions up- and downstream of the C-terminus of the target gene as described for the TAP tag (3.1.1.1, Figure 3.2). The vectors pKT146 and pKT176 differ only in the selection marker, which is *S. pombe HIS5* or *C. albicans URA3*, respectively, which complement the depletions of the corresponding yeast genes in the strain TR2a (Sikorski and Hieter, 1989). Upon tDimer2-tagging of Snu114p using plasmid pKT176 a strong background of small colonies was observed on the SC-URA plates used for transformant selection. We therefore chose the plasmid pKT146 for tDimer2 labeling of the other proteins.

The correct integration of the tagging cassette was confirmed by PCR analysis as described in Figure 3.8 A. A tDimer2-specific antibody was not available. Therefore, the expression of the fusion proteins was tested by small scale TAP purification of tri-snRNPs from 2 L cultures. Tri-snRNPs carrying the tDimer2 tag at Brr2p were purified via TAP-tagged

Snu114p. Tri-snRNPs carrying the tDimer2 tag at Prp8p, Snu114p, Prp6p, Prp31p, Prp4p, or Prp3p, respectively, were purified via TAP-tagged Brr2p. Proteins were extracted from the calmodulin column eluate and analyzed by SDS-PAGE followed by silver staining. In case of correct expression of the tag the band of the labeled protein shifted to a higher molecular weight as indicated by arrows in Figure 3.8 B (shown are tri-snRNP-containing gradient fractions of a large scale purification). Adjacent lanes in Figure 3.8 B were run on the same gel and therefore serve as reference for the position of the native protein.

The shift of the labeled protein could be additionally verified by western blot analysis using protein-specific antibodies against Prp8p (Grainger and Beggs, 2005), Prp31p (kind gift of Dr. J. L. Woolford), and Prp3p (Anthony et al., 1997) (not shown). Note that the near absence of the Snu66p-band (at about 75 kDa) in case of tDimer2-labeling of Snu114p and Prp6p is not caused by the tag. This effect was always observed, when the yeast cells were broken using a French Press. Moreover, the splicing activity of extracts prepared with the French Press was very low (not shown). The French Press was therefore replaced by a mortar grinder (RM100, Retsch). This method proved to be much gentler for braking the yeast cells and provided highly active splicing extracts.

The tDimer2 tag was successfully fused to the C-terminus of Prp8p, Brr2p, Snu114p, Prp6p, Prp31p, and Prp3p (Figure 3.8 B). For Snu66p and Dib1p we could not prove the correct expression of the tDimer2 fusion protein by SDS-PAGE (not shown). Interestingly, for almost all tDimer2-tagged proteins a faint band could be detected in SDS-PAGE gels (Figure 3.8 B) as well as in western blot analysis at the position of the native protein, indicating the loss of the tDimer2 tag in a subpopulation of particles during purification. For EM analysis of tDimer2-labeled tri-snRNPs the particles were fixed during gradient centrifugation following the 'GraFix' protocol. Particles were embedded in negative stain and the tDimer2 tag was directly visualized in the electron microscope with and without class averaging.

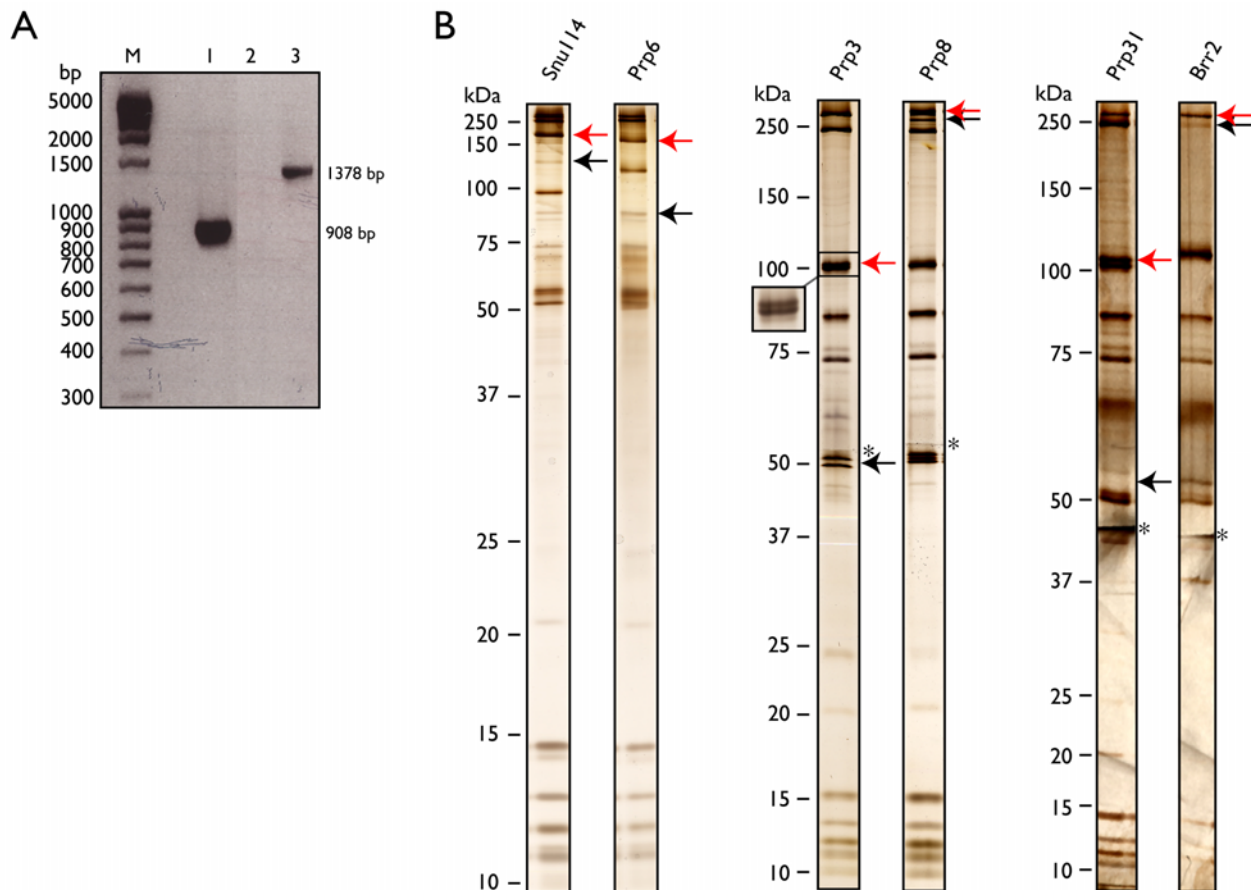


Figure 3.8 Verification of the correct integration and expression of the C-terminal tDimer2 tag.

The procedure for the verification of the integration and expression of the C-terminal tDimer2 tag is explained for the tri-snRNP protein Prp8p. A: Chromosomal DNA was isolated from transformant colonies and was checked for correct integration of the tDimer2 tag by PCR analysis using a forward primer complementary to a sequence in the C-terminal region of the target gene (check.for.Prp8) and two different reverse primers, check.rev.tD2.U and check.rev.Prp8, respectively (used in separate PCR reactions). check.rev.tD2.U bound to the tDimer2 sequence, check.rev.Prp8 to a sequence downstream of the PRP8 stop codon. The PCR products were analyzed on a 1% agarose gel. In case of a correct tDimer2 tag integration event the check.rev.tD2.U primer produced a PCR product of 1378 bp in combination with the check.for.Prp8 primer (lane 3). If the tag was not integrated no PCR product was obtained (lane 2). A 908 bp fragment was obtained using the check.rev.Prp8 primer in combination with the check.for.Prp8 primer when the tag was not integrated (lane 1). In case of correct integration a 3834 bp PCR product would have been expected. M = marker (lengths (bp) of the DNA fragments are indicated) B: For verification of the correct expression of the tDimer2 fusion protein, tri-snRNPs were purified with the TAP method. Proteins were extracted, acetone precipitated, separated by SDS-PAGE (12% or 8%/12% step gels) and stained with silver. In case of correct expression of the tDimer2 tag (54 kDa) the band of the tagged protein was shifted to a higher molecular weight (red arrows). The black arrows indicate the position of the respective native proteins. Inset: Prp3p-tDimer2 migrates almost identically with Snu114p, visible as two very closely migrating bands. The molecular weights (kDa) of protein standards are indicated on the left. The border between 8% PAA and 12% PAA is marked by asterisks.

Initial tagging with the yECitrine tag was performed with Brr2p, Snu114p, Prp6p, and Prp31p, respectively. The correct integration of the construct into the genome was verified by PCR analysis (not shown). The expression of the yECitrine-fusion proteins was verified by western blot analysis using an anti-HA antibody (Figure 3.9 A). Moreover, the shift of the tagged protein to a higher molecular weight in a SDS-PAGE gel compared to its native form was monitored by silver staining of the proteins (Figure 3.9 B). Tri-snRNPs carrying the yECitrine tag at Brr2p were purified via TAP-tagged Snu114p. Tri-snRNPs carrying the yECitrine tag at Prp6p, or Prp31p, respectively, were purified via TAP-tagged Brr2p.

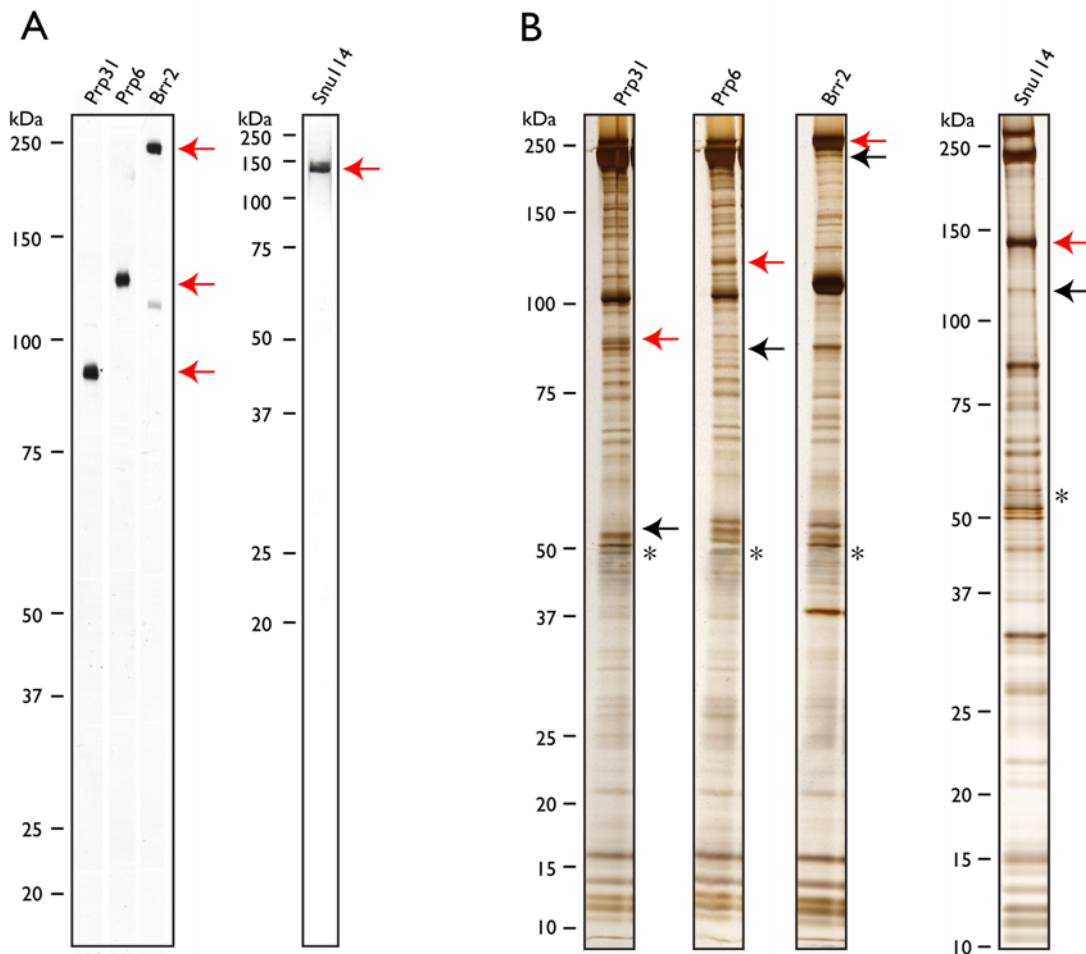


Figure 3.9 Verification of the expression of the C-terminal yECitrine tag. One clone of each protein that was successfully tested by PCR analysis for the correct integration of the yECitrine tag (not shown) was selected for tri-snRNP purification via the TAP method. Proteins were extracted from the calmodulin eluate, acetone precipitated, separated by SDS-PAGE (8%/12% step gels) and either blotted on a nitrocellulose membrane to detect the fusion protein using an antibody against the 3HA tag contained in the yECitrine cassette (anti-HA) (A) or stained with silver (B). In case of yECitrine tag (27 kDa) expression the band of the tagged protein was shifted in the SDS-PAGE gel to a higher molecular weight (red arrows). The black arrows indicate the position of the respective native proteins (B). The molecular weights (kDa) of protein standards are indicated on the left. The border between 8% PAA and 12% PAA is marked by asterisks.

3.1.4.2 Immunolabeling of tri-snRNP proteins

To set up a second independent labeling method for the localization of tri-snRNP proteins by EM, we screened for antibodies suitable for immunolabeling studies. Conventional protein-specific antibodies often have different sensitivities and specificities and therefore require individual testing and optimization of each antibody. To avoid this we tested antibodies against the yECitrine tag and the TAP tag for their applicability for immunolabeling studies. For the yECitrine tag (containing the fluorescence-optimized YFP variant Citrine and a 3-HA tag; 3.1.3.1) we tested a polyclonal anti-HA antibody, a monoclonal anti-YFP antibody, and a polyclonal anti-GFP antibody. For the TAP tag we tested a polyclonal peptide antibody against the CBP-part of the TAP tag, which we named anti-CBP (see 2.1.3). Antibodies were first tested in co-immunoprecipitation (Co-IP) assays (Figure 3.10) by immobilizing the antibodies on ProtA-sepharose beads followed by incubation with TAP-purified tri-snRNPs. As a control we used an anti-Snu114 antibody (Bartels et al., 2003) and an anti-Prp4 antibody (Banroques and Abelson, 1989).

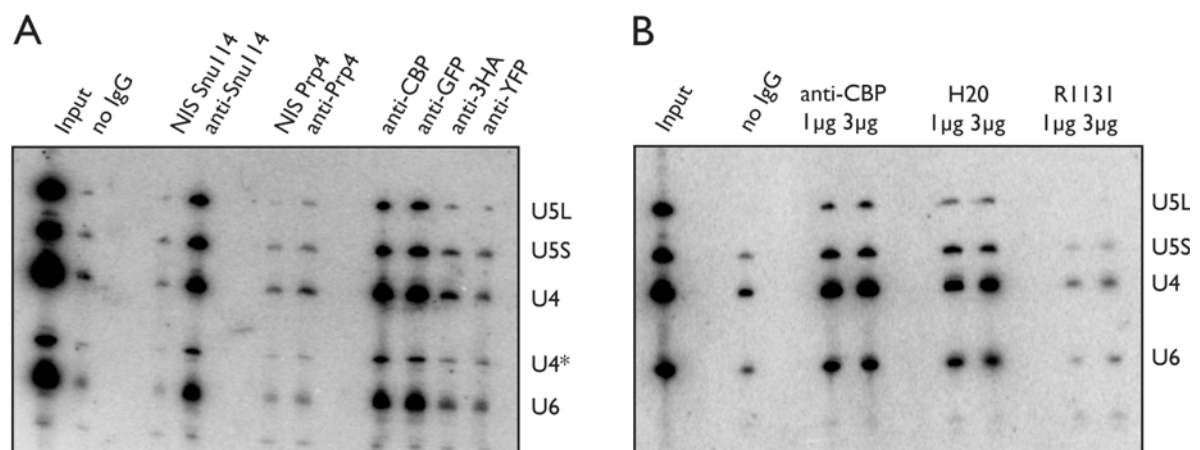


Figure 3.10 Testing of different antibodies for their ability to co-immunoprecipitate tri-snRNPs. A: Antibodies against the yECitrine tag (anti-GFP, anti-YFP, anti-HA) and the TAP tag (anti-CBP) were tested in Co-IP assays. The antibodies were immobilized on ProtA-sepharose beads in separate reaction tubes and incubated each with the same amount of TAP-purified tri-snRNPs. The 'input' shows the amount of tri-snRNPs that was incubated with each ProtA-sepharose-coupled antibody. Co-immunoprecipitated snRNAs were extracted (see 2.2.4.3) and analyzed by northern blot using radioactively labeled DNA probes against the U4, U5, and U6 snRNAs. Hybridized DNA probes were detected by autoradiography. The Co-IP efficiency of the tag-specific antibodies was compared to that of the protein-specific anti-Snu114 and anti-Prp4 antibodies. Note that tri-snRNPs incubated with anti-CBP, anti-Snu114 or anti-Prp4 antibody did not carry a yECitrine tag. As a control, TAP-purified tri-snRNPs were incubated with the ProtA-sepharose in the absence of an antibody ('no IgG'). The 'input' is the amount of tri-snRNPs that was used in each reaction. The positions of the snRNAs are indicated on the right; U4* is a fragment of U4 snRNA lacking the 3' end (Anthony et al., 1997). NIS: Non-immune serum. B: Antibodies against the m3G-cap of U4 and U5 snRNA (H-20, R1131) were tested in two different concentrations in Co-IP assays as described in (A). The Co-IP efficiency was compared to that of the anti-CBP antibody.

The anti-Prp4 antibody co-immunoprecipitated tri-snRNP snRNAs only at background levels (Figure 3.10 A). The anti-CBP and anti-GFP antibodies co-precipitated tri-snRNPs with a yield comparable to anti-Snu114. The co-precipitation efficiency with the anti-YFP antibody was at background levels, with the anti-HA antibody slightly above background levels. Additionally, we tested antibodies that recognize the 2,2,7-trimethylguanosin (m_3G) containing cap structure of the U snRNAs, the H-20 antibody (Bochnig et al., 1987) and the R1131 antibody (Lührmann et al., 1982) (Figure 3.10 B). The Co-IP efficiency of the H-20 and R1131 antibody was compared to that of the anti-CBP antibody. H-20 co-precipitated tri-snRNPs almost as efficiently as anti-CBP, whereas the Co-IP with the R1131 antibody did not work (Figure 3.10 B).

The antibodies that co-immunoprecipitated tri-snRNPs (anti-CBP, anti-GFP, anti-HA, H-20) were subsequently tested in small-scale immunolabeling assays (Figure 3.11). The tri-snRNPs used for these experiments carried a C-terminal TAP tag at Brr2p, and if an antibody against the yECitrine tag was tested they additionally contained a yECitrine tag at the C-terminus of Prp6p. TAP-purified tri-snRNPs were incubated with an excess of the antibodies (as described in Figure 3.11) for 90 min at 4°C prior to subjecting the reactions to glycerol gradient centrifugation. As negative control, the anti-CBP antibody was loaded on a gradient in the absence of tri-snRNPs (Figure 3.11 E). Gradients were fractionated and the gradient fractions were analyzed for the presence of antibody by enzyme linked immunosorbent assays (ELISA) (Figure 3.11 A-E). The free anti-CBP in the negative control peaked in the upper third of the gradient (Figure 3.11 E, fractions 3-7), whereas in the bottom half of the gradient no antibody could be detected in the absence of tri-snRNPs. Except for the anti-CBP antibody (Figure 3.11 C) all antibody profiles were very similar to that of the negative control. Only upon incubation of tri-snRNPs with the anti-CBP antibody considerable amounts of antibody could be detected in the lower gradient fractions, indicating an association of anti-CBP with high molecular weight complexes.

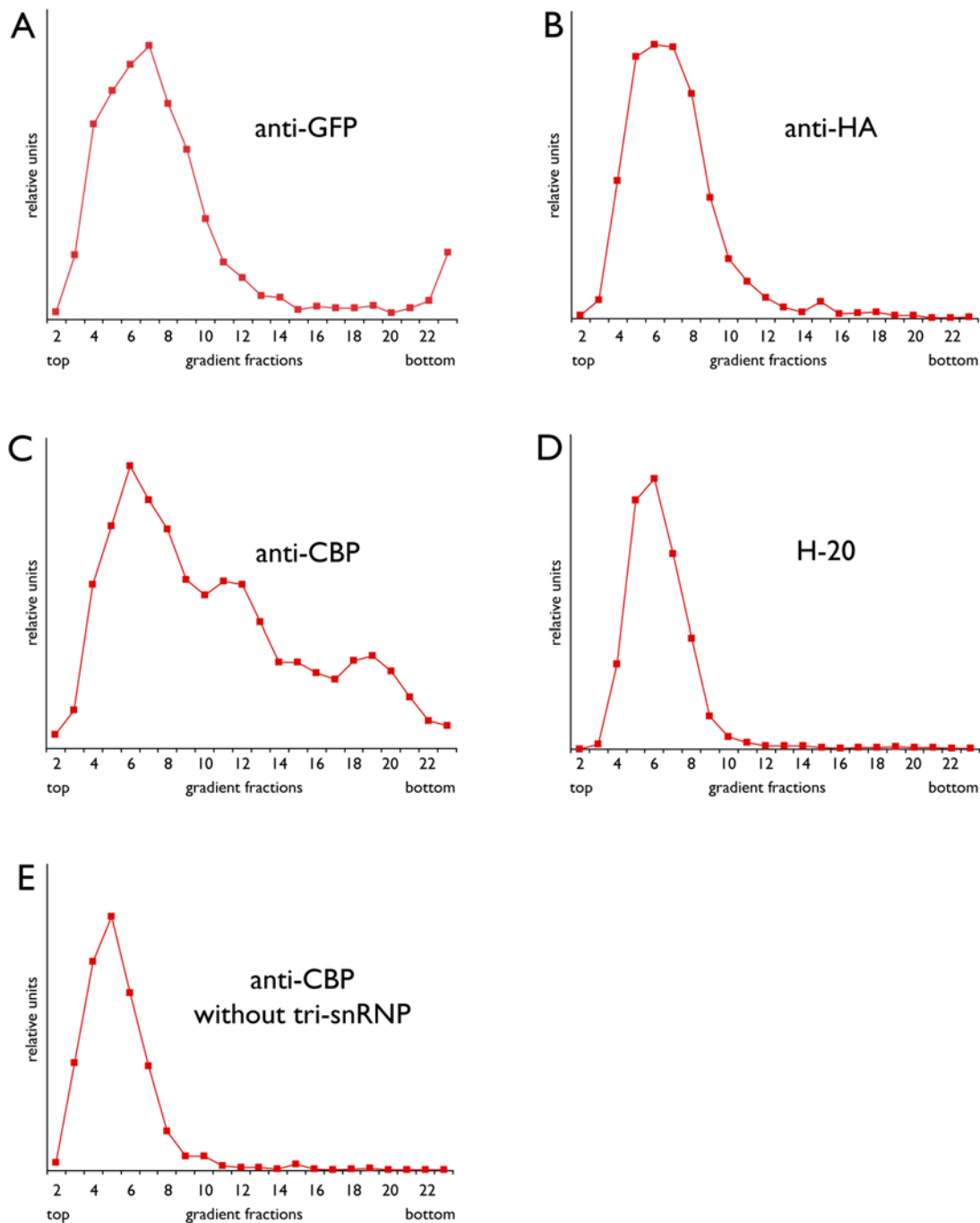


Figure 3.11 Testing of antibodies in immunolabeling assays. The ability of different antibodies to form stable immunocomplexes with TAP-tagged and yECitrine-tagged tri-snRNPs was tested by small scale immunolabeling experiments. An approximately 20-fold molar excess of anti-GFP (A), anti-HA (B), and anti-CBP (C) antibody was incubated with TAP-purified tri-snRNPs. For the H-20 antibody (D) a 6-fold molar excess was chosen according to results obtained from H-20-labeling of human B-complexes (E. Wolf, personal communication). As negative control, the anti-CBP antibody was loaded on a gradient in the absence of tri-snRNPs (E). The reactions were subjected to gradient centrifugation to separate immunocomplexes from unbound antibody. The relative amount of antibody in each gradient fraction was measured by ELISA using a peroxidase-coupled anti-rabbit antibody as well as TMB (3,3',5,5'-tetramethylbenzidine) for detection. Shown are the line charts obtained by plotting the signal intensity in each fraction (= relative amount of antibody) against the gradient fractions to visualize the sedimentation behavior of the antibodies in the gradient in presence (A-D) or absence (E) of tri-snRNPs.

The sedimentation profile of the anti-CBP antibody shows different peaks (Figure 3.11 C). The one at the top of the gradient very likely corresponds to the unbound antibody as determined by comparison with the negative control (Figure 3.11 E). To identify the other peaks and to check if the tri-snRNPs are still intact after incubation with the anti-CBP antibody and gradient centrifugation, we analyzed an aliquot of each gradient fraction by northern blot probing for the U4, U5, and U6 snRNAs. Northern blot analysis showed that all three tri-snRNP snRNAs co-migrated with the antibody peak in fractions 18-21, whereas the U5 snRNAs also co-migrated with the small peak in fractions 15/16 (Figure 3.12 A, B). An additional strong antibody peak was detected in fractions 11-13, which were essentially free of snRNAs. These fractions probably contained the immunocomplex with the free TAP-tagged protein (in this case Brr2p). With the ultracentrifugation conditions typically applied for tri-snRNP purification (see 2.2.4.2) the single Brr2 protein usually peaked around fractions 7 to 9 (Figure 3.4). The shift of 4 fractions would be in agreement with a considerable increase of the molecular weight (from 246 kDa to ~ 400 kDa) and probably also of the sedimentation coefficient upon formation of an immunocomplex of Brr2p with the anti-CBP antibody. Compared with the unlabeled particles the peak of the immunolabeled tri-snRNP is also shifted to fractions containing particles of higher molecular weight due to the formation of immunocomplexes (compare Figure 3.12 B and C). Moreover, in contrast to unlabeled particles, noticeable amounts of U4, U5, and U6 snRNAs were detected in the fractions towards the bottom of the gradient, indicating the presence of hetero-trimeric immunocomplexes and larger aggregates.

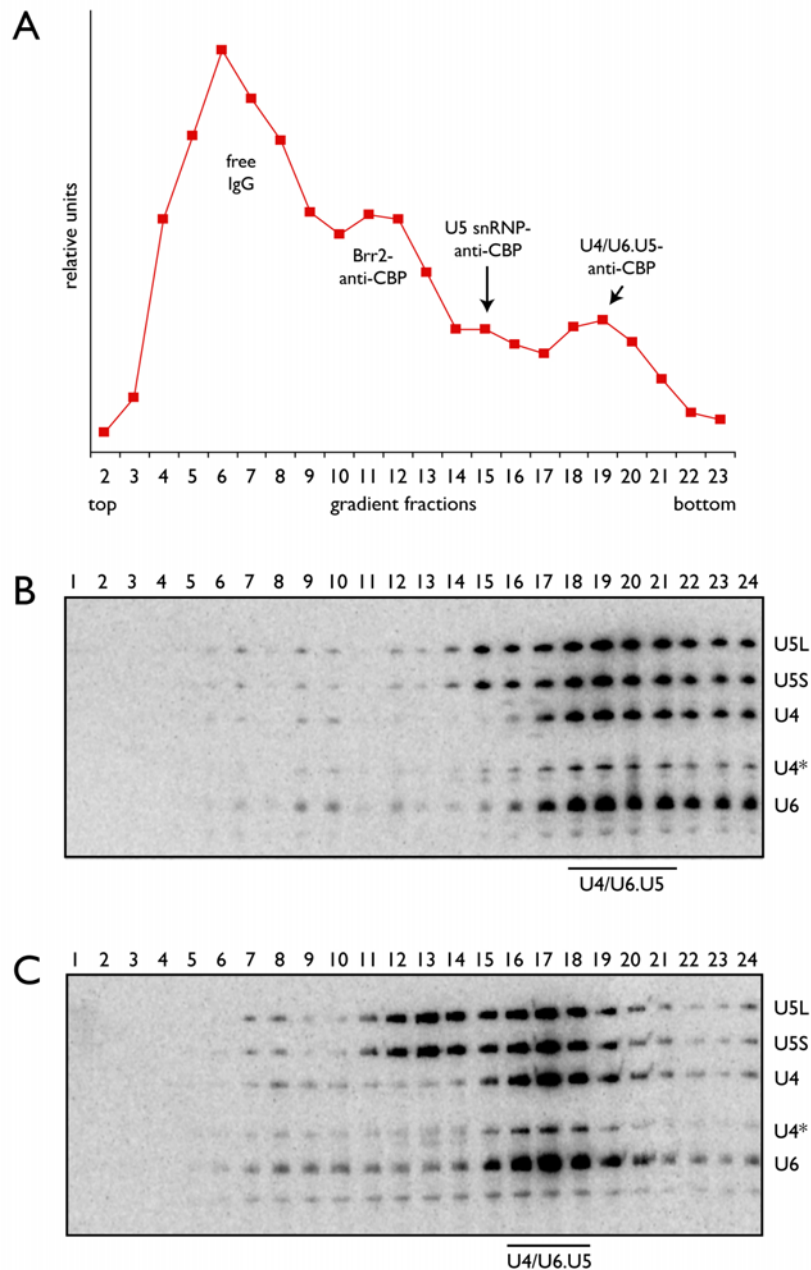


Figure 3.12 Identification of the immunocomplexes obtained upon incubation with the anti-CBP antibody. TAP-purified tri-snRNPs were immunolabeled with anti-CBP antibody and sedimented on a glycerol gradient. **A:** Gradient fractions were analyzed by ELISA as described in Figure 3.11 to detect the anti-CBP antibody. **B:** To identify the snRNAs contained in the gradient fractions, the RNAs were extracted, ethanol precipitated and separated by denaturing PAGE, followed by northern blot analysis using radioactively labeled DNA probes against the U4, U5, and U6 snRNAs. Hybridized DNA probes were detected by autoradiography. The migration of the snRNAs of anti-CBP labeled tri-snRNPs in the gradient (**B**) was compared to that of unlabeled tri-snRNPs run in a parallel experiment (**C**). The positions of the tri-snRNP snRNAs are indicated on the right. U4* is a fragment of U4 snRNA lacking the 3' end (Anthony et al., 1997).

The failure of the other tested antibodies to form immunocomplexes with the tri-snRNP might be due to the inability of these antibodies to stably bind to the particles. However, it could also be due to a disintegration of tri-snRNPs upon incubation with the antibody, which could have several reasons. First, the tri-snRNPs could be disrupted by the binding of the antibody, an effect that is often observed upon immunolabeling. Second, the particle could be degraded by proteases or RNases contained in the antibody solution. To investigate these possibilities we analyzed the gradient fractions of the reaction with the anti-HA antibody (representative for all other yECitrine-tag-specific antibodies) and of the reaction with H-20 antibody by northern blot. If the tri-snRNPs had been destroyed upon incubation with the anti-HA or the H-20 antibody, respectively, then the tri-snRNPs snRNAs would no longer co-migrate in the gradient. Since the gradients were run under standard conditions (see 2.2.4.2), intact tri-snRNPs were expected to migrate approximately in fractions 17-19.

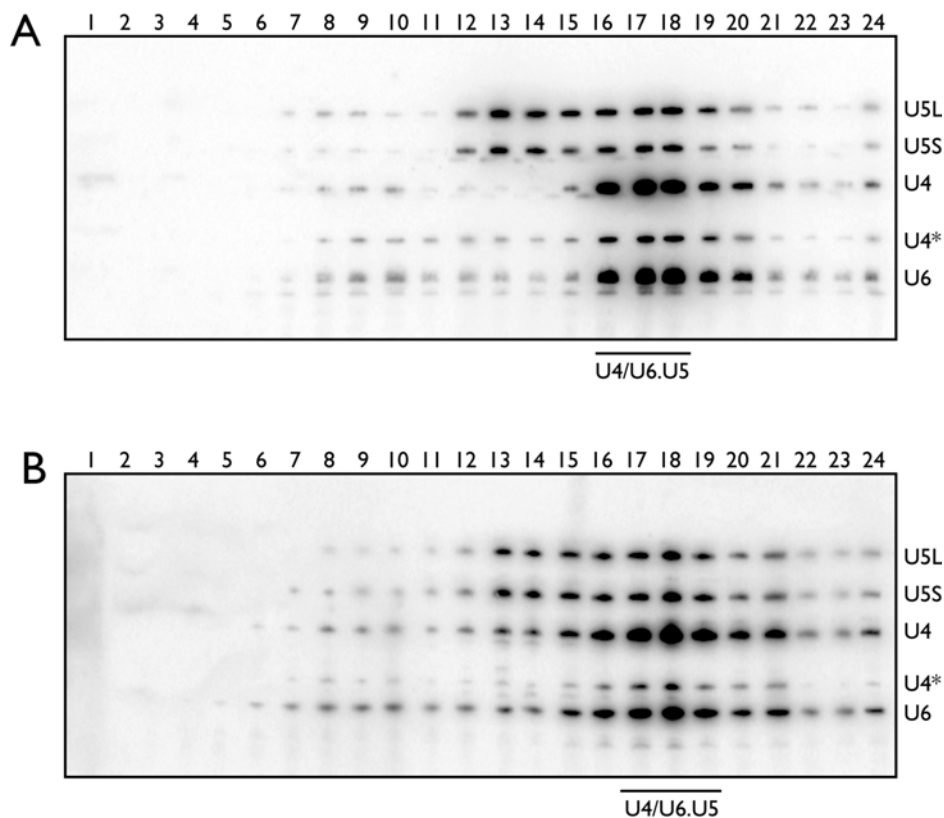


Figure 3.13 Testing of the tri-snRNP integrity upon incubation with the anti-HA and H-20 antibodies. Aliquots of the gradient fractions of the immunolabeling reactions with the anti-HA and the H-20 antibody (Figure 3.11 B and D) were analyzed for their snRNA content by denaturing PAGE and northern blot analysis using radioactively labeled DNA probes against the U4, U5, and U6 snRNAs, which were detected by autoradiography A: tri-snRNPs incubated with anti-HA antibody; B: tri-snRNPs incubated with H-20 antibody. The positions of the tri-snRNP snRNAs are indicated on the right. U4* is a fragment of U4 snRNA lacking the 3' end (Anthony et al., 1997).

Indeed, with both antibodies the tri-snRNP snRNAs were detected in the expected gradient fractions (Figure 3.13 A and B), showing that the particles are not destroyed upon incubation with the antibodies. It can therefore be assumed that the antibodies (except for anti-CBP) are not able to stably bind to the tri-snRNP.

Of all antibodies that were successfully tested in Co-IP assays only the anti-CBP antibody forms a stable complex with the tri-snRNP. However, experiments presented so far do not prove that this complex formation is the result of a specific interaction between the antigen binding site (ABS) of anti-CBP with the CBP tag. The ABS could as well cross-react with intrinsic epitopes on the surface of the tri-snRNP or the interaction could even occur unspecifically via the Fc-portion (C-terminal constant domains CH2 and CH3 of the heavy chains) of the antibody. To test if the anti-CBP antibody binds the tri-snRNP via its ABS, the ABS was blocked by incubation with increasing amounts of the anti-CBP immunizing peptide (see 2.1.4) prior to incubation with TAP-purified tri-snRNPs (Figure 3.14 A). A 1:1 ratio of antibody and peptide has only a weak influence on the Co-IP efficiency of anti-CBP compared to unblocked anti-CBP (Figure 3.14 A, lanes 3 and 5). However, the Co-IP efficiency of anti-CBP is already strongly reduced at a 10-fold molar excess of peptide over antibody (Figure 3.14 A, lane 6). An increase to a 100-fold molar excess does not further reduce the binding efficiency (Figure 3.14 A, lane 7). At the same time, the peptide has no influence on the Co-IP efficiency of tri-snRNPs by the anti-Snu114 antibody (lanes 8-12), showing that binding of the tri-snRNP is indeed blocked by the specific interaction between the peptide (= antigen) and the ABS of anti-CBP. The blocking of anti-CBP with the immunizing peptide was additionally tested in immunolabeling experiments (Figure 3.14 B), which were performed as described above (Figure 3.11) except for the pre-incubation of anti-CBP with a 100-fold molar excess of the immunizing peptide prior to incubation with TAP-purified tri-snRNPs. Pre-incubation with the peptide completely abolished anti-CBP-tri-snRNP complex formation since no antibody could be detected in the tri-snRNP fractions (Figure 3.14 B, black triangles), while the unblocked anti-CBP stably bound to the TAP-purified tri-snRNPs (Figure 3.14 B, red squares). Thus, the anti-CBP interacts with the tri-snRNP via its ABS.

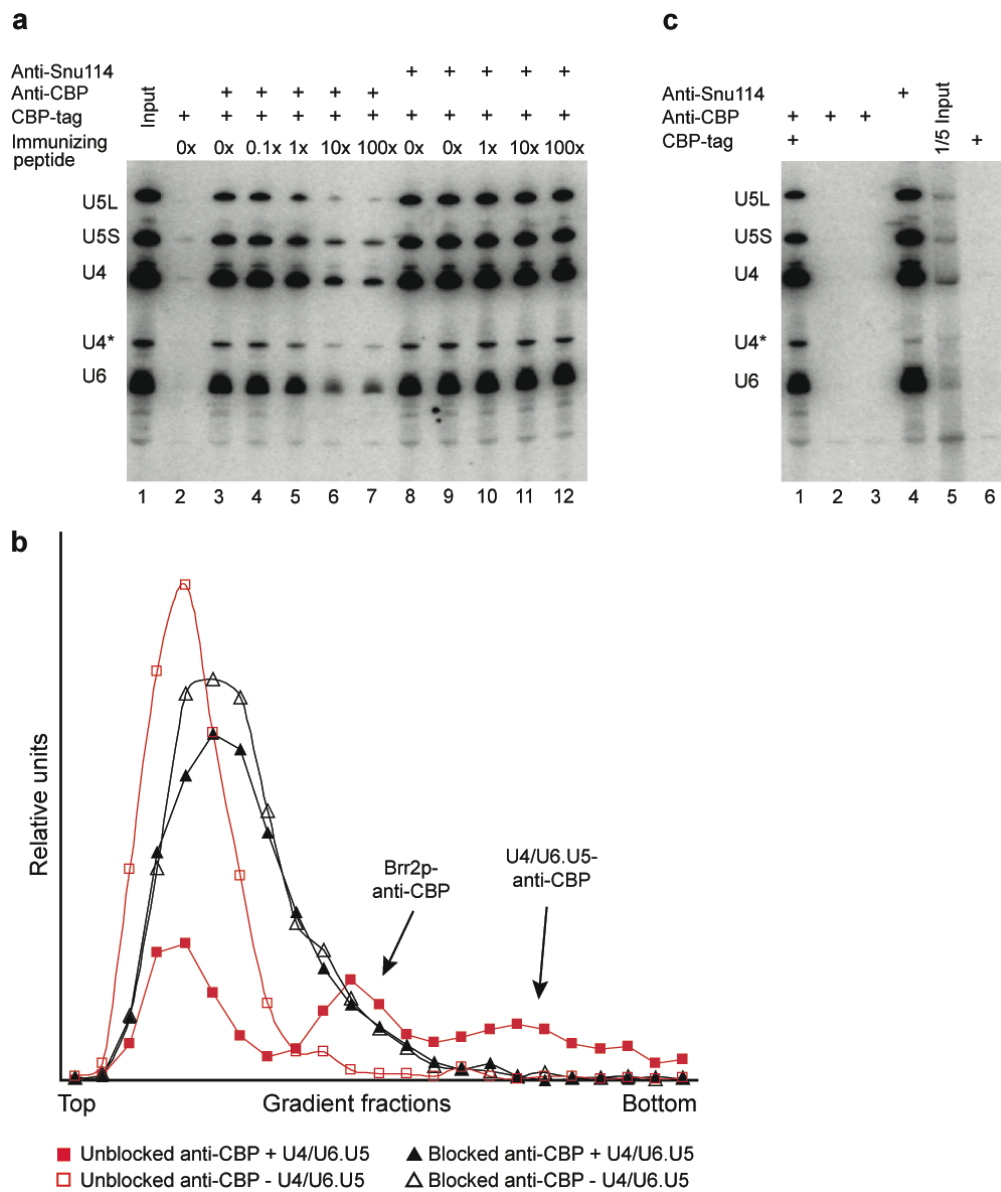


Figure 3.14 Testing of the specificity of the anti-CBP antibody interaction with CBP-tagged tri-snRNPs. Different specificity tests were performed to analyze if the anti-CBP antibody binds specifically and exclusively to the CBP of CBP-tagged tri-snRNPs. **A:** ProtA-sepharose bound anti-CBP was incubated with increasing molar excess of its immunizing peptide (see 2.1.4) prior to Co-IP of TAP-purified tri-snRNPs (lane 3-7). Co-IP with the anti-Snu114 antibody under identical conditions served as a control (lane 8-12; lanes 8 and 9: identical conditions as internal control). Co-precipitated snRNAs were extracted (see 2.2.4.3) and analyzed by northern blot using radioactively labeled DNA probes against U4, U5, and U6 snRNA, which were detected by autoradiography. **B:** Anti-CBP was blocked with a 100-fold molar excess of the immunizing peptide prior to incubation with TAP-purified tri-snRNPs. The reaction was sedimented on a glycerol gradient. The relative amount of antibody (y-axis) in the gradient fractions was analyzed by ELISA as described (Figure 3.11). The sedimentation of equal amounts of blocked and unblocked anti-CBP in presence and absence of tri-snRNP was compared. **C:** The specificity of anti-CBP was tested in a Co-IP of tri-snRNPs that do not contain a CBP tag (strain TR2a) from yeast total cell extract (lanes 2 and 3, identical, independent reactions). As control untagged tri-snRNPs were co-immunoprecipitated with anti-Snu114 antibody (lane 4) and TAP-purified tri-snRNPs were co-immunoprecipitated with anti-CBP antibody (lane 1). Co-precipitated snRNAs were analyzed as described in (A). **A/C:** The 'input' is the amount of tri-snRNPs that was used in each reaction. As a control, tri-snRNPs were incubated with the ProtA-sepharose in absence of an antibody (A, lane 2; C, lane 6).

To test if the tri-snRNP contains intrinsic epitopes for the anti-CBP antibody, Co-IPs were performed using extract from the untagged parent strain TR2a. In contrast to the anti-Snu114 antibody, anti-CBP could not co-precipitated tri-snRNPs from this strain (Figure 3.14 C, lanes 2, 3), showing that the tri-snRNP does not contain additional intrinsic epitopes for anti-CBP. Together these experiments demonstrate that the anti-CBP antibody specifically and exclusively interacts with the CBP of TAP-tagged tri-snRNPs.

To optimize the amount of anti-CBP antibody for immunolabeling studies, the antibody was titrated against TAP-purified tri-snRNPs (TAP tag at Brr2p). To estimate the amount of tri-snRNP purified from 1 L yeast culture, the concentration of the snRNAs (A_{260}) in tri-snRNP gradient peak fractions of large-scale purifications (from 12 to 16 L culture) was measured. Due to the still low amount of particles this measurement provided just a rough estimate of 0.5 to 1 pmol tri-snRNP per 1 L culture. However, this was sufficient for our purpose because we were only interested in the optimal ratio of antibody to tri-snRNP. For the titration experiments it was assumed that from 1 L culture approximately 0.75 pmol of tri-snRNP can be purified and the anti-CBP antibody was titrated from a 10-fold to a 40-fold molar excess (Figure 3.15).

The reactions were subjected to gradient centrifugation and gradient fractions were analyzed by ELISA. Figure 3.15 shows that an increase of the antibody concentration from a 10-fold to a 20-fold molar excess increases the amount of anti-CBP-tri-snRNP complexes, whereas a further increase of antibody concentration to a 40-fold molar excess does not, indicating that the binding is saturated. We therefore chose a 20-fold molar excess of anti-CBP for further labeling studies.

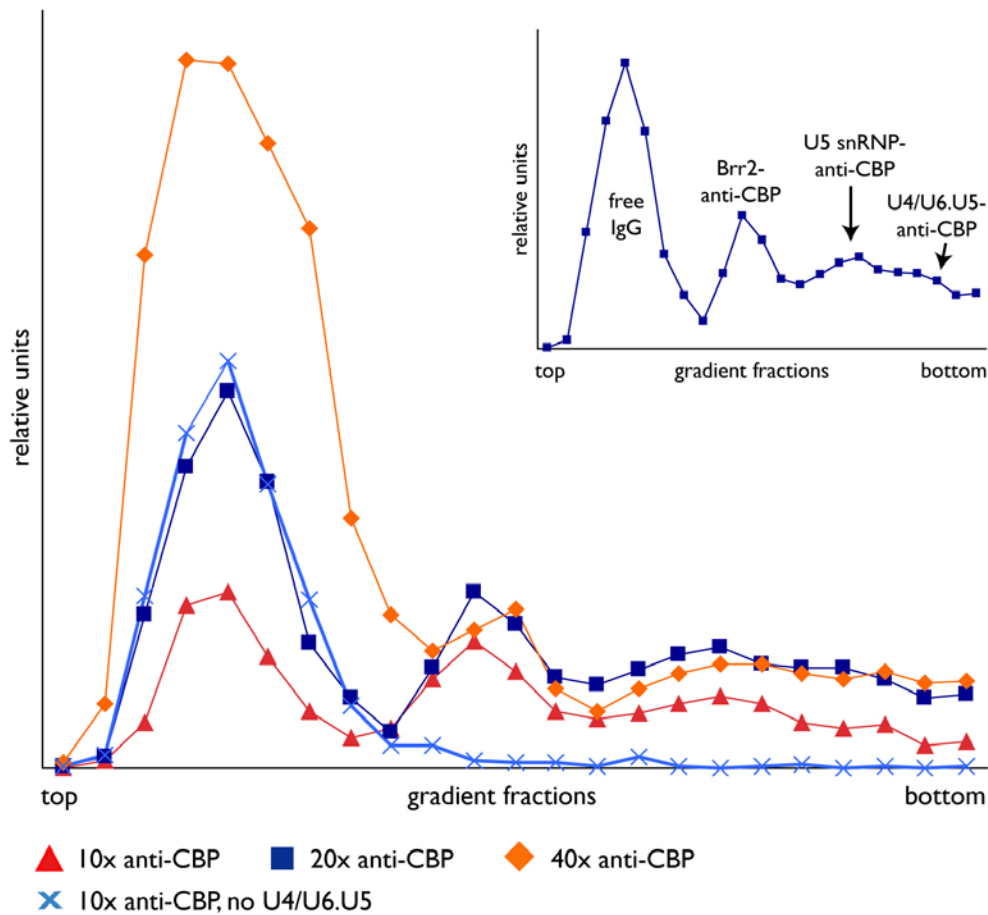


Figure 3.15 Titration of anti-CBP against TAP-purified tri-snRNPs. Tri-snRNPs were incubated with a 10- to 40-fold molar excess of anti-CBP antibody. Reactions were loaded on glycerol gradients and the relative amount of anti-CBP (y-axis) in the gradient fractions was determined by ELISA as described (Figure 3.11). As control a 10-fold molar excess of anti-CBP was loaded on a gradient in the absence of tri-snRNPs. Small line plot: the 20-fold molar excess of anti-CBP was selected for the labeling studies.

By using the TAP tag and the anti-CBP antibody for immunolabeling we could combine purification of the particles with localization of the tag in the electron microscope. For EM analysis of immunolabeled tri-snRNPs the complexes were fixed during gradient centrifugation according to the ‘GraFix’ protocol (Kastner et al., 2008). Particles were embedded in negative stain and grids were screened in the microscope for antibody-tri-snRNP-complexes. In addition to the direct inspection of the raw images, single-particle images were processed including multivariate classification (see 1.8) to corroborate the antibody position. Moreover, to confirm the antibody position by an independent method, the immunocomplexes were incubated after gradient centrifugation but prior to preparation of the EM-specimen with ProtA-coated colloidal gold (ProtA-gold), which specifically binds to the Fc-portion of the antibody via the ProtA. The ProtA-gold labeling experiments were performed in collaboration with E. Wolf (Cellular Biochemistry, Max Planck Institute for Biophysical Chemistry, Göttingen). The colloidal gold has a high electron density and is therefore visible as black dots in the EM images. Thus, ProtA-gold enhances the visualization of the antibody on the single particle level and allowed us to additionally verify the position of the antibody-labels. A sample that was incubated with ProtA-gold in the absence of anti-CBP served as a control (Figure 3.16, A). In this sample the gold particles were found predominantly in the background, whereas in the sample with the anti-CBP antibody, the gold was predominantly found attached to the tri-snRNP particles (Figure 3.16, B).

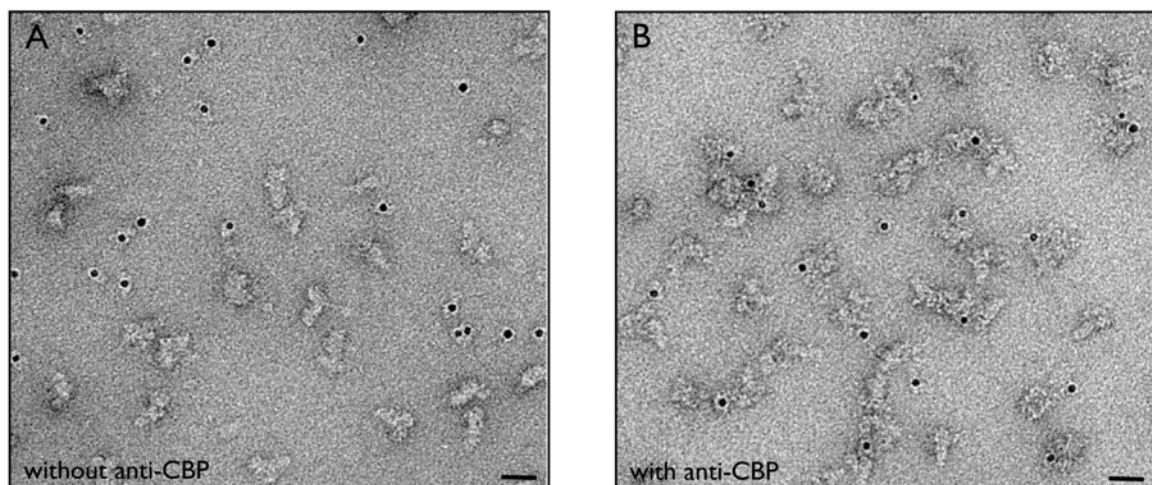


Figure 3.16 ProtA-gold labeling of anti-CBP antibody-tri-snRNP-complexes. Gradient fractions containing TAP-purified, anti-CBP labeled tri-snRNPs (or unlabeled particles as a control) were incubated with ProtA-coated colloidal gold. This reaction was directly used for EM-grid preparation. Shown is an EM overview of Prp8p-TAP-tagged tri-snRNPs incubated with ProtA-gold in the absence (A) or presence (B) of anti-CBP antibody. The bar represents 30 nm. The raw images were kindly provided by E. Wolf (Cellular Biochemistry, Max Planck Institute for Biophysical Chemistry, Göttingen)

In the case of ProtA-gold labeling less glutaraldehyde was used in the gradient (0.04% instead of 0.1%) to avoid a reduction of the antibody reactivity with the ProtA due to internal cross-linking reactions with the glutaraldehyde. We performed ProtA-gold labeling with the immunolabeled U5-specific proteins Brr2p, Prp8p and Snu114p (3.1.4, Figures 3.17 and 3.18).

3.1.5 Localization of the U5-specific proteins Brr2p, Prp8p and Snu114p

First, we focused on the mapping of the U5 proteins Brr2p, Prp8p, and Snu114p, which have been assigned a part in the catalytic activation of the spliceosome. At the same time we used the mapping of Brr2p to validate the applied labeling strategies. Tri-snRNPs purified via TAP-tagged Brr2p were incubated with an optimized amount (3.1.3.2, Figure 3.15) of anti-CBP antibody and subjected to gradient centrifugation according to the ‘Grafix’ protocol (Kastner et al., 2008). The anti-CBP antibody bound to Brr2p-CBP was visualized in the raw images as additional density close to the head of the particle (Figure 3.17 A, ‘single’). Upon alignment and multivariate classification, the class averages (‘avg’) exhibited a significantly improved SNR and statistically confirmed the uniqueness of the immunolabel and corroborated the antibody position. In most class averages the contact point between the antibody and the tri-snRNP was well defined, while the outline of the immunolabel was less well defined upon averaging due to the different orientations of the antibody with respect to the tri-snRNP (see 1.8).

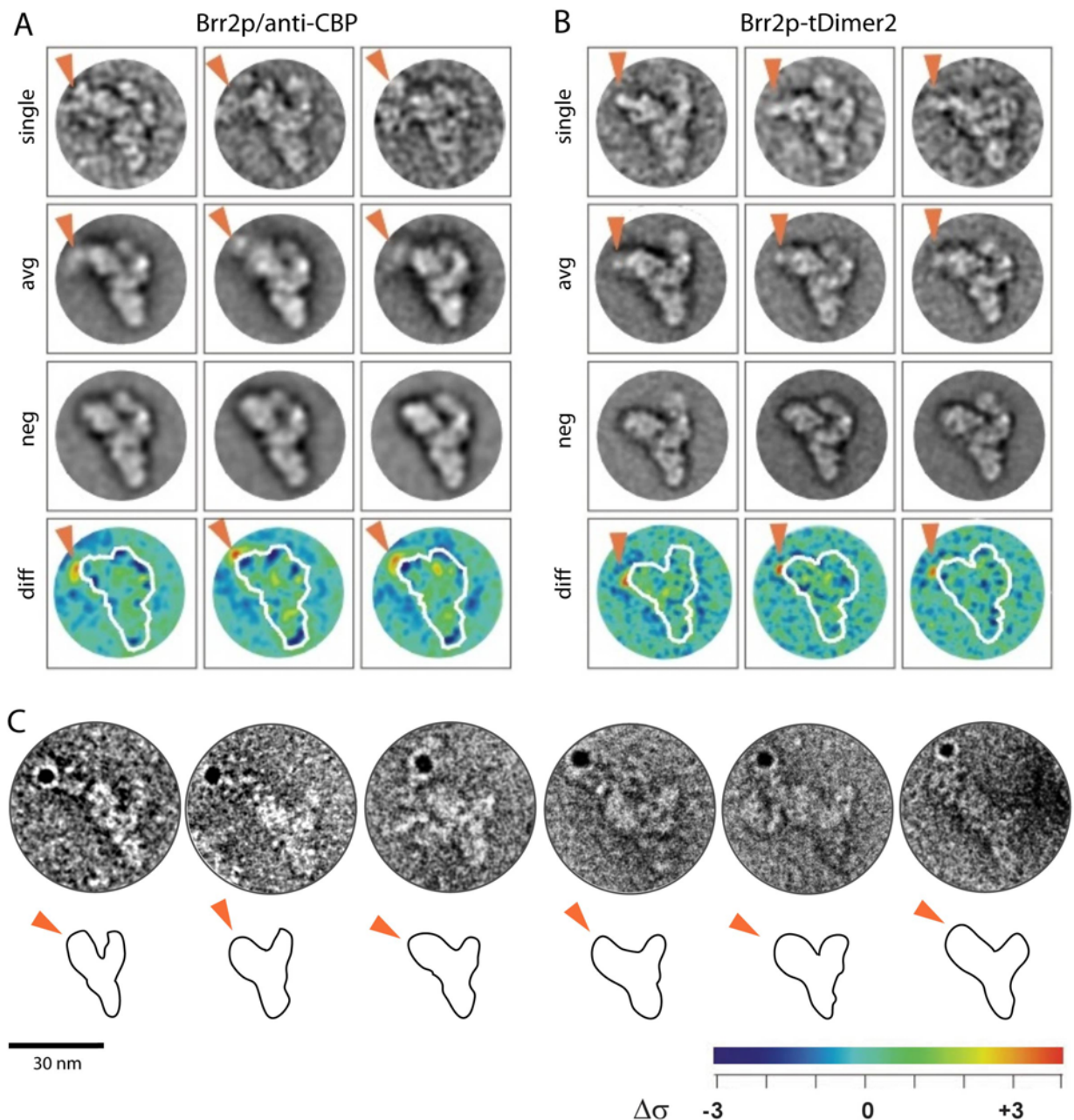


Figure 3.17 EM analysis of tri-snRNPs labeled at the C-terminus of Brr2p. Tri-snRNPs were prepared for EM as described (3.1.2). A: Anti-CBP antibody labeling of Brr2p-CBP tri-snRNPs with raw images (first row, 'single'), class averages ('avg'), corresponding unlabeled class averages ('neg'), and difference maps computed by subtracting the unlabeled from the labeled class averages ('diff'). Orange-red indicates a difference in density of $\geq 3\sigma$. B: Same analysis as in (A) with tri-snRNPs labeled at the C-terminus of Brr2p by the globular tag tDimer2. C: Raw images of ProtA-gold bound to anti-CBP antibody-tri-snRNP complexes. A – C: the red arrows highlight the position of the immunolabel and the tDimer2 label. Figure 3.17 A and B were kindly provided by B. Sander and M. Golas (Cryo-Electron Microscopy, Max Planck Institute for Biophysical Chemistry, Göttingen). Raw images from which ProtA-gold labeled tri-snRNPs were selected, were kindly provided by E. Wolf (Cellular Biochemistry, Max Planck Institute for Biophysical Chemistry, Göttingen).

By subtracting corresponding unlabeled ('neg') from the labeled averages ('avg') difference maps ('diff') were created. The class average pairs used for the calculation of the difference maps were selected such that the shape and the fine structural details of the average pairs were as similar as possible as determined by visual comparison. The difference in densities between labeled and unlabeled particles is specified as the standard deviation ' $\Delta\sigma$ ' and is visualized by a color code. $\Delta\sigma$ is zero when there is no difference in densities between the labeled and the unlabeled average (green and light blue color). $\Delta\sigma > 0$ indicates densities that are only present in the labeled average (yellow and red); $\Delta\sigma < 0$ represents densities unique to the unlabeled average (dark blue). The difference maps showed that the antibody caused a significant, i.e. $\geq 3\sigma$ change in density adjacent to the head domain. To confirm this result with a different method, the immunolabeled particles were incubated after gradient centrifugation with colloidal gold coupled to ProtA. In the raw images the antibody is visible as a bridge connecting the ProtA-gold to the tip of the head (Figure 3.17 C).

In our second independent approach we directly visualized the globular tDimer2 tag at the C-terminus of Brr2p. The tag was visualized in the raw images as pronounced, globular density at the very tip of the head-like structure (Figure 3.17 B, 'single'). In class averages of Brr2-tDimer2-tri-snRNPs the tDimer2 tag appeared as a bright density element (Figure 3.17 B, 'avg'), showing that the tag has a high structural stability. The structural stability together with the small size of the tDimer2 tag allowed to very precisely narrow down the position of the C-terminus of Brr2p to a small region at the tip of the head. Thus, the results of both labeling methods independently located the C-terminus of Brr2p to the same position, i.e. to the tip of the head.

Prp8p and Snu114p tightly interact with each other (Achsel et al., 1998; Liu et al., 2006), indicating that they might co-localize in the tri-snRNP. To investigate this, the C-termini of both proteins were first immunolabeled with the anti-CBP antibody. The antibodies bound to the C-terminus of Prp8p could be visualized in single images as well as in class averages in the middle of the main body, at the periphery opposite to the small arm (Figure 3.18 A). This result was additionally confirmed by ProtA-gold labeling of the immunocomplexes (Figure 3.18 C). Interestingly, upon incubation of Prp8p-CBP-tagged tri-snRNPs with the anti-CBP antibody the number of particles that display the typical view of the tri-snRNP in the electron microscope decreased. Instead, several untypical views were observed, where the binding site of the antibody could not be determined.

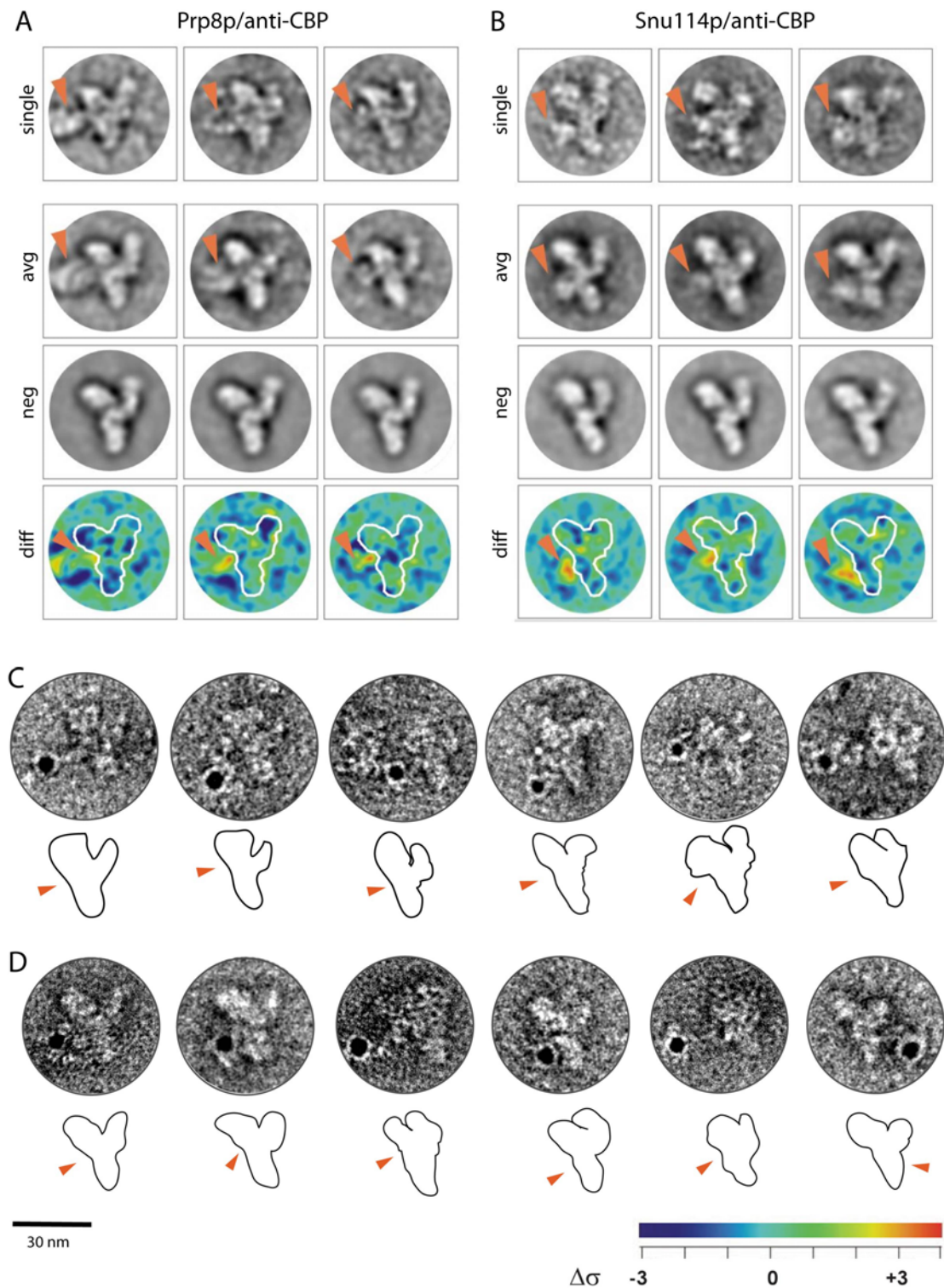


Figure 3.18 EM analysis of tri-snRNPs labeled at the C-terminus of Prp8p or Snu114p, respectively. Labeling analysis of tri-snRNP proteins as described in Figure 3.17. A: anti-CBP antibody labeling of Prp8p-CBP tri-snRNPs, B: anti-CBP antibody labeling of Snu114p-CBP tri-snRNPs, C: Raw images of ProtA-gold labeled anti-CBP antibody-tri-snRNP complexes CBP-tagged at Prp8p, D: Raw images of ProtA-gold labeled anti-CBP antibody-tri-snRNP complexes CBP-tagged at Snu114p. A – D: the red arrows highlight the position of the labels. Figure 3.18 A and B were kindly provided by B. Sander and M. Golas (Cryo-Electron Microscopy, Max Planck Institute for Biophysical Chemistry, Göttingen). Raw images from which ProtA-gold labeled tri-snRNPs were selected, were kindly provided by E. Wolf (Cellular Biochemistry, Max Planck Institute for Biophysical Chemistry, Göttingen).

Class averaging of Snu114p labeled tri-snRNPs revealed two antibody positions. (1) In most averages the antibody was located in the same region as the antibody bound to the C-terminus of Prp8p (Fig 3.18 B, left and central column). (2) In some averages, the antibody label pointed more towards the foot of the tri-snRNP (Figure 3.18 B, right column). These different positions of the antibody were also visible with the ProtA-gold labeled immunocomplexes (Figure 3.18 D). In ProtA-gold labeled anti-CBP-tri-snRNP complexes the antibody was visible as a bridge between the ProtA-gold and the tri-snRNP, pointing out the binding site of the antibody. Additionally, it could be observed that in a small subpopulation of particles the antibody bound to Prp8p and Snu114p was indeed bound to the middle of the main body, but it fell over to the opposite side of the tri-snRNP, next to the arm as shown in Figure 3.18 D for Snu114p (rightmost image). This indicated that the C-terminus of these proteins might not be located directly at the periphery on the left side of the particle but more central.

In contrast to the results obtained with Brr2p, the tDimer2 tag fused to Prp8p and Snu114p merely resulted in some subtle changes of the densities within the central portion of the main body (not shown), rather than in an additional domain that would protrude from the particle. Therefore, the tDimer2 tag was not considered for the localization of the C-termini of Prp8p and Snu114p. Our results show that the C-termini of Prp8p and Snu114p, in line with their tight association, are located in proximity to each other in the central part of the main body.

3.1.6 Localization of the U4/U6 portion of the tri-snRNP

We next identified the U4/U6 snRNP within the tri-snRNP. Prp3p and Prp4p form a heterodimer that is stably associated with U4/U6 snRNA. Moreover, the human Prp3p could be crosslinked to the 3' terminal half of U6 snRNA within stem II of the U4/U6 duplex (Nottrott et al., 2002). We therefore chose Prp3p as an indicator for the position of U4/U6 stem II. The C-terminus of Prp3p could be located in the central and upper region of the small arm by anti-CBP antibody labeling (Figure 3.19 A). The position of the tDimer2 tag at Prp3p could not be clearly identified (not shown). Therefore, the tDimer2 tag was not considered for the localization of the Prp3p C-terminus. We further corroborated the mapping of the U4/U6 snRNP to the small arm by anti-CBP antibody labeling of the Lsm8 protein, which in the Lsm core structure contacts the U6 snRNA 3' end (Achsel et al., 1999; Vidal et al., 1999) not far from the site at which Prp3p contacts the U6 snRNA. Immunolabeling of Lsm8p resulted in an additional antibody density at the upper part of the small arm, facing away either from the tip of the small arm or to the right side of the arm (Figure 3.19 B). The Lsm8p label is located more to the tip of the arm than

Prp3p. In comparison with the biochemical interaction data this provides first hints about the orientation of the U4/U6 duplex within the arm (see 4.4.3).

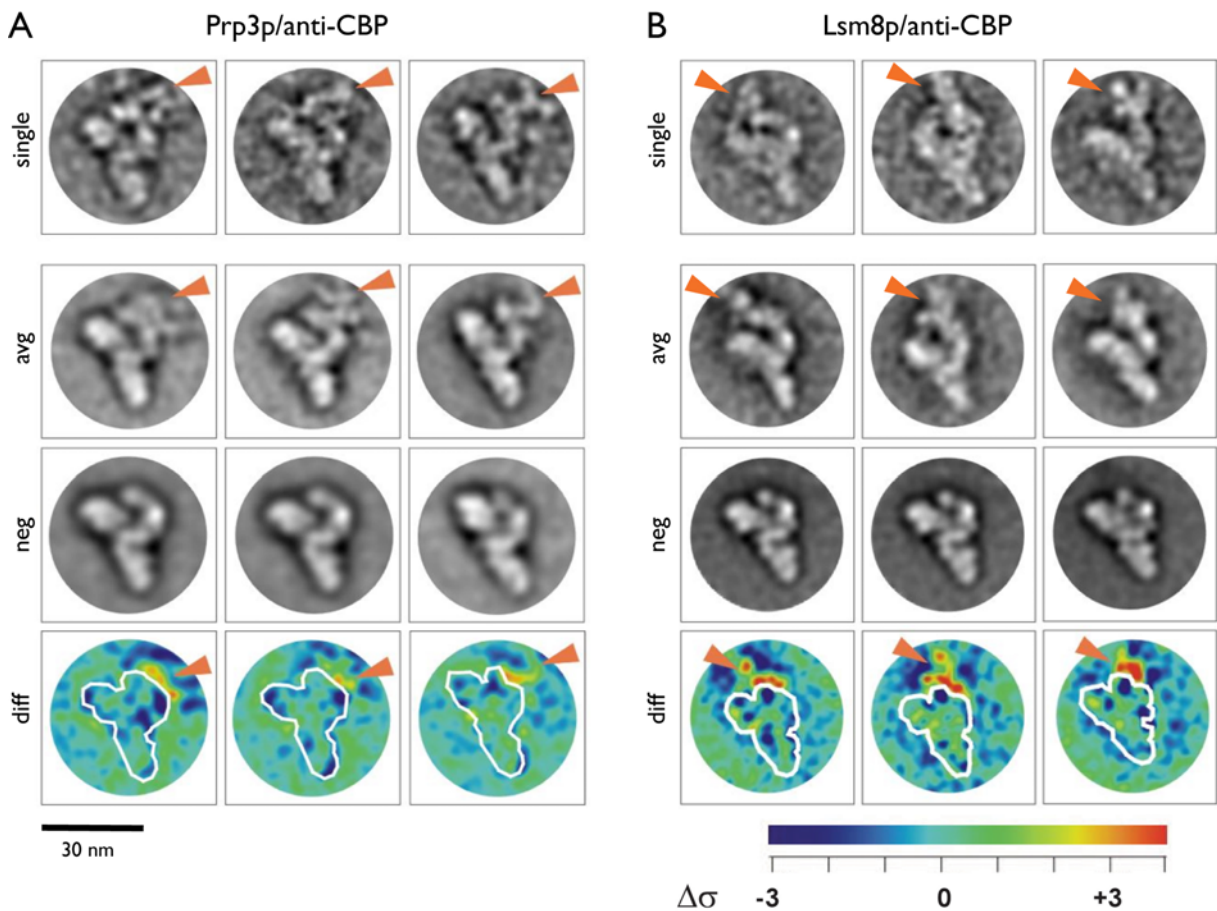


Figure 3.19 EM analysis of tri-snRNPs labeled at the C-terminus of Prp3p or Lsm8p, respectively. Labeling analysis of tri-snRNP proteins as described in Figure 3.17. A: anti-CBP antibody labeling of Prp3p-CBP tri-snRNPs, B: anti-CBP antibody labeling of Lsm8p-CBP tri-snRNPs. A and B: red arrows highlight the position of the labels. This figure was kindly provided by B. Sander and M. Golas (Cryo-Electron Microscopy, Max Planck Institute for Biophysical Chemistry, Göttingen)

We also investigated the position of the C-terminus of Prp4p by antibody- and tDimer2-labeling. However, although the tDimer2 tagging of Prp4p was successful (Figure 3.20, lane 2), we could not detect significant amounts of Prp4-tDimer2-tagged tri-snRNPs upon SDS-PAGE analysis of TAP-purified tri-snRNPs after gradient centrifugation. In contrast, U5 snRNP purification seemed to be unaffected (not shown). Moreover, almost no intact Prp4p-tDimer2-tagged tri-snRNP particles could be detected on the EM grids. The latter was also observed upon anti-CBP labeling of Prp4p-CBP-tagged tri-snRNPs, although

tri-snRNPs could be purified via TAP-tagged Prp4p (not shown). This indicated that tri-snRNPs were destroyed upon C-terminal labeling of Prp4p.

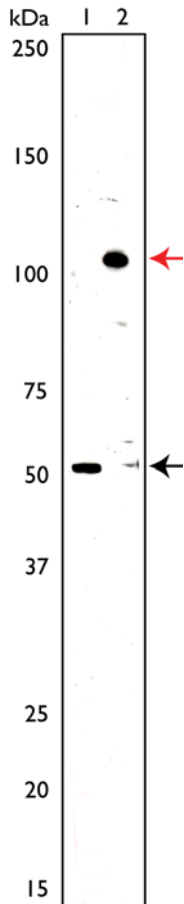


Figure 3.20 Verification of the expression of the Prp4p-tDimer2 fusion protein by western blot analysis. Prp4p-tDimer2-tagged tri-snRNPs were TAP-purified; proteins were extracted, ethanol precipitated, separated on a SDS-PAGE gel and blotted to a nylon membrane. The Prp4p-tDimer2 fusion protein was detected using an anti-Prp4p antibody (lane 2). As a control, tri-snRNPs without a tDimer2 tag at Prp4p were investigated (lane 1). The protein band is shifted from 52 kDa for the native protein (black arrow) to approximately 110 kDa (red arrow) upon tDimer2 tagging of Prp4p. The molecular weights (kDa) of protein standards are indicated on the left.

3.1.7 Localization of Prp6p and Prp31p

Finally, we mapped the position of Prp6p and Prp31p in the tri-snRNP, which in the human tri-snRNP act as bridging proteins between U5 and U4/U6 (Liu et al., 2006; Makarova et al., 2002; Schaffert et al., 2004). For this we performed immunolabeling as well as tDimer2-labeling. The tDimer2 tag at the C-terminus of Prp6p could be identified as a small, well defined protuberance in the linker region (Figure 3.21 B). It was located very close to a characteristic bright globular density element visible in the class averages at the base of the small arm (Figure 3.21 B and D). Immunolabeling of Prp6p consistently created an additional density next to the bright density element at the base of the small arm, facing away from the main body (Figure 3.21 A).

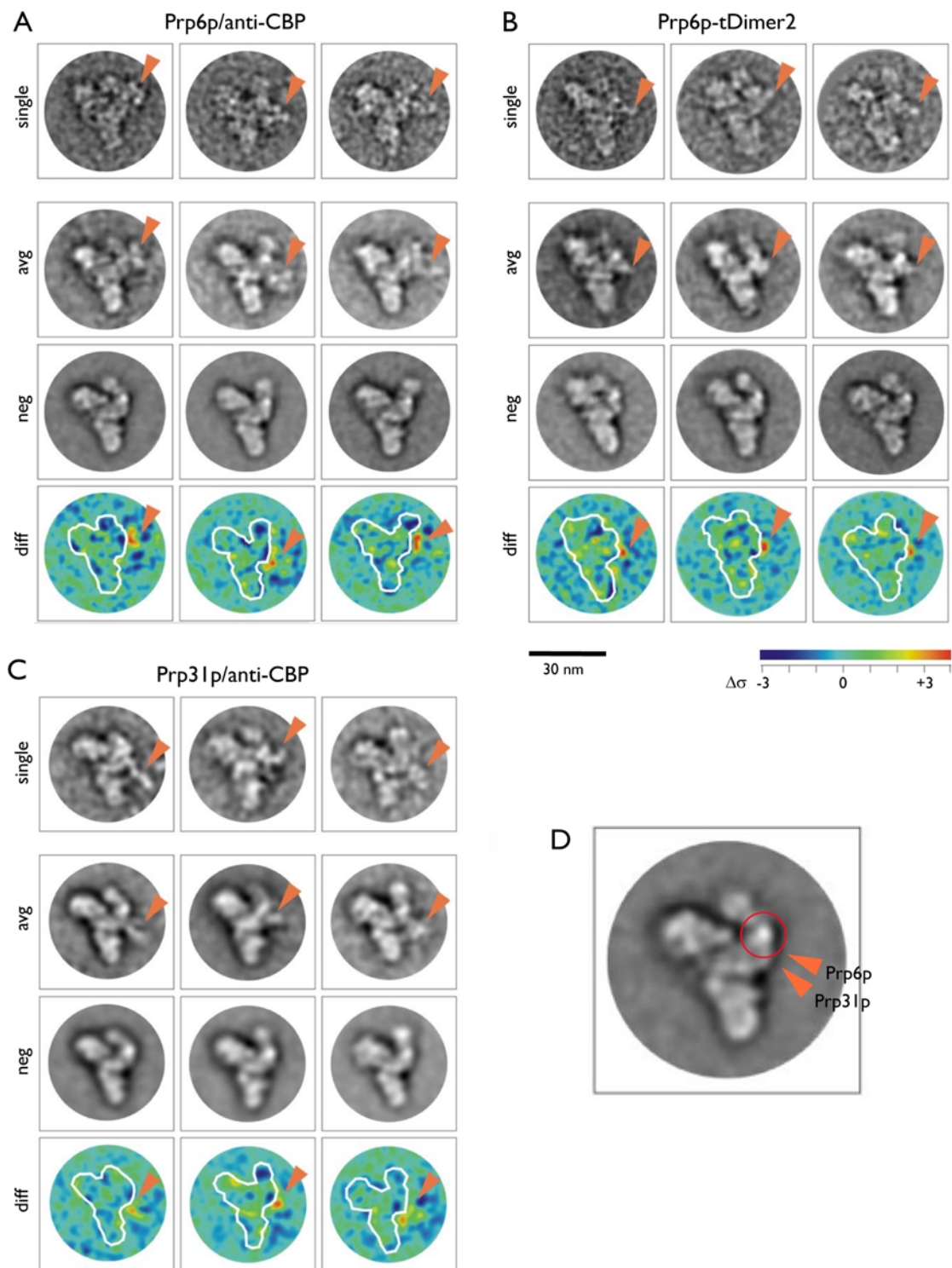


Figure 3.21 EM analysis of tri-snRNPs labeled at the C-terminus of Prp6p or Prp31p, respectively. Labeling analysis of tri-snRNP proteins as in Figure 3.17. Red arrows show the positions of the labels. A: anti-CBP antibody labeling of Prp6p-CBP-tagged tri-snRNPs, B: tri-snRNPs labeled at Prp6p with the tDimer2 tag, C: anti-CBP antibody labeling of Prp31p-CBP-tagged tri-snRNPs. D: Class average of an unlabeled tri-snRNP. A very characteristic bright density element at the base of the small arm is pointed out by a red circle. The red arrows indicate the slightly different positions of the labels attached to the C-terminus of Prp6p and Prp31p with respect to the bright density element, as determined from the labeled class averages. Figures A-C were kindly provided by B. Sander and M. Golas (Cryo-Electron Microscopy, Max Planck Institute for Biophysical Chemistry, Göttingen)

Interestingly, antibodies bound to the C-terminus of Prp31p were visualized at an almost identical position in the linker domain. However, the antibody bound to Prp31p appeared to be located more distant to the bright density than the tDimer2 tag and the antibody attached to Prp6p, closer to the main body (Figure 3.21 C and D). This indicated that Prp31p is located next to Prp6p within the linker region, but closer to the main body (Figure 3.21 C). The position of the tDimer2 tag at Prp31p could not be clearly identified (not shown). Therefore, the tDimer2 tag was not considered for the localization of the Prp3p C-terminus. Thus, our labeling studies indicate that the C-termini of Prp6p and Prp31p are located in the linker region between U5 and U4/U6, consistent with the biochemical and genetic data that indicate their function as bridging proteins.

3.1.8 N-terminal TAP tagging of tri-snRNP proteins for future labeling studies

C-terminal labeling of tri-snRNP proteins provided a comprehensive map of the yeast tri-snRNP (see 4.3). However, C-terminal labeling of the interesting U4/U6 protein Prp4p was not possible because it interfered with tri-snRNP stability. Moreover, by labeling the C-terminus of Prp8p and Brr2p, we localized only small regions of these rather extended proteins and we do not know where the rest of these proteins is located. For these reasons it would be highly desirable to also label other regions of the proteins. We therefore fused the TAP tag to the N-terminus of Prp4p, Brr2p, and Prp8p for future immunolabeling studies.

N-terminal TAP tagging works essentially in the same way as C-terminal TAP tagging (Figure 3.22) (Puig et al., 2001). A major difference is that the tagging cassette contains a *GAL1* promoter between the selection marker and the TAP tag (Figure 3.22). This is necessary because by integration of the N-terminal TAP-tagging cassette, the distance between the start codon of the target gene and its endogenous promoter becomes too big for the endogenous promoter to maintain the regulation of the target gene expression. After selection and testing of transformants, the *GAL1* promoter (which could in principle be used for overexpressing the tagged protein) is removed together with the marker gene using site-specific recombination via loxP-sites, induced by Cre recombinase. In the resulting strains the N-terminally TAP-tagged target gene is again placed under the control of its endogenous promoter (Figure 3.22).

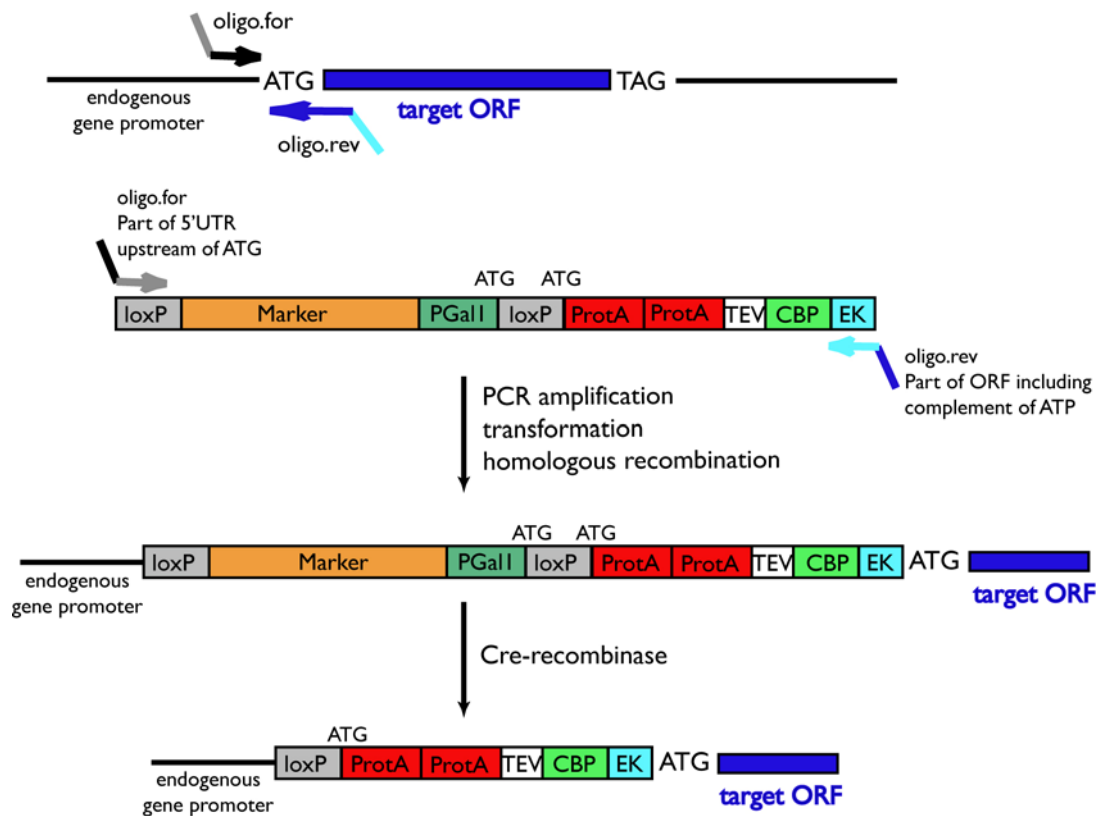


Figure 3.22: N-terminal TAP tagging strategy. The tagging cassette is amplified by primers containing regions of homology to the target gene upstream of the start codon (excluding ATG) and downstream of the start codon including ATG, respectively. The primers are designed such that the tag is fused in frame to the N-terminus of the target gene. The integration of the TAP cassette places the target gene under control of the GAL1 promoter. Finally, the GAL1 promoter and the marker are removed by Cre recombinase which is transformed into the cells on the plasmid pSH62 (Güldener et al., 1996), placing the TAP-tagged target gene again under the control of its natural promoter. The N-terminal TAP tag additionally contains a cleavage site for an enterokinase (EK), allowing for the complete removal of the tag after purification (which was not necessary for our studies).

Primers for PCR amplification of the tagging cassette from plasmid pBS1761 were designed as described in (Puig et al., 2001), introducing regions complementary to the sequences up- and downstream of the start codon of *PRP4*, *PRP8*, and *BRR2*, respectively. The yeast strain YPH499 (Sikorski and Hieter, 1989) was transformed with the purified PCR products and incubated on galactose-containing SC-TRP plates at 30°C for 3-4 days. Grown colonies were picked, streaked out on fresh selective plates and further incubated for 2-3 days at 30°C. Clones were tested for correct integration and expression of the tag by PCR and western blot analysis, respectively, as described for C-terminal TAP tagging (3.1.1.1). Of twelve tested Prp4p-transformants five showed correct integration and expression of the N-terminal TAP tag (Figure 3.23 A, B). 36 colonies were tested both of the Brr2p- and Prp8p-transformants. This

yielded in eight positive integrations for Brr2p and ten for Prp8p, respectively as determined by PCR analysis (Figure 3.23 A, and data not shown).

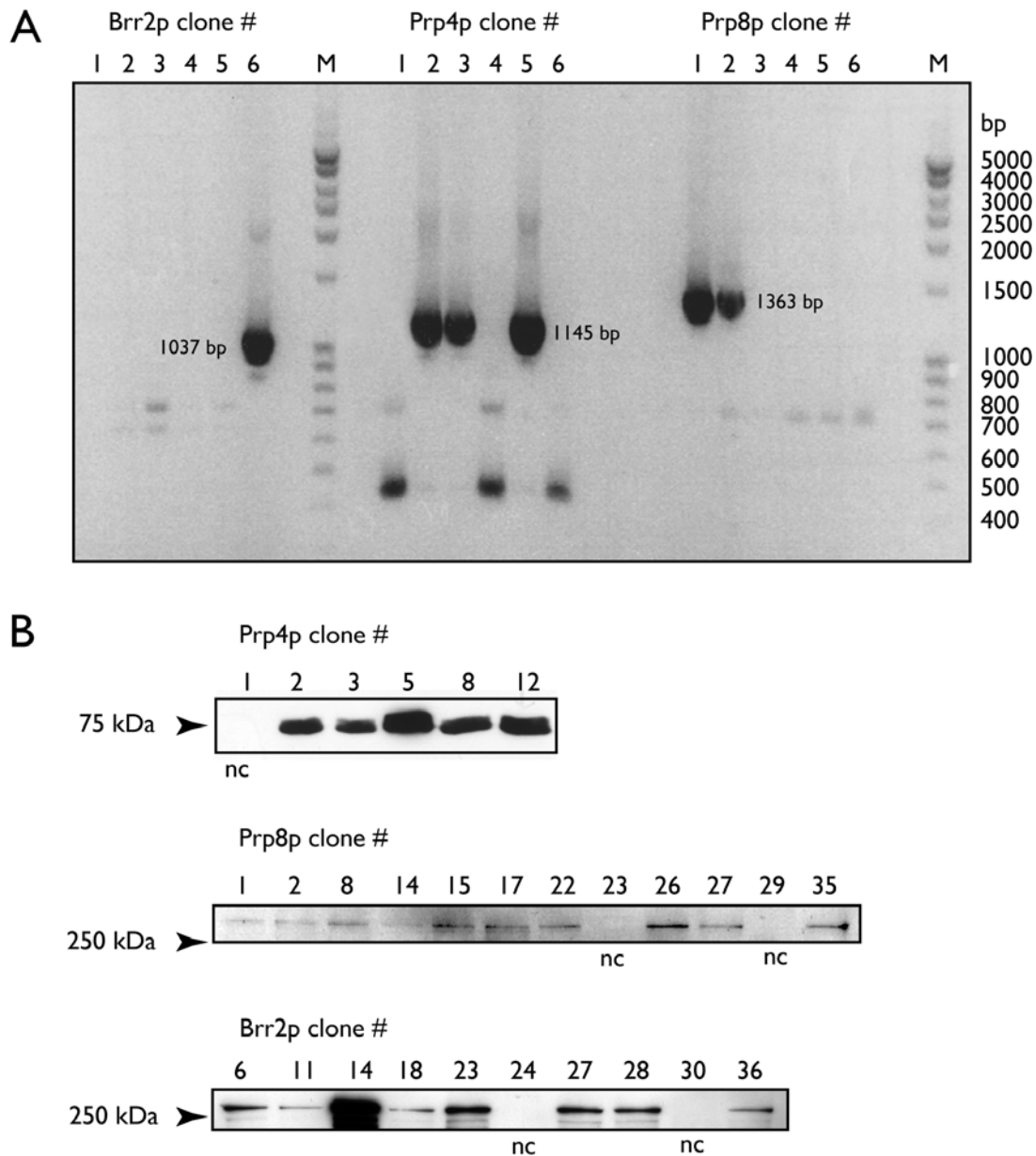


Figure 3.23: N-terminal TAP tagging of Prp4p, Brr2p, or Prp8p, respectively. A: Transformants were tested by PCR analysis for the correct integration of the N-terminal TAP tag. The forward primer (check.N.for; see 2.1.6) was designed such that it bound to the CBP part of the TAP tag, the reverse primer (check.N.rev; see 2.1.6) was complementary to a short sequence in the N-terminal region of the target gene. Thus, a PCR product was only obtained in case of correct integration of the tag as exemplified for the clones #1-6 of each protein. Expected product lengths in case of correct integration: Brr2p: 1037 bp, Prp4p: 1145 bp, Prp8p: 1363 bp. M = marker (lengths (bp) of the DNA fragments are indicated) B: All clones with a correctly integrated tag as shown by PCR analysis were tested for the expression of the fusion protein by western blot analysis using the PAP-antibody which binds to the ProtA of the TAP tag. Clones for which no product was obtained were selected as a negative control (nc): Prp4p clone #1; Brr2p clone #24 and #30; Prp8p clone #23 and #29

However, it was difficult to detect the fusion protein of Brr2p and Prp8p with the TAP tag by western blot analysis, probably due to the extended size of the proteins, which made the transfer from the gel to the nitrocellulose membrane very inefficient. Only with one Brr2p-transformant (#14) we obtained a strong western blot signal with the PAP-antibody at a size of approximately 270 kDa (Figure 3.23 B). However, we also obtained strong degradation bands of this protein (not shown).

After extension of the transfer time from 3 hr at 70 V to 24 hr at 20 V we detected signals also for the other Brr2p-transformants, as well as very weak signals for the Prp8p-transformants (Figure 3.23 B). As a negative control, transformants of Prp4p, Brr2p, and Prp8p, respectively, were selected, which had not shown a correctly integrated tag in PCR analysis. With these transformants we did not obtain a band in western blot (Figure 3.23 B, Prp4p clone #1, Brr2p clone #24 and #30; Prp8p clone #23 and #29). Two positive clones of each protein were selected (Brr2p #14 and #23; Prp8p #26 and #35; Prp4p #2 and #3) and transformed with the plasmid pSH62 (Güldener et al., 1996), containing the Cre recombinase. Upon incubation of liquid cultures of the clones at 30°C for transformation, we observed that the Brr2p clone #14 grew much slower than the other five clones (about one third of their speed), indicating that the integration of the tag in this clone causes problems. The transformed cells were plated on histidine-deficient YPG plates and incubated at 30°C for four days. The transformants grew very dense, similar to the transformation with the control plasmid (pRS313). The transformants were therefore streaked out again on histidine-deficient YPG plates to obtain single colonies. Then, six colonies of each transformation were streaked out on YPD medium to test for the excision of the *GAL1* promoter associated with the marker and for the loss of the plasmid. All streaked out colonies grew very well on YPD medium at 30°C, which shows that the *GAL1* promoter (together with the marker gene) was removed by the Cre recombinase. Thus, the N-terminally TAP-tagged proteins (Prp8p, Brr2p, and Prp4p) were placed again under the control of their endogenous promoter.

3.2 Investigation of the yeast U5 snRNP

3.2.1 Isolation of yeast U5 snRNPs using the TAP purification method

To obtain highly pure U5 snRNPs for mass spectrometry and EM analysis the particle was purified by the TAP method followed by glycerol gradient centrifugation. U5 snRNPs were purified via different TAP tagging strategies: In the strain YCB3 the TAP tag was fused to the C-terminus of the U5 snRNP protein Snu114p, and an additional ProtA tag lacking the TEV cleavage site was fused to the C-terminus of the U4/U6 snRNP protein Prp4p. Since both proteins are also components of the tri-snRNP, in the first affinity purification step (IgG-sepharose) U5 snRNPs, as well as U4/U6 snRNPs and tri-snRNPs were retained on the column. However, only U5 snRNPs can then be eluted by TEV cleavage because they do not contain ProtA tagged Prp4p. Figure 3.24 shows the snRNA (A) and protein distribution (B) of U5 snRNPs purified from this strain in the gradient after TAP purification.

Long and short U5 snRNAs (U5L and U5S) peak in fractions 9-11, which are essentially free of other snRNAs. Proteins co-sedimenting with the U5 snRNA were identified by mass spectrometry (in collaboration with Dr. H. Urlaub, Bioanalytic Mass Spectrometry, Max Planck Institute for Biophysical Chemistry, Göttingen) as indicated in Figure 3.24 C on the right. The protein composition was essentially the same as that of previously purified U5 snRNPs (Stevens and Abelson, 1999). However, from the excised protein bands no tryptic fragments of Prp28p and SmBp could be detected.

The U5 snRNPs purified from the strain YCB3 contained the protein Aar2p (Figure 3.24 C) which is a component of the yeast 16S U5 snRNP, a simpler form of the 18S U5 snRNP. The 16S Aar2p-U5 comprises only Prp8p, Snu114p, Aar2p, and the Sm proteins (Gottschalk et al., 2001), whereas the 18S U5 contains Brr2p instead of Aar2p, as well as Prp28p and Lin1p (Stevens et al., 2001). Thus, using TAP-tagged Snu114p we purified a mixture of the smaller (16S) and the larger (18S) U5 snRNPs that could not be separated with our purification procedure. To purify only the large form of U5, we TAP-tagged the 40 kDa protein Lin1p, which is unique for the 18S U5 snRNP. Although we could prove the correct integration and expression of the TAP tag at the C-terminus of Lin1p (not shown), we could not purify sufficient amounts of the 18S U5 snRNP for EM and MS analysis via TAP-tagged Lin1p. We therefore used a different strategy: TAP-tagged Brr2p (strain YEK2) co-purifies 18S U5 snRNP and tri-snRNP, but not the 16S Aar2p-U5 snRNP. The 18S U5 and the tri-snRNP can be separated by gradient centrifugation as shown in Figure 3.4. The protein composition of this 18S U5 snRNP was similar to that obtained from strain YCB3, except for the absence of Aar2p (Figure 3.24 D).

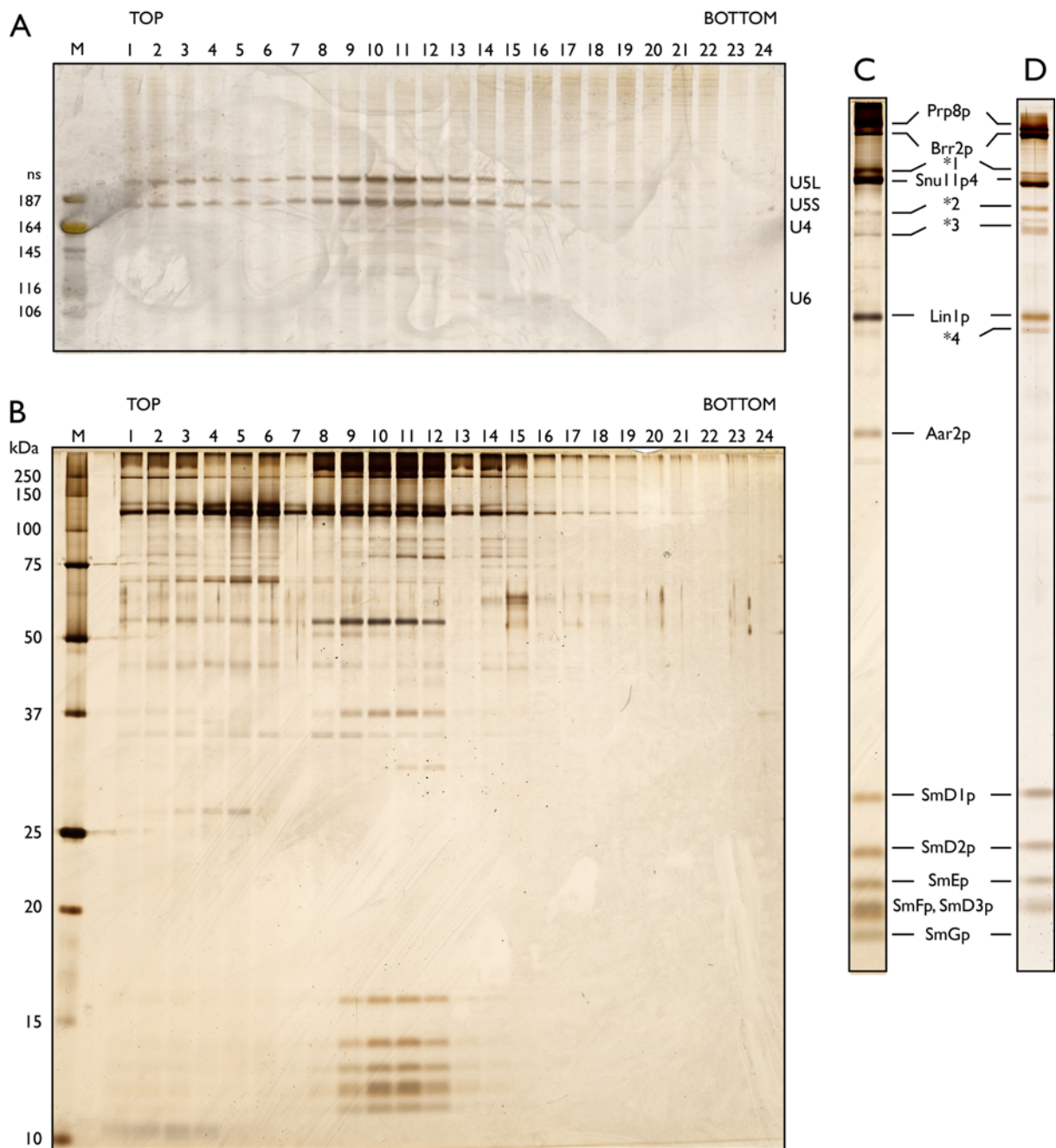


Figure 3.24 Purification of yeast U5 snRNPs by the TAP method. A – C: U5 snRNPs TAP-tagged at Snu114p and ProtA-tagged at Prp4p were TAP-purified and sedimented on a glycerol gradient. Gradient fractions were analyzed for their RNA (A) and protein (B) content by denaturing PAGE and SDS-PAGE, respectively. Gels were stained with silver. The molecular weights (kDa) of protein standards (B) as well as the lengths (ns) of the human snRNAs used as a marker (A; 'M') are indicated on the left. The yeast snRNA names are shown on the right (A). The protein bands of gradient fraction 10 were cut out and the proteins were identified by MS analysis as indicated in C. D: Silver stained proteins of a gradient fraction containing U5 snRNPs purified via TAP-tagged Br2p were also identified by MS analysis *1 = Snu114p, *2 = Prp6p, *3 = Spp381p, *4 = Prp4p.

3.2.2 Electron microscopy of TAP-purified yeast U5 snRNPs

To obtain first insight into the structure of the yeast U5 snRNP, TAP-purified particles were analyzed by negative stain EM. Sample preparation for EM was performed as described for the tri-snRNP (3.1.2). U5 snRNPs purified from strain YCB3 (Snu114p-TAP tag/Prp4p-ProtA) are not shown here because the particles were prepared by the sandwich method (enclosing the particles between two carbon films) (Sander et al., 2006), which turned out to have a flattening effect on the yeast U5 snRNP. Therefore, the U5 snRNPs purified via TAP-tagged Snu114p or Brr2p were prepared using a single carbon film.

EM analysis of U5 snRNPs purified via TAP-tagged Brr2p showed a population of elongated particles with a maximum dimension of 25 nm (Figure 3.25 A). Single particle image processing and image classification were performed, providing class averages at a good signal to noise ratio. The class averages showed that the particles possess one pointed and one broader end (Figure 3.25 B). The pointed end in several cases displays a roughly annular density, which appears to have a ring-like shape due to the accumulation of stain in its centre. However, the particles in the different averages differed strongly, not only in their structural details, but also in their overall shape. To test, if the different shapes represent different views of the same particle, the EM specimen was tilted in the microscope (not shown). The tilted images revealed that the different shapes did not result from different viewing angles.

We additionally analyzed U5 snRNPs purified via Snu114p, which contained at least a subpopulation of 16S Aar2p-U5 snRNPs. The particles revealed a very similar diversity of shapes (Figure 3.25 C), which in this case could at least be partially due to the presence of the Aar2p-U5 snRNP. However, it was not possible to distinguish between the two forms of the U5 snRNP in the electron microscope. Due to the heterogeneous appearance of the U5 snRNPs in the electron microscope and the difficulty to identify the different shapes, the yeast U5 snRNP was not used for 3D structure determination or labeling studies.

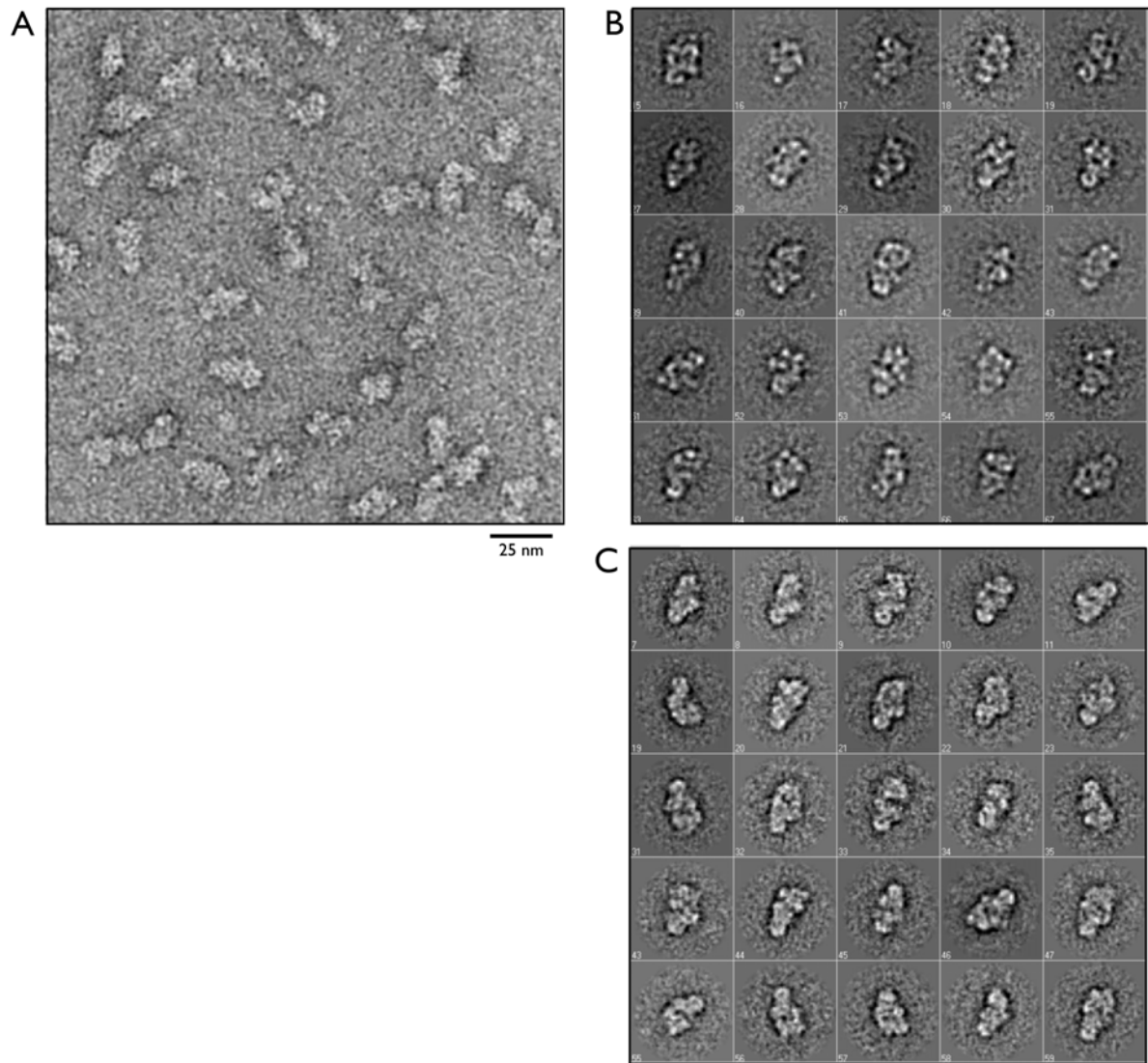


Figure 3.25 EM analysis of yeast U5 snRNPs purified via different TAP strategies. A: Representative EM overview image of negatively stained U5 snRNPs (Br2p-TAP tag). B: Class averages of U5 snRNPs purified via TAP-tagged Br2p, C: Class averages of U5 snRNPs purified via TAP-tagged Snu114p. Bar represents 25 nm. Raw image and class averages shown in this figure were kindly provided by B. Sander and M. Golas (Cryo-Electron Microscopy, Max Planck Institute for Biophysical Chemistry, Göttingen)

4 Discussion

Spliceosomal complexes have been characterized so far mainly biochemically by investigating the protein composition, protein-protein or protein-RNA interactions, as well as by functional studies of specific components. Moreover, EM structures of spliceosomal complexes [A, B, B Δ U1, and C (Behzadnia et al., 2007; Boehringer et al., 2004; Deckert et al., 2006; Jurica et al., 2004)] are available. On the other hand, not much is known about the structural arrangements of functionally important components (snRNAs, proteins, conserved regions of the pre-mRNA) within these complexes. Understanding the structures of spliceosomal complexes on the molecular level would help to understand how the different factors involved in pre-mRNA splicing cooperate to fulfill their intricate tasks.

We therefore established EM labeling studies in the yeast U4/U6.U5 tri-snRNP, an important building block of the spliceosome. Although it is well established that several components of the evolutionarily highly conserved tri-snRNP are involved in the formation and activation of the catalytic core as well as in disassembly of the spliceosome, the molecular architecture of this particle is still unknown. Of special interest is the position of the U5-specific proteins Prp8p, Brr2p and Snu114p, which are involved in a key step of the catalytic activation of the spliceosome, the U4/U6 snRNA unwinding. The present study describes the structural investigation of the yeast tri-snRNP by negative stain EM. By applying a twofold labeling strategy, we have mapped the positions of functionally important U5, U4/U6 and tri-snRNP-specific proteins in two dimensions and can thus provide the first structural model of the yeast tri-snRNP. This model has several implications for the interactions between tri-snRNP proteins during the unwinding of the U4/U6 snRNA.

4.1 The native yeast tri-snRNP is a dynamic particle and shows structural differences to the human tri-snRNP

EM investigation of purified yeast tri-snRNPs revealed a characteristic view of the complex, owing to a preferential orientation of the particles on the carbon film. The EM images obtained by negative staining display high contrast and reveal numerous fine-structural details of the triangular particles, which exhibit a slim main body with a pointed lower end and a broader 'head' structure. A smaller 'arm' domain is connected to the main body at a central linker region. Interestingly, the head and the arm domain adopt different positions relative to each other and to the main body, resulting in a 'closed' and an 'open' state (see 3.1.2). We suggest that the dynamics

of particle shape reflect a structural flexibility of the yeast tri-snRNP, although we cannot completely exclude the existence of subpopulations of tri-snRNPs with different protein compositions that could not be separated by our purification strategy. Such a subpopulation of tri-snRNPs could contain the Prp28 protein. The DExD/H-box helicase could not be detected in the tri-snRNPs purified in this study, as well as in previous purifications performed at 150–250 mM salt (Gottschalk et al., 1999; Stevens and Abelson, 1999; Stevens et al., 2001). However, Eliza Small and coworkers (Small et al., 2006) could purify tri-snRNPs via TAP-tagged Prp28p at 50 mM salt. Thus, Prp28p might be only loosely associated with the yeast tri-snRNP and in the majority of cases is easily lost during purification at physiological salt concentration (~ 150 mM KCl) due to its high salt lability.

The yeast tri-snRNP has a maximum dimension of 30–34 nm and thus is 3–4 nm longer than the human U4/U6.U5 particle (Sander et al., 2006). EM images of the human tri-snRNP also displayed a triangular particle that – in its overall shape –resembles the closed form of the yeast tri-snRNP, showing that in addition to the high evolutionary conservation of the tri-snRNP's components also the structure is partially conserved. However, the yeast tri-snRNP appears to be slimmer than the human tri-snRNP, especially in the central region of the particle, which could be due to the additional proteins contained in the human tri-snRNP that are not part of the yeast particle (100K/Prp28p, 65K/Sad1p, 40K, 27K, 20K; see 1.5, Table 1.1). A major difference between the yeast and the human tri-snRNP is the pronounced separation of the upper part of the yeast tri-snRNP into a head and a smaller arm domain. This was not observed in the human tri-snRNP, although the broader (upper) part of the human complex is also divided into two parts by a cleft, including a roughly annular head domain (Sander et al., 2006). However, in contrast to the yeast particle, where head and arm are well separated from each other in the 'open' state (see 3.1.2, Figure 3.6 C), the two subdomains created by the cleft in the human tri-snRNP stay in proximity to each other (Sander et al., 2006).

The head domain of the human tri-snRNP contains part of the U5 snRNP – as determined by fitting the 3D structure of the human U5 snRNP into the tri-snRNP structure (Sander et al., 2006) – and likely corresponds to the head-like structure of the yeast tri-snRNP containing the U5-specific protein Brr2p (4.3). Interestingly, the head domain of the human tri-snRNP shows a structural flexibility relative to the main body (Sander et al., 2006), which might be similar to the movements of the head domain observed in the yeast tri-snRNP (see 3.1.2, Figure 3.6, C).

4.2 A two-fold labeling strategy allows for the clear localization of functionally important proteins within the yeast tri-snRNP

Due to the structural dynamics of the yeast tri-snRNP a 3D structure determination of the particle and the localization of its proteins in 3D was not possible (see 1.8). Therefore, the labeling studies were performed in 2D, namely on the level of single images and class averages. In principal, the preferential orientation of the yeast tri-snRNP on the carbon film together with the high quality of the images obtained by negative staining makes the yeast tri-snRNP an ideal particle for 2D localization studies (see 1.8) without the necessity for 3D structure determination. However, the structural dynamics of the particle also posed a challenge for the 2D localization of the labels, especially for the image processing (see 1.8).

To localize selected proteins within the yeast tri-snRNP by EM, we genetically fused a 54 kDa globular protein tag, tDimer2, to the C-terminus of the proteins in a haploid yeast strain by homologous recombination. Thus, every copy of the protein that is expressed in the cell should carry the tag. This is an advantage compared to traditional labeling methods such as immunolabeling, where usually not more than 40-50% of the proteins are labeled. Interestingly, during testing of the transformants for correct expression of the tDimer2 fusion protein by SDS-PAGE analysis (see 3.1.3.1, Figure 3.8), for several of the tagged proteins we observed a weak band migrating like the native (untagged) protein. Possibly, the tag is very sensitive to cleavage by proteases and is sometimes lost during tri-snRNP purification. Since this was not observed to the same extent for all tagged proteins, this effect might also depend on the position of the tag within the particle and its accessibility for proteolytic cleavage.

The direct visualization of a 54 kDa tag within a particle of 1.5 MDa in 2D EM images is challenging and requires high-quality EM data obtained by uniform staining, high image contrast, good SNR and careful image processing. The tag can be seen most easily if it protrudes from the periphery of the particle in the image plane. However, if the tag protrudes from the particle in direction of the electron beam, the visualization in 2D becomes difficult (see 1.8). EM analysis of tDimer2-labeled tri-snRNPs showed that the tag has a high structural stability, because it appeared in the class averages as a well defined protuberance (see 3.1.4, Figure 3.17 B, and 3.1.6, Figure 3.21 B). The structural stability in combination with the small size of the tDimer2 tag allowed for the very precise definition of the label's position within the tri-snRNP (4.3). However, due to the structural flexibility of the tri-snRNP in the arm region and in the central part of the main body, the tDimer2 tag could not be clearly visualized for all labeled proteins.

In a complementary and independent labeling approach we immunolabeled the C-terminally tagged proteins using a tag-specific antibody. This ensured that the antibody binds with the same sensitivity and specificity to all tagged proteins, providing a better comparability of the labeling data than the use of different protein-specific antibodies. Moreover, we wanted to localize the cap-structure of the snRNAs using a cap-specific antibody. Interestingly, of the three antibodies that efficiently precipitated tri-snRNPs in Co-IP assays (anti-CBP, and anti-GFP, both tag-specific; and H-20, cap-specific), only the anti-CBP antibody remained stably associated with the tri-snRNP also during gradient centrifugation. It could be excluded experimentally that the absence of antibody-tri-snRNP complexes was the result of a disintegration of the particles upon antibody binding (see 3.1.3.2, Figure 3.13). Another possibility for the absence of antibody-tri-snRNP complexes could be a destruction of the immunocomplexes due to the forces applied on the particles during gradient centrifugation. However, glutaraldehyde fixation of tri-snRNPs incubated with the H-20 antibody, which should stabilize possible immunocomplexes during gradient centrifugation did not yield higher amounts of H-20-tri-snRNP complexes (not shown). Together, these results indicate that no stable immunocomplexes were formed with the H-20 and the anti-GFP antibody. However, the question remains why those antibodies precipitated tri-snRNPs in Co-IPs. One explanation could be that in the Co-IPs a much higher excess of antibody (at least 40-fold higher than in the immunolabeling assays) was used. Due to the high excess of antibody, the Co-IP efficiency might appear to be satisfying, although the binding efficiency of the antibody in reality is quite low.

The comparatively large anti-CBP antibody could be visualized with all CBP-labeled proteins except for Prp4p. Interestingly, the density of the label was sometimes larger than expected from a single antibody. By TAP purification not only tri-snRNPs are purified but also the free TAP-tagged protein. Since the anti-CBP antibody was incubated directly with the eluate of the calmodulin column, the antibody possibly formed heterotrimeric complexes with the tri-snRNP and the free TAP-tagged protein. The increased size of the immunolabel strongly facilitated its visualization in the electron microscope. The antibody was directly visualized in single images. In addition, the careful selection and alignment of immunolabeled particles allowed to perform image classification and class averaging. Although the density of the antibody is less well defined upon averaging due to the flexibility of the immunolabel, image processing proved the statistical significance and uniqueness of the label positions with all seven labeled proteins.

The position of the antibody could be determined very precisely when the binding site of the antibody was located at exposed positions within the tri-snRNP (i.e. at the tip of the head or

in the linker region; see 3.1.4, Figure 3.17 A, and 3.1.6, Figure 3.21 C and Figure 4.1 A). If the binding site was not exposed, like in the central part of the main body or of the arm domain, the rotational freedom of the antibody complicated the localization (see 1.8). In these cases the labeling data required the definition of larger areas for the possible localization of the labeled C-terminus (Figure 4.1 A). Altogether, the flexibility of the immunolabel in combination with the structural dynamics of the tri-snRNP posed quite a challenge for the exact localization of the antibody position. Nevertheless, the immunolabeling of tri-snRNP proteins provided highly specific results of satisfactory quality [as shown by biochemical (see 3.1.3.2, Figure 3.14) and statistical analysis (see 3.1.4-3.1.6)].

Importantly, the localization data obtained by the two independent methods were very consistent, confirming the validity of our approach. The two-fold labeling strategy in combination with the unique quality of the EM data for the first time allowed for the comprehensive mapping of a spliceosomal particle and to propose a structural model.

4.3 Structural model of the yeast tri-snRNP based on the labeling studies

Applying a set of diverse, independent techniques, we localized the C-termini of seven targeted proteins, Prp8p, Brr2p, Snu114p, Prp3p, Lsm8p, Prp6p, and Prp31p. The colored areas depicted in Figure 4.1 A indicate the regions in which the C-termini of the investigated proteins are located with the highest probability. They were defined by visual comparison of the label positions in a large number of class averages and fitted manually into the tri-snRNP's 2D image. The indicated outlines of these areas are therefore not to be taken as the definite border of the region in which the C-termini are located. The size of the areas reflects the accuracy with which the position of the label (tDimer2 tag or anti-CBP antibody) could be determined. This accuracy depended strongly on the flexibility and size of the label, as well as on the position of the label within the tri-snRNP (see 1.8 and 4.2).

In case of Prp6p and Brr2p, the very precise information obtained from the small and structurally stable tDimer2-tag allowed to narrow down the position of the C-termini to a strikingly small region in the linker and at the tip of the head, respectively (Figure 4.1 A). Due to the exposed position of the Prp31p C-terminus in the structurally stable linker region, the immunolabeling of this protein also provided very precise information (see also 3.1.6, Figure 3.21 C). The antibody bound to the C-terminus of Lsm8p was detected at the upper part of the small arm, facing away either from the top of the arm or to the right side of the arm (see 3.1.5, Figure 3.19 B). This did not allow to determine the exact binding position of the antibody

and therefore required the definition of a larger area (Figure 4.1 A). Similarly, due to the rotational freedom of the anti-CBP antibody, the positions of the C-termini of Prp8p, Snu114p, and Prp3p in the central part of the main body and in the smaller arm domain, respectively could not be determined as precisely as that of Brr2p, Prp31p, and Prp6p. Moreover, the antibody bound to Snu114p seemed to vary between a central and a lower position, which additionally increased the area defined for the Snu114p C-terminus (Figure 4.1 A).

Long and short U5 snRNAs (U5L and U5S) peak in fractions 9-11, which are essentially free of other snRNAs. Proteins co-sedimenting with the U5 snRNA were identified by mass spectrometry (in collaboration with Dr. H. Urlaub, Bioanalytic Mass Spectrometry, Max Planck Institute for Biophysical Chemistry, Göttingen) as indicated in Figure 3.24 C on the right. The protein composition was essentially the same as that of previously purified U5 snRNPs (Stevens and Abelson, 1999). However, from the excised protein bands no tryptic fragments of Prp28p and SmBp could be detected.

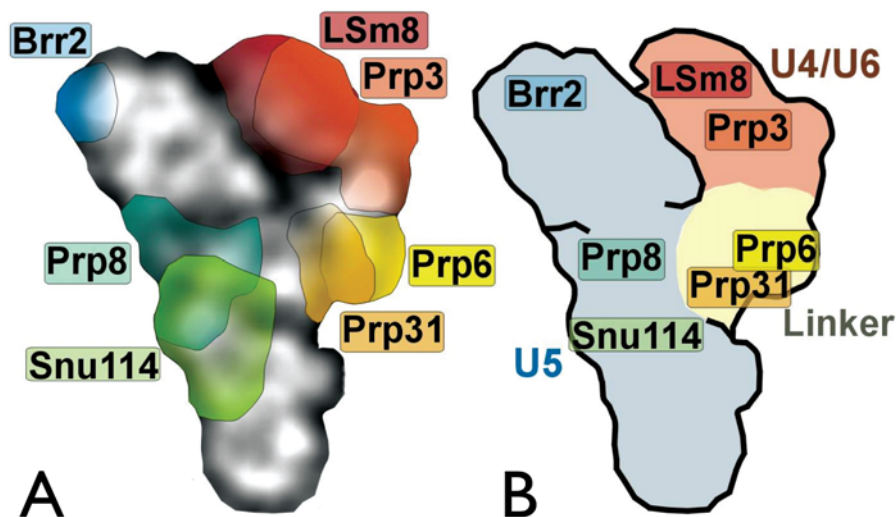


Figure 4.1 Structural model of the yeast tri-snRNP (see main text). A: The location assignment of the C-termini of Brr2p and Prp6p is based on the precise labeling by tDimer2 resulting in the smallest of all consensus regions. The areas defined for the C-termini of the other proteins are based on the immunolabeling data. B: The labeling data suggest that the main body of the tri-snRNP comprises the U5 snRNP, whereas the arm consists of the U4/U6 snRNP. Prp6p and Prp31p, which have been suggested to connect U5 to U4/U6 (Liu et al., 2006; Makarova et al., 2002; Schaffert et al., 2004) are located in the linker region that connects the arm to the tri-snRNP's main body. This figure was kindly provided by B. Sander and M. Golas (Cryo-Electron Microscopy, Max Planck Institute for Biophysical Chemistry, Göttingen)

Our labeling studies located the C-termini of the tightly interacting U5-specific proteins Brr2p, Prp8p, and Snu114p in the tri-snRNP's main body, suggesting that the main body harbors

the U5-snRNP (Figure 4.1 B). The C-terminus of the 246 kDa protein Brr2p is located at the very tip of the head region. Since head and arm domain are well separated in many class averages, the only possible direction in which this large protein can extend is towards the centre of the main body. In contrast, the central localization of the C-termini of Prp8p and Snu114p does not allow to make a statement about the orientation of these proteins within the particle.

However, yeast two-hybrid studies in yeast and human have shown that fragments of Prp8p can bind to fragments of Brr2p and vice versa (van Nues and Beggs, 2001). These data indicate that the two proteins might directly interact in native tri-snRNPs. We therefore propose that at least a part of the 280 kDa protein Prp8p extends towards the head domain of the tri-snRNP and might thus be in proximity to or even in direct contact with Brr2p. Similarly, the proximity of the C-termini of Prp8p and Snu114p allows to suggest a direct interaction between these two proteins, a model supported also by yeast two-hybrid interaction data (Dix et al., 1998; Liu et al., 2006) and the tight physical interaction of human Prp8p and Snu114p in an RNA-free complex (Achsel et al., 1998).

The localization of Prp3p and Lsm8p maps the U4/U6 snRNP to the small arm of the tri-snRNP (Figure 4.1 B). Lsm8p is located in the upper region of this arm, while Prp3p seems to map to a lower, more central region of the arm. It has been shown that the Lsm proteins and Prp3p contact the U6 snRNA at the extreme 3' end (Vidal et al., 1999) and in the region of the U4/U6 stem II (Nottrott et al., 2002), respectively. Thus, our labeling studies might provide initial insight into the orientation of the U4/U6 duplex within the small arm of the tri-snRNP. According to our results the 3' end of the U6 snRNA would then be located in the upper part of the arm, which thus might also contain the Lsm ring, whereas the U4/U6 stem I might be located shortly below.

Since in many particles the arm is well separated from the head, we exclude an extension of U4/U6 into the head domain. Moreover, the size of the U4/U6 snRNP (~ 0.3 MDa) makes it unlikely that the U4/U6 snRNP extends beyond the linker region. Thus, the arm comprises the U4/U6 snRNP, which is connected by Prp6p and Prp31p in the linker region to the main body containing the U5 snRNP (Figure 4.1 B). This corresponds well to the proposed function of Prp6p and Prp31p as bridging proteins between U5 and U4/U6 in the human tri-snRNP (Liu et al., 2006; Makarova et al., 2002; Schaffert et al., 2004). The localization of U5 and U4/U6 within the yeast tri-snRNP corresponds well to the position of their human counterparts in the human tri-snRNP, which was determined by fitting the 3D structures of purified U5 and U4/U6 snRNPs into the 3D structure of the human tri-snRNP (Sander et al., 2006).

4.4 Functional implications from the labeling studies

4.4.1 Snu114p might regulate the activity of downstream proteins by structural rearrangements

It is well established that the U5-specific protein Brr2p is the factor which catalyzes U4/U6 snRNA unwinding during the catalytic activation of the spliceosome, and that, as an integral component of the spliceosome, its activity has to be tightly controlled throughout the splicing cycle. Two other U5 snRNP proteins, Prp8p and Snu114p, have been strongly suggested to control Brr2p. However, the currently available biochemical and genetic data (Bartels et al., 2002; Bartels et al., 2003; Brenner and Guthrie, 2005; Fabrizio et al., 1997; Kuhn et al., 2002; Small et al., 2006) do not explain the exact mechanism of (1) U4/U6 snRNA unwinding and (2) the regulation of Brr2p activity.

One possible mechanism for Brr2p regulation would be a direct control by Snu114p. This GTPase has been shown to regulate U4/U6 snRNA unwinding in purified yeast tri-snRNPs in a guanine nucleotide state dependent manner (Small et al., 2006). The GTP-bound state of Snu114p seems to promote U4/U6 unwinding, whereas the GDP-bound state represses unwinding. Snu114p is a homolog of the eukaryotic ribosomal translocation factor 2 (eEF-2) (Fabrizio et al., 1997) as well as of the bacterial elongation factor G (EF-G). Because of the high sequence similarity between the two proteins (26% homology, 46% similarity) (Fabrizio et al., 1997), the domain structure of eEF-2 most likely also applies to Snu114p, with the exception of a 120-amino-acid N-terminal extension, which is unique to Snu114p. In Figure 4.2 two crystal structures of eEF-2 are shown, the apo eEF-2 (ExotoxinA-eEF2 complex, (Jorgensen et al., 2005); Figure 4.2 A), and the eEF-2 in complex with the translocation inhibitor sordarin (EF-2-sor, (Jorgensen et al., 2003); Figure 4.2 B). Both structures provide clear evidence that the eEF-2 is a highly flexible protein. Upon sordarin binding the domains IV and V undergo a large conformational change relative to the domains I and II, rotating around a linker between domain II and III. The conformational change in eEF-2/EF-G is thought to trigger the GTP-driven translocation of the aminoacyl-tRNA from the A to the P site (Stark, Holger et al., 2000; Stark, H. et al., 2000; Taylor et al., 2007) by inducing long-range and large scale conformational rearrangements in the ribosome (Stark, H. et al., 2000). Due to the strong homology between eEF-2 and Snu114p a similar flexibility of domain IV and V is assumed for the C-terminal region of Snu114p (Brenner and Guthrie, 2005).

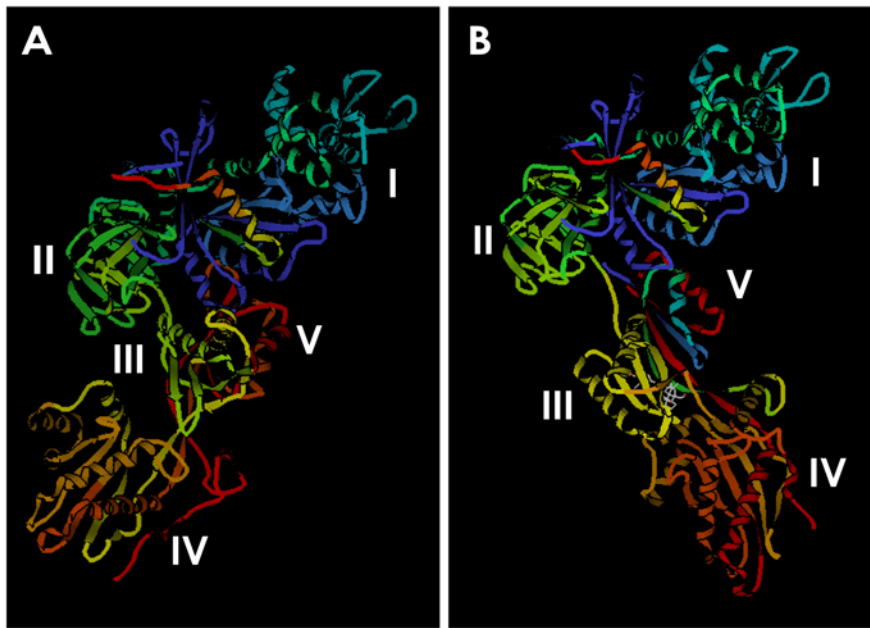


Figure 4.2 Crystal structures of the eukaryotic elongation factor eEF-2 in ExotoxinA-bound state (apo eEF-2, **A**) and in the sordarin-bound state (eEF-2-sor, **B**). The structures were taken from the RCSB protein data bank; PDB identification of apo-eEF-2: 1zm3; PDB identification of eEF-2-sor: 1n0u; the domains were assigned according to (Jorgensen et al., 2003).

Strikingly, in our immunolabeling studies we observed two different positions of the antibody bound to the C-terminus of Snu114p, a central and a lower position. These different antibody positions might result from large scale structural rearrangements in the tri-snRNP, induced by a GTP-driven conformational change of Snu114p's domains IV and V, analogous to the situation in the ribosome. These structural rearrangements could serve to regulate the activities of downstream proteins. Thus, as an integral GTPase of the spliceosome, Snu114p would be a good candidate to function as a continuous regulator that triggers Brr2p activity by inducing conformational changes.

On the other hand, Prp8p has been suggested to be a direct regulator of Brr2p. It has been speculated that Prp8p might undergo a conformational rearrangement which changes its interaction with Brr2p and thereby activates the helicase (van Nues and Beggs, 2001). Moreover, Prp8p has been suggested to simultaneously control the activity of Prp28p (Kuhn et al., 2002), which is involved in U1 snRNA/5' SS unwinding, another key step of spliceosome activation. Recent investigations of the function of the Snu114p C-terminus led to the proposal of a model that would allow to combine these data (Brenner and Guthrie, 2005). In this model (Figure 4.3), GTP hydrolysis drives a conformational change in domain IV of Snu114p, which modifies its

interaction with Prp8p. This induces a conformational change in Prp8p, which in turn alters the interaction of Prp8p with Brr2p and Prp28p and thereby activates the two helicases.

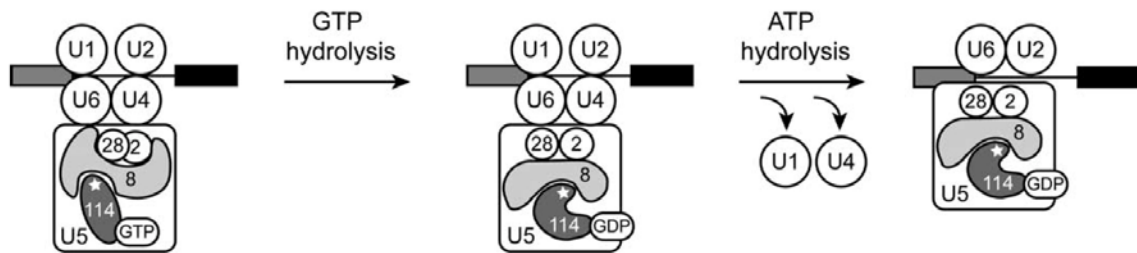


Figure 4.3 Model for the regulation of Brr2p and Prp28p activity during the catalytic activation of the spliceosome. In the fully assembled spliceosome GTP-hydrolysis induces a conformational change in Snu114p ('114'). Thereby, the interaction between domain IV of Snu114p (marked by a star) and Prp8p ('8') is changed, resulting in a conformational change of Prp8p, which activates the ATPases Brr2p ('2') and Prp28p ('28'). Subsequently U1 and U4 are released from the spliceosome (Brenner and Guthrie, 2005).

The different positions of the antibody bound to Snu114p indicate that there might indeed be a movement of the C-terminus of Snu114p, which might induce structural rearrangements in the tri-snRNP. Our studies located the C-terminus of Snu114p in proximity to the C-terminal region of Prp8p in the central part of the main body. Therefore, it would indeed be possible that a conformational change of Snu114p alters its interaction with Prp8p. Although we located only the C-terminal domains of Prp8p and Brr2p, their positions in the main body of the tri-snRNP, in combination with the size of the proteins and their proposed interaction in yeast two-hybrid studies, would allow the possibility of a direct interaction in the native yeast tri-snRNP (4.3). The C-terminus of Snu114p seems to be located slightly more distant to Brr2p (Figure 4.1 A). Considering the smaller size of Snu114p, a direct interaction with Brr2p might be less likely (however not impossible because due to its homology with eEF-2 a maximum dimension of ~ 12 nm can be assumed for Snu114p, which would be sufficient to reach up into the head region). In line with the model proposed by Brenner and Guthrie, our data would therefore support the model of a regulation of Brr2p by Snu114p, in which Prp8p functions as a mediator transferring the activation signals from the centrally located GTPase Snu114p to Brr2p. Since it has been shown, that the U4/U6 snRNA unwinding in purified tri-snRNPs does not require GTP-hydrolysis (Small et al., 2006), Snu114p might function in this process like a classic signalling G protein

Our findings also raised the question if there is a correlation between the ‘open’ and ‘closed’ state of the tri-snRNP on the one hand and the variable positions of the antibody bound to Snu114p on the other hand. However, we could not observe a correlation between the position of the antibody bound to Snu114p and the position of the head or arm domain. We therefore suggest that the ‘closed’ and ‘open’ state of the tri-snRNP merely reflect a structural flexibility of the particle and do not represent different functional states.

4.4.2 How is the U4/U6 snRNA unwound in the tri-snRNP?

In yeast, U4/U6 snRNA unwinding is not only catalyzed during the activation of the spliceosome, but can be also induced in the tri-snRNP upon addition of ATP in ammonium sulfate precipitates of yeast whole cell extracts known as ‘fraction I’ (Cheng and Abelson, 1987; Raghunathan and Guthrie, 1998a). Purified yeast tri-snRNPs dissociate into U5 and U4/U6 in the presence of ATP (Gottschalk, 1999; Stevens et al., 2001)(this study, data not shown). Recent studies indicate that also U4/U6 unwinding might be catalyzed in yeast tri-snRNPs purified at 50 mM salt (Small et al., 2006), suggesting that all factors involved in the unwinding reaction might be present in the U4/U6.U5 particle. Therefore, the yeast tri-snRNP would be an interesting model for understanding the U4/U6 snRNA unwinding during spliceosome activation. The ATPase Brr2p might trigger the unwinding of U4/U6 either directly (Laggerbauer et al., 1998) or by destabilizing an RNA-protein interaction that stabilizes the U4/U6 snRNA duplex, a mode of action suggested also for Prp28p (Chen et al., 2001). This putative U4/U6 snRNA stabilizing protein is possibly a U4/U6 snRNP component, since the snRNAs are already base-paired in the U4/U6 di-snRNP. A possible candidate would be the Prp3 protein, which has been shown to be necessary for the integrity of the yeast U4/U6 snRNP as well as of the tri-snRNP (Anthony et al., 1997). Both possible mechanisms of U4/U6 unwinding by Brr2p suggest a direct contact of Brr2p either with the U4/U6 snRNAs or with a duplex-stabilizing factor.

The observed separation between the head and arm domain in our purified particles raises the question of how the unwinding of U4/U6 snRNA is triggered in the tri-snRNP. We think that the ‘open’ and ‘closed’ form of the tri-snRNP do not represent different functional states, but are merely the result of the structural dynamics of the particle. The unwinding signal of Brr2p, which is located in the head domain of the main body, might therefore not be relayed to the U4/U6 snRNA in the arm by a direct contact but rather indirectly, possibly through protein-protein interactions. In the ‘open’ form of the yeast tri-snRNP the linker region is the only connection between U5 and U4/U6. Thus, the unwinding signal possibly would have to be

relayed from Brr2p to the bridging proteins Prp6p and Prp31p in the linker, and from them to the U4/U6 snRNA in the arm domain. This might also involve additional proteins such as Snu66p, which has been shown in yeast to be able to bind to Brr2p as well as to Prp6p in yeast two-hybrid studies (van Nues and Beggs, 2001).

4.4.3 The interaction between the C-terminus of Prp4p and Prp3p might be important for tri-snRNP stability

The C-terminal labeling of Prp4p with the tDimer2 tag as well as with the anti-CBP antibody resulted in the disintegration of the tri-snRNP upon purification (see 3.1.5) although the tDimer2-tagging of Prp4p was successful (see 3.1.5, Figure 3.20) and tri-snRNPs could be purified using TAP-tagged Prp4p (not shown). The C-terminus of Prp4p is formed by seven Tryptophan-Aspartat- (WD) repeats. The WD-repeats are typical for the G β subunits of heteromeric G proteins (Dalrymple et al., 1989). In G protejns these subunits have been shown to fold into a seven-bladed propeller-like structure (Lambright et al., 1996; Sondek et al., 1996) and they are known to form interfaces for protein-protein interactions (Neer et al., 1994). By introduction of targeted mutations into the C-terminal domain of the yeast Prp4p in combination with co-immunoprecipitation assays, Ayadi and coworkers (Ayadi et al., 1998) showed that Prp4p directly contacts Prp3p via the wide surface of its C-terminal propeller-like structure. The C-terminal labeling of Prp4p most probably interferes with this interaction and destabilizes the tri-snRNP, which leads to its disintegration upon purification. Previous studies already indicated that Prp4p and Prp3p interact (Last et al., 1987; Maddock et al., 1994) and that Prp3p is important for the integrity of the U4/U6 and the tri-snRNP (Anthony et al., 1997). Together with these studies, our results suggest that it is not Prp3p alone but its interaction with the C-terminal WD-repeats of Prp4p that might be important for stabilizing the tri-snRNP.

4.5 The yeast U5 snRNP

The yeast U5 snRNP would be an interesting particle for labeling studies because of its small size (~ 0.9 kDa), where it can be expected that a tag would be easier visible in the electron microscope. Moreover, it would be interesting to compare the location of Prp8p, Brr2p, and Snu114p in the U5 snRNP to their position in the tri-snRNP to learn, if these proteins are rearranged upon binding of U4/U6 snRNP.

4.5.1 Comparison of the yeast and human U5 snRNP

The yeast U5 snRNP contains seven Sm proteins and at least four particle-specific proteins (see 3.2.1, Figure 3.24 D). The yeast particle is smaller than its human counterpart. Prp6p and Snu66p (SART-1) are not present in the yeast U5 snRNP (Stevens et al., 2001) (and this study), however, their corresponding human orthologs are components of the human U5 particle (Makarov et al., 2000) (Makarova, 2002). Moreover, the human U5 contains an additional protein, U5-40K, of which no confirmed ortholog is known in yeast. Interestingly, in our U5 snRNP purifications Prp28p could not be detected by MS. This DExD/H-box helicase, which is involved in the U1 snRNA displacement from the 5' SS (see 1.6), is associated with the human U4/U6.U5 tri-snRNP (Teigelkamp et al., 1997), and the U5 snRNP (Behrens and Lührmann, 1991) although its association with U5 was only observed at low salt. Moreover, Prp28 was identified in previous purifications of the yeast U5 snRNP (Stevens et al., 2001) but never in the tri-snRNP (Gottschalk et al., 1999; Stevens et al., 2001) (this study). A possible reason for its absence in our U5 purifications could be a loss during purification due to a loose association of the Prp28p with the U5 snRNP. On the other hand, the amount of protein could have simply been too low for detection by MS. Similarly, the SmB protein could not be detected by MS, probably also due to too low amounts of protein. Moreover, MS analysis was performed only of the silver stained protein bands, not of the complete lane of the gel. Therefore, Prp28p and SmBp bands might have been cut out because of too weak staining.

MS analysis of U5 snRNPs purified via TAP-tagged Snu114p (with or without ProtA tag at Prp4p) revealed the presence of an additional protein, the Aar2p (see 3.2.1, Figure 3.24 C), which is a component of the 16S Aar2p-U5, a small form of the U5 snRNP which was co-purified with the U1 snRNP in yeast (Gottschalk et al., 2001). In human, no confirmed ortholog of Aar2p is known. The Aar2p-U5 was suggested to be a precursor of the U5 snRNP assembling in the cytoplasm during snRNP biogenesis. It is thought, to be then transported into the cell

nucleus where Aar2p is exchanged for Brr2p, and where additional U5-specific proteins associate with the snRNP (Boon et al., 2007).

4.5.2 The U5 snRNP is too heterogeneous for labeling studies and 3D structure determination

Although the U5 snRNPs were purified via three steps, including the tandem affinity purification followed by gradient centrifugation, the particles appeared to be very heterogeneous in the electron microscope (see 3.2.2, Figure 3.25). To investigate if the heterogeneous appearance of the particles was due to different orientations on the carbon film, the EM specimen was tilted in the microscope and tilt pairs (images of the particle before and after tilting) were analyzed. This analysis showed that the different observed shapes of the U5 snRNP were not created by different viewing angles of the same particle. Thus, the observed heterogeneity probably is due to conformational or biochemical heterogeneity. The obtained biochemical and electron microscopic data of the purified U5 snRNPs indicated that an improvement of sample quality (either biochemically or on the EM side) would have required enormous efforts, which would have been beyond the scope of this work. Therefore, the yeast U5 snRNP was not further considered for 3D structure determination or labeling studies.

4.5.3 Possible reasons for heterogeneous appearance of the yeast U5 snRNP in the electron microscope

In case of U5 snRNP purification via TAP-tagged Snu114p, which results in the co-purification of the 16S Aar2p-U5 and the 18S U5 snRNP, the heterogeneity could be due to the mixture of the two particles. However, comparison with U5 snRNPs purified via Brr2p (which purifies only the 18S U5) showed that those particles had the same heterogeneous appearance. Thus, the observed heterogeneity is not only due to the presence of the Aar2p-U5 in the sample purified via Snu114p. The analysis of the silver gels of TAP-purified U5 snRNPs indicated that the heterogeneous appearance might also reflect a biochemical heterogeneity. Several protein bands were observed that were either predominantly present in the lighter U5 snRNP fractions and nearly absent in the heavier fractions or vice versa (see 3.2.1, Figure 3.24, fractions 8-12). This indicates that different subpopulations of U5 snRNPs might exist, which contain additional proteins. These subpopulations of U5 snRNPs could not be separated by the applied purification

procedure. The identity of the associated proteins is unknown, because the protein concentration was too low for MS analysis.

The U5 snRNP undergoes several changes in its protein composition during pre-mRNA splicing. Upon integration into the tri-snRNP the Lin1 protein dissociates, and in the activated spliceosome only the core of Prp8p, Brr2p, and Snu114p is present. Upon spliceosome disassembly, the U5 snRNP has to be recycled in a complete 18S U5 to be incorporated into the tri-snRNP. Thus, discrete intermediate states of the U5 snRNP might exist, which all contain the three core proteins Prp8p, Brr2p, and Snu114p, and were therefore co-purified in our purifications.

4.6 Comparison of the yeast U5 snRNP and the tri-snRNP

The labeling data mapped the U5 snRNP to the main body of the tri-snRNP. A size comparison of the U5 and the tri-snRNP shows that the maximum dimension of the U5 snRNP (~ 25 nm) is smaller than that of the tri-snRNP (~ 33 nm). On the other hand, the U5 snRNP in many views appears to be broader than the main body of the tri-snRNP (Figure 4.4). Thus, upon integration into the tri-snRNP the U5 snRNP probably has to be rearranged to fit into the main body. A structural rearrangement of the U5 snRNP was also proposed in human. There, the lower part of U5 (foot and central domain) fitted well into the structure of the tri-snRNP. However, for the head domain of U5 a structural rearrangement had to be assumed to be able to fit the 3D structure of U5 into the 3D structure of the tri-snRNP (Sander et al., 2006). These rearrangements resulted in an upward movement of the head domain of U5.

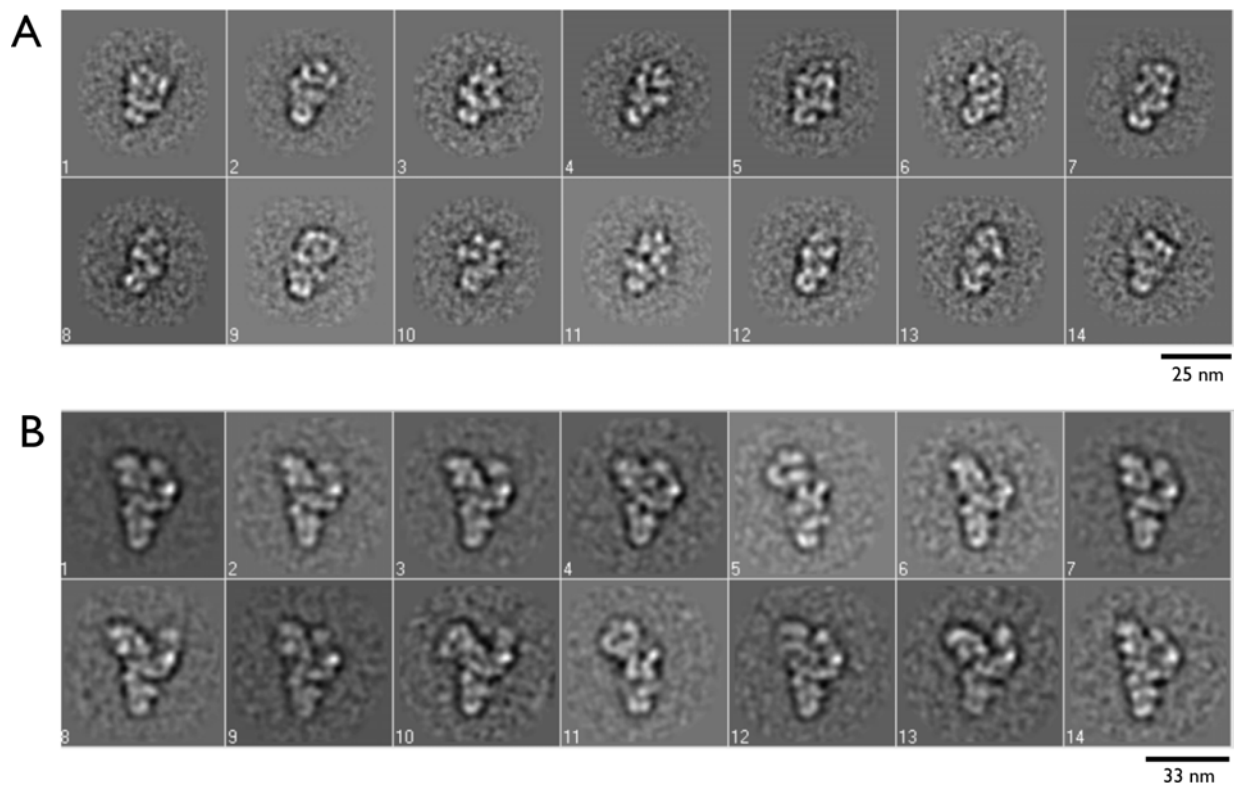


Figure 4.4 Comparison of the structures of the yeast U5 snRNP and the tri-snRNP. The maximum dimension of the U5 snRNP is 25 nm, of the tri-snRNP 33 nm. The class averages shown in this figure were kindly provided by B. Sander and M. Golas (Cryo-Electron Microscopy, Max Planck Institute for Biophysical Chemistry, Göttingen)

4.7 Perspectives

The labeling data obtained by two independent approaches provided reliable information about the structural organization of the yeast tri-snRNP. To refine this information it would be highly desirable to identify the positions of other domains, especially of the large proteins (Prp8p, Brr2p) and to map additional proteins like Snu66p, Prp38p or Prp4p to the tri-snRNP. This might provide more information about how the unwinding signal is relayed from Brr2p to the U4/U6 snRNA duplex. For this purpose N-terminal TAP-tagging of tri-snRNP proteins has already been initiated. Moreover, Gauss et al. (Gauss et al., 2005) constructed plasmids that allow the internal labeling of proteins in yeast. This would allow to directly target functionally important domains of proteins, if the labeling does not interfere with protein folding, function or stability.

In addition, the position of the snRNAs could be located within the tri-snRNP structure using oligonucleotides complementary to single stranded regions of the snRNAs. These oligonucleotides would be coupled to a molecular label that allows the localization of the binding site of the oligonucleotide. Here, several possibilities exist, e.g. a biotin label could be detected by

an anti-biotin antibody. A new method published recently (Alcid and Jurica, 2008) uses a sequence-specific RNA binding protein fused to a doughnut-shaped structure that can be easily detected in the electron microscope. Interesting regions of snRNAs to be investigated would be the highly conserved ACAGAG-box of the U6 snRNA, which base pairs with the 5'SS in the activated spliceosome (see 1.6.2) and is known to be single-stranded in the tri-snRNP, or the internal stem-loop of the U5 snRNA, which is close to the U5 loop I (see 1.5) that is thought to tether the exons for the second step of splicing in cooperation with Prp8p (see 1.6.2).

A long-term goal would be the labeling of the U5-specific proteins Prp8p, Snu114p, and Brr2p in different spliceosomal complexes. These three proteins, which stay associated with the spliceosome throughout the splicing cycle, are involved in several crucial steps in the splicing cycle (see 1.6.3). Thus, it would be exciting to locate their position in different spliceosomal complexes representing the different states of the splice cycle. Their position within these complexes, as well as their orientation relative to each other at different steps of the splice cycle might provide further interesting hints about their cooperative activity in pre-mRNA splicing and the dynamic rearrangements in the spliceosome.

5 References

- Abou Elela, S. and Ares, M.** (1998). Depletion of yeast RNase III blocks correct U2 3' end formation and results in polyadenylated but functional U2 snRNA. *EMBO J.* **17**, 3738-46.
- Achsel, T. et al.** (1998). The human U5-220kD protein (hPrp8) forms a stable RNA-free complex with several U5-specific proteins, including an RNA unwindase, a homologue of ribosomal elongation factor EF-2, and a novel WD-40 protein. *Mol. Cell. Biol.* **18**, 6756-66.
- Achsel, T. et al.** (1999). A doughnut-shaped heteromer of human Sm-like proteins binds to the 3'- end of U6 snRNA, thereby facilitating U4/U6 duplex formation *in vitro*. *EMBO J.* **18**, 5789-802.
- Alcid, E. A. and Jurica, M. S.** (2008). A protein-based EM label for RNA identifies the location of exons in spliceosomes. *Nat. Struct. Mol. Biol.* **15**, 213-5.
- Anthony, J. G., Weidenhammer, E. M. and Woolford, J. L., Jr.** (1997). The yeast Prp3 protein is a U4/U6 snRNP protein necessary for integrity of the U4/U6 snRNP and the U4/U6.U5 tri-snRNP. *RNA* **3**, 1143-52.
- Arenas, J. and Hurwitz, J.** (1987). Purification of a RNA debranching activity from HeLa cells. *J. Biol. Chem.* **262**, 4274-79.
- Ayadi, L. et al.** (1998). Functional and structural characterization of the prp3 binding domain of the yeast prp4 splicing factor. *J. Mol. Biol.* **284**, 673-87.
- Banroques, J. and Abelson, J. N.** (1989). PRP4: a protein of the yeast U4/U6 small nuclear ribonucleoprotein particle. *Mol. Cell. Biol.* **9**, 3710-9.
- Bartels, C., Klatt, C., Lührmann, R. and Fabrizio, P.** (2002). The ribosomal translocase homologue Snu114p is involved in unwinding U4/U6 RNA during activation of the spliceosome. *EMBO Rep.* **3**, 875-80.
- Bartels, C., Urlaub, H., Lührmann, R. and Fabrizio, P.** (2003). Mutagenesis Suggests Several Roles of Snu114p in Pre-mRNA Splicing. *J. Biol. Chem.* **278**, 28324-34.
- Behrens, S. E. and Lührmann, R.** (1991). Immunoaffinity purification of a [U4/U6.U5] tri-snRNP from human cells. *Genes Dev.* **5**, 1439-52.
- Behzadnia, N. et al.** (2007). Composition and three-dimensional EM structure of double affinity-purified, human prespliceosomal A complexes. *EMBO J.* **26**, 1737-48.
- Bellare, P. et al.** (2008). A role for ubiquitin in the spliceosome assembly pathway. *Nat. Struct. Mol. Biol.* **advanced online publication**.
- Blum, H., Beier, H. and Gross, H. J.** (1987). Improved silver staining of plant proteins, RNA and DNA in polyacrylamide gels. *Electrophoresis* **8**, 93-99.
- Bochnig, P., Reuter, R., Bringmann, P. and Lührmann, R.** (1987). A monoclonal antibody against 2,2,7-trimethylguanosine that reacts with intact, class U, small nuclear ribonucleoproteins as well as with 7-methylguanosine-capped RNAs. *Eur. J. Biochem.* **168**, 461-7.
- Boehringer, D. et al.** (2004). Three-dimensional structure of a pre-catalytic human spliceosomal complex B. *Nat. Struct. Mol. Biol.* **11**, 463-8.

- Boon, K.-L. et al.** (2007). Prp8 mutations that cause human retinitis pigmentosa lead to a U5 snRNP maturation defect in yeast. *Nat. Struct. Mol. Biol.* **14**, 1077-83.
- Bordonne, R., Banroques, J., Abelson, J. and Guthrie, C.** (1990). Domains of yeast U4 spliceosomal RNA required for PRP4 protein binding, snRNP-snRNP interactions, and pre-mRNA splicing *in vivo*. *Genes Dev.* **4**, 1185-96.
- Bouveret, E. et al.** (2000). A Sm-like protein complex that participates in mRNA degradation. *EMBO J.* **19**, 1661-71.
- Brenner, T. J. and Guthrie, C.** (2005). Genetic Analysis Reveals a Role for the C Terminus of the *Saccharomyces cerevisiae* GTPase Snu114 During Spliceosome Activation. *Genetics* **170**, 1063-80.
- Brenner, T. J. and Guthrie, C.** (2006). Assembly of Snu114 into U5 snRNP requires Prp8 and a functional GTPase domain. *RNA* **12**, 862-71.
- Brow, D. A.** (2002). Allosteric cascade of spliceosome activation. *Annu. Rev. Genet.* **36**, 333-60.
- Brow, D. A. and Guthrie, C.** (1988). Spliceosomal RNA U6 is remarkably conserved from yeast to mammals. *Nature* **334**, 213-8.
- Burge, C. B., Tuschl, T. and Sharp, P. A.** (1999). Splicing of Precursors to mRNAs by the Spliceosomes. In *The RNA World*, (ed. R. F. Gesteland T. R. Cech and J. F. Atkins), pp. 525-60. Cold Spring Harbor, New York: Cold Spring Harbor Laboratory Press.
- Burnette, W. N.** (1981). 'Western Blotting': Electrophoretic transfer of proteins from sodium dodecyl sulfate-polyacrylamide gels to unmodified nitrocellulose and radiographic detection with antibody and radioiodinated protein A. *Anal. Biochem.* **112**, 195-203.
- Busch, H., Reddy, R., Rothblum, L. and Choi, Y. C.** (1982). SnRNAs, snRNPs, and RNA Processing. *Annu. Rev. Biochem.* **51**, 617-54.
- Campbell, R. E. et al.** (2002). A monomeric red fluorescent protein. *Proc. Natl. Acad. Sci. U. S. A.* **99**, 7877-82.
- Cao, S. and Chen, S. J.** (2006). Free energy landscapes of RNA/RNA complexes: with applications to snRNA complexes in spliceosomes. *J. Mol. Biol.* **357**, 292-312.
- Chanfreau, G., Elela, S. A., Ares, M., Jr. and Guthrie, C.** (1997). Alternative 3'-end processing of U5 snRNA by RNase III. *Genes Dev.* **11**, 2741-51.
- Chen, C.-H. et al.** (2002). Functional and physical interactions between components of the Prp19p-associated complex. *Nucleic Acids Res.* **30**, 1029-37.
- Chen, J. Y. et al.** (2001). Specific alterations of U1-C protein or U1 small nuclear RNA can eliminate the requirement of Prp28p, an essential DEAD box splicing factor. *Mol. Cell* **7**, 227-32.
- Cheng, S. C. and Abelson, J.** (1987). Spliceosome assembly in yeast. *Genes Dev.* **1**, 1014-27.
- Colgan, D. F. and Manley, J. L.** (1997). Mechanism and regulation of mRNA polyadenylation. *Genes Dev.* **11**, 2755-66.
- Cormack, B. P. et al.** (1997). Yeast enhanced green fluorescent protein (yEGFP) a reporter of gene expression in *Candida albicans*. *Microbiology* **143 (Pt 2)**, 303-11.
- Dalrymple, M. A., Petersen-Bjorn, S., Friesen, J. D. and Beggs, J. D.** (1989). The product of the PRP4 gene of *S. cerevisiae* shows homology to beta subunits of G proteins. *Cell* **58**, 811-2.

- Das, R., Zhou, Z. and Reed, R.** (2000). Functional association of U2 snRNP with the ATP-independent spliceosomal complex E. *Mol. Cell* **5**, 779-87.
- Datta, B. and Weiner, A. M.** (1991). Genetic evidence for base pairing between U2 and U6 snRNA in mammalian mRNA splicing. *Nature* **352**, 821-4.
- Deckert, J. et al.** (2006). Protein composition and electron microscopy structure of affinity-purified human spliceosomal B complexes isolated under physiological conditions. *Mol. Cell. Biol.* **26**, 5528-43.
- Dix, I. et al.** (1998). Protein-RNA interactions in the U5 snRNP of *Saccharomyces cerevisiae*. *RNA* **4**, 1239-50.
- Dube, P., Tavares, P., Lurz, R. and van Heel, M.** (1993). The portal protein of bacteriophage SPP1: a DNA pump with 13-fold symmetry. *EMBO J.* **12**, 1303-9.
- Fabrizio, P. et al.** (1997). An evolutionarily conserved U5 snRNP-specific protein is a GTP-binding factor closely related to the ribosomal translocase EF-2. *EMBO J.* **16**, 4092-106.
- Fairman, M. E. et al.** (2004). Protein displacement by DExH/D 'RNA helicases' without duplex unwinding. *Science* **304**, 730-4.
- Frank, D. N., Roiha, H. and Guthrie, C.** (1994). Architecture of the U5 small nuclear RNA. *Mol. Cell. Biol.* **14**, 2180-90.
- Frank, J. and van Heel, M.** (1982). Correspondence analysis of aligned images of biological particles. *J. Mol. Biol.* **161**, 134-37.
- Fromont-Racine, M. et al.** (2000). Genome-wide protein interaction screens reveal functional networks involving Sm-like proteins. *Yeast* **17**, 95-110.
- Galisson, F. and Legrain, P.** (1993). The biochemical defects of prp4-1 and prp6-1 yeast splicing mutants reveal that the PRP6 protein is required for the accumulation of the [U4/U6.U5] tri-snRNP. *Nucleic Acids Res.* **21**, 1555-62.
- Gauss, R., Trautwein, M., Sommer, T. and Spang, A.** (2005). New modules for the repeated internal and N-terminal epitope tagging of genes in *Saccharomyces cerevisiae*. *Yeast* **22**, 1-12.
- Goffeau, A. et al.** (1996). Life with 6000 genes. *Science* **274**, 546, 63-7.
- Golas, M. M. et al.** (2003). Molecular Architecture of the Multiprotein Splicing Factor SF3b. *Science* **300**, 980-84.
- Gottschalk, A.** (1999). Umfassende Analyse der Protein-Komponenten spleißosomaler Ribonukleoprotein-Komplexe aus *Saccharomyces cerevisiae*. Institut für Molekularbiologie und Tumorforschung, Marburg: Philipps-Universität.
- Gottschalk, A., Kastner, B., Lührmann, R. and Fabrizio, P.** (2001). The yeast U5 snRNP coisolated with the U1 snRNP has an unexpected protein composition and includes the splicing factor Aar2p. *RNA* **7**, 1554-65.
- Gottschalk, A. et al.** (1999). Identification by mass spectrometry and functional analysis of novel proteins of the yeast [U4/U6.U5] tri-snRNP. *EMBO J.* **18**, 4535-48.
- Grainger, R. J. and Beggs, J. D.** (2005). Prp8 protein: at the heart of the spliceosome. *RNA* **11**, 533-57.
- Griesbeck, O. et al.** (2001). Reducing the Environmental Sensitivity of Yellow Fluorescent Protein. MECHANISM AND APPLICATIONS. *J. Biol. Chem.* **276**, 29188-94.

- Güldener, U. et al.** (1996). A new efficient gene disruption cassette for repeated use in budding yeast. *Nucleic Acids Res.* **24**, 2519-24.
- Guthrie, C. and Patterson, B.** (1988). Spliceosomal snRNAs. *Annu. Rev. Genet.* **22**, 387-419.
- Hartmuth, K. et al.** (2002). Protein composition of human prespliceosomes isolated by a tobramycin affinity-selection method. *Proc. Natl. Acad. Sci. U. S. A.* **99**, 16719-24.
- Hilliker, A. K. and Staley, J. P.** (2004). Multiple functions for the invariant AGC triad of U6 snRNA. *RNA* **10**, 921-8.
- Horowitz, D. S., Kobayashi, R. and Krainer, A. R.** (1997). A new cyclophilin and the human homologues of yeast Prp3 and Prp4 form a complex associated with U4/U6 snRNPs. *RNA* **3**, 1374-87.
- Jankowsky, E., Gross, C. H., Shuman, S. and Pyle, A. M.** (2001). Active Disruption of an RNA-Protein Interaction by a DExH/D RNA Helicase. *Science* **291**, 121-25.
- Jiang, W. et al.** (2008). Backbone structure of the infectious epsilon15 virus capsid revealed by electron cryomicroscopy. *Nature* **451**, 1130-4.
- Jorgensen, R. et al.** (2005). Exotoxin A-eEF2 complex structure indicates ADP ribosylation by ribosome mimicry. *Nature* **436**, 979-84.
- Jorgensen, R. et al.** (2003). Two crystal structures demonstrate large conformational changes in the eukaryotic ribosomal translocase. *Nat. Struct. Mol. Biol.* **10**, 379-85.
- Jurica, M. S. et al.** (2002). Purification and characterization of native spliceosomes suitable for three-dimensional structural analysis. *RNA* **8**, 426-39.
- Jurica, M. S. and Moore, M. J.** (2003). Pre-mRNA Splicing. Awash in a Sea of Proteins. *Mol. Cell* **12**, 5-14.
- Jurica, M. S., Sousa, D., Moore, M. J. and Grigorieff, N.** (2004). Three-dimensional structure of C complex spliceosomes by electron microscopy. *Nat. Struct. Mol. Biol.* **11**, 265-9.
- Kambach, C. et al.** (1999). Crystal structures of two Sm protein complexes and their implications for the assembly of the spliceosomal snRNPs. *Cell* **96**, 375-87.
- Karaduman, R.** (2006). Determination of the Structure of the Spliceosomal U6 snRNP from Yeast, *Saccharomyces cerevisiae*. Biologische Fakultät, Göttingen: Georg-August Universität.
- Karagöz, E. G.** (2006). Localization of functionally important proteins of the yeast *S. cerevisiae* U4/U6.U5 tri-snRNP spliceosomal particle using specific labeling tags and Electron Microscopy. Biologische Fakultät, Göttingen: Georg August Universität.
- Kastner, B., Bach, M. and Lührmann, R.** (1990). Electron microscopy of small nuclear ribonucleoprotein (snRNP) particles U2 and U5: evidence for a common structure-determining principle in the major U snRNP family. *Proc. Natl. Acad. Sci. U. S. A.* **87**, 1710-4.
- Kastner, B. et al.** (2008). GraFix: sample preparation for single-particle electron cryomicroscopy. *Nat. Methods* **5**, 53-5.
- Kastner, B. and Lührmann, R.** (1999). Purification of U small nuclear ribonucleoprotein particles. *Methods Mol. Biol.* **118**, 289-98.
- Kent, O. A. and MacMillan, A. M.** (2002). Early organization of pre-mRNA during spliceosome assembly. *Nat. Struct. Biol.* **9**, 576-81.

- Kent, O. A., Ritchie, D. B. and Macmillan, A. M.** (2005). Characterization of a U2AF-independent commitment complex (E') in the mammalian spliceosome assembly pathway. *Mol. Cell. Biol.* **25**, 233-40.
- Kim, D. H. and Rossi, J. J.** (1999). The first ATPase domain of the yeast 246-kDa protein is required for *in vivo* unwinding of the U4/U6 duplex. *RNA* **5**, 959-71.
- Kretzner, L., Krol, A. and Rosbash, M.** (1990). *Saccharomyces cerevisiae* U1 small nuclear RNA secondary structure contains both universal and yeast-specific domains. *Proceedings of the National Academy of Sciences* **87**, 851-5.
- Krol, A. et al.** (1981). Primary and secondary structures of chicken, rat and man nuclear U4 RNAs. Homologies with U1 and U5 RNAs. *Nucleic Acids Res.* **9**, 2699-716.
- Krol, A. et al.** (1990). Solution structure of human U1 snRNA. Derivation of a possible three-dimensional model. *Nucleic Acids Res.* **18**, 3803-11.
- Kuhn, A. N., Li, Z. and Brow, D. A.** (1999). Splicing factor Prp8 governs U4/U6 RNA unwinding during activation of the spliceosome. *Mol. Cell* **3**, 65-75.
- Kuhn, A. N., Reichl, E. M. and Brow, D. A.** (2002). Distinct domains of splicing factor Prp8 mediate different aspects of spliceosome activation. *Proc. Natl. Acad. Sci. U. S. A.* **99**, 9145-9.
- Laemmli, U. K.** (1970). Cleavage of Structural Proteins during the Assembly of the Head of Bacteriophage T4. *Nature* **227**, 680-85.
- Laggerbauer, B., Achsel, T. and Lührmann, R.** (1998). The human U5-200kD DEXH-box protein unwinds U4/U6 RNA duplexes *in vitro*. *Proc. Natl. Acad. Sci. U. S. A.* **95**, 4188-92.
- Lambright, D. G. et al.** (1996). The 2.0 Å crystal structure of a heterotrimeric G protein. *Nature* **379**, 311-9.
- Lamond, A. I., Sproat, B., Ryder, U. and Hamm, J.** (1989). Probing the structure and function of U2 snRNP with antisense oligonucleotides made of 2'-OMe RNA. *Cell* **58**, 383-90.
- Last, R. L., Maddock, J. R. and Woolford, J. L., Jr.** (1987). Evidence for related functions of the RNA genes of *Saccharomyces cerevisiae*. *Genetics* **117**, 619-31.
- Li, Z. and Brow, D. A.** (1996). A spontaneous duplication in U6 spliceosomal RNA uncouples the early and late functions of the ACAGA element *in vivo*. *RNA* **2**, 879-94.
- Liu, S., Rauhut, R., Vornlocher, H. P. and Lührmann, R.** (2006). The network of protein-protein interactions within the human U4/U6.U5 tri-snRNP. *RNA* **12**, 1418-30.
- Lopez, P. J. and Seraphin, B.** (2000). Uncoupling yeast intron recognition from transcription with recursive splicing. *EMBO Rep.* **1**, 334-9.
- Lopez, P. J. and Séraphin, B.** (1999). Genomic-scale quantitative analysis of yeast pre-mRNA splicing: implications for splice-site recognition [letter]. *RNA* **5**, 1135-7.
- Lührmann, R. et al.** (1982). Isolation and characterization of rabbit anti-m3 2,2,7G antibodies. *Nucleic Acids Res.* **10**, 7103-13.
- Lund, M. and Kjems, J.** (2002). Defining a 5' splice site by functional selection in the presence and absence of U1 snRNA 5' end. *RNA* **8**, 166-79.
- Maddock, J. R. et al.** (1994). Extragenic suppressors of *Saccharomyces cerevisiae* prp4 mutations identify a negative regulator of PRP genes. *Genetics* **136**, 833-47.

- Madhani, H. D. and Guthrie, C.** (1992). A novel base-pairing interaction between U2 and U6 snRNAs suggests a mechanism for the catalytic activation of the spliceosome. *Cell* **71**, 803-17.
- Makarov, E. M., Makarova, O. V., Achsel, T. and Lührmann, R.** (2000). The human homologue of the yeast splicing factor prp6p contains multiple TPR elements and is stably associated with the U5 snRNP via protein-protein interactions. *J. Mol. Biol.* **298**, 567-75.
- Makarov, E. M. et al.** (2002). Small Nuclear Ribonucleoprotein Remodeling During Catalytic Activation of the Spliceosome. *Science* **298**, 2205-08.
- Makarova, O. V. et al.** (2002). Protein 61K, encoded by a gene (PRPF31) linked to autosomal dominant retinitis pigmentosa, is required for U4/U6*U5 tri-snRNP formation and pre-mRNA splicing. *EMBO J.* **21**, 1148-57.
- Makarova, O. V. et al.** (2004). A subset of human 35S U5 proteins, including Prp19, function prior to catalytic step 1 of splicing. *EMBO J.* **23**, 2381-91.
- Maroney, P. A., Romfo, C. M. and Nilsen, T. W.** (2000). Functional recognition of 5' splice site by U4/U6.U5 tri-snRNP defines a novel ATP-dependent step in early spliceosome assembly. *Mol. Cell* **6**, 317-28.
- Mayes, A. E., Verdone, L., Legrain, P. and Beggs, J. D.** (1999). Characterization of Sm-like proteins in yeast and their association with U6 snRNA. *EMBO J.* **18**, 4321-31.
- McCracken, S. et al.** (1997). 5'-Capping enzymes are targeted to pre-mRNA by binding to the phosphorylated carboxy-terminal domain of RNA polymerase II. *Genes Dev.* **11**, 3306-18.
- Merril, C. R., Goldman, D., Sedman, S. A. and Ebert, M. H.** (1981). Ultrasensitive stain for proteins in polyacrylamide gels shows regional variation in cerebrospinal fluid proteins. *Science* **211**, 1437-8.
- Moore, M. J., Query, C. C. and Sharp, P. A.** (1993). Splicing of precursors to mRNA by the spliceosome. In *The RNA World*, (ed. A. Gesteland), pp. 303-57. Cold Spring Harbor, New York: Cold Spring Harbor Laboratory Press.
- Moore, M. J. and Sharp, P. A.** (1993). Evidence for two active sites in the spliceosome provided by stereochemistry of pre-mRNA splicing. *Nature* **365**, 364-8.
- Mura, C., Cascio, D., Sawaya, M. R. and Eisenberg, D. S.** (2001). The crystal structure of a heptameric archaeal Sm protein: Implications for the eukaryotic snRNP core. *Proc. Natl. Acad. Sci. U. S. A.* **98**, 5532-7.
- Neer, E. J., Schmidt, C. J., Nambudripad, R. and Smith, T. F.** (1994). The ancient regulatory-protein family of WD-repeat proteins. *Nature* **371**, 297-300.
- Nilsen, T. W.** (1998). RNA-RNA interactions in nuclear pre-mRNA splicing. In *RNA Structure and Function*, (ed. R. W. S. a. M.Grundber-Manago), pp. 279-307. Cold Spring Harbor, New York.: Cold Spring Harbor Laboratory Press.
- Nottrott, S. et al.** (1999). Functional interaction of a novel 15.5kD [U4/U6.U5] tri-snRNP protein with the 5' stem-loop of U4 snRNA. *EMBO J.* **18**, 6119-33.
- Nottrott, S., Urlaub, H. and Lührmann, R.** (2002). Hierarchical, clustered protein interactions with U4/U6 snRNA: a biochemical role for U4/U6 proteins. *EMBO J.* **21**, 5527-38.
- O'Keefe, R. T. and Newman, A. J.** (1998). Functional analysis of the U5 snRNA loop 1 in the second catalytic step of yeast pre-mRNA splicing. *EMBO J.* **17**, 565-74.

- Ohi, M. D. et al.** (2002). Proteomics analysis reveals stable multiprotein complexes in both fission and budding yeasts containing Myb-related Cdc5p/Cef1p, novel pre-mRNA splicing factors, and snRNAs. *Mol. Cell. Biol.* **22**, 2011-24.
- Padgett, R. A.** (2005). mRNA Splicing: Role of snRNAs. In *Encyclopedia of Life Sciences*. Chichester: John Wiley & Sons, Ltd.
- Puig, O. et al.** (2001). The tandem affinity purification (TAP) method: a general procedure of protein complex purification. *Methods* **24**, 218-29.
- Rader, S. D. and Guthrie, C.** (2002). A conserved Lsm-interaction motif in Prp24 required for efficient U4/U6 di-snRNP formation. *RNA* **8**, 1378-92.
- Raghunathan, P. L. and Guthrie, C.** (1998a). RNA unwinding in U4/U6 snRNPs requires ATP hydrolysis and the DEIH-box splicing factor Brr2. *Curr. Biol.* **8**, 847-55.
- Raghunathan, P. L. and Guthrie, C.** (1998b). A spliceosomal recycling factor that reanneals U4 and U6 small nuclear ribonucleoprotein particles. *Science* **279**, 857-60.
- Rappsilber, J., Ryder, U., Lamond, A. I. and Mann, M.** (2002). Large-scale proteomic analysis of the human spliceosome. *Genome Res.* **12**, 1231-45.
- Ruby, S. W. and Abelson, J.** (1991). Pre-mRNA splicing in yeast. *Trends Genet.* **7**, 79-85.
- Salgado-Garrido, J., Bragado-Nilsson, E., Kandels-Lewis, S. and Séraphin, B.** (1999). Sm and Sm-like proteins assemble in two related complexes of deep evolutionary origin. *EMBO J.* **18**, 3451-62.
- Sambrook, J., Russell, D. W. and Maniatis, T.** (1989). *Molecular Cloning: A Laboratory Manual*. Cold Spring Harbor, NY: Cold Spring Harbor Laboratory Press.
- Sander, B. et al.** (2006). Organization of core spliceosomal components U5 snRNA loop I and U4/U6 Di-snRNP within U4/U6.U5 Tri-snRNP as revealed by electron cryomicroscopy. *Mol. Cell* **24**, 267-78.
- Sander, B., Golas, M. M. and Stark, H.** (2003). Corrim-based alignment for improved speed in single-particle image processing. *J. Struct. Biol.* **143**, 219-28.
- Sashital, D. G. et al.** (2004). U2-U6 RNA folding reveals a group II intron-like domain and a four-helix junction. *Nat. Struct. Mol. Biol.* **11**, 1237-42.
- Schaffert, N. et al.** (2004). RNAi knockdown of hPrp31 leads to an accumulation of U4/U6 di-snRNPs in Cajal bodies. *EMBO J.* **23**, 3000-9.
- Schwer, B.** (2001). A new twist on RNA helicases: DExH/D box proteins as RNPsases. *Nat. Struct. Mol. Biol.* **8**, 113-6.
- Segault, V. et al.** (1999). Conserved loop I of U5 small nuclear RNA is dispensable for both catalytic steps of pre-mRNA splicing in HeLa nuclear extracts. *Mol. Cell. Biol.* **19**, 2782-90.
- Seipelt, R. L., Zheng, B., Asuru, A. and Rymond, B. C.** (1999). U1 snRNA is cleaved by RNase III and processed through an Sm site-dependent pathway [In Process Citation]. *Nucleic Acids Res.* **27**, 587-95.
- Shatkin, A. J.** (1976). Capping of eucaryotic mRNAs. *Cell* **9**, 645-53.
- Sheff, M. A. and Thorn, K. S.** (2004). Optimized cassettes for fluorescent protein tagging in *Saccharomyces cerevisiae*. *Yeast* **21**, 661-70.

- Shevchenko, A., Wilm, M., Vorm, O. and Mann, M.** (1996). Mass spectrometric sequencing of proteins silver-stained polyacrylamide gels. *Anal. Chem.* **68**, 850-8.
- Shuster, E. O. and Guthrie, C.** (1988). Two conserved domains of yeast U2 snRNA are separated by 945 nonessential nucleotides. *Cell* **55**, 41-8.
- Sikorski, R. S. and Hieter, P.** (1989). A system of shuttle vectors and yeast host strains designed for efficient manipulation of DNA in *Saccharomyces cerevisiae*. *Genetics* **122**, 19-27.
- Singh, R. and Reddy, R.** (1989). Gamma-monomethyl phosphate: a cap structure in spliceosomal U6 small nuclear RNA. *Proc. Natl. Acad. Sci. U. S. A.* **86**, 8280-3.
- Small, E. C., Leggett, S. R., Winans, A. A. and Staley, J. P.** (2006). The EF-G-like GTPase Snu114p regulates spliceosome dynamics mediated by Brr2p, a DExD/H box ATPase. *Mol. Cell* **23**, 389-99.
- Smith, P. K. et al.** (1985). Measurement of protein using bicinchoninic acid. *Anal. Biochem.* **150**, 76-85.
- Sondek, J. et al.** (1996). Crystal structure of a G-protein beta gamma dimer at 2.1A resolution. *Nature* **379**, 369-74.
- Spingola, M., Grate, L., Haussler, D. and Ares, M., Jr.** (1999). Genome-wide bioinformatic and molecular analysis of introns in *Saccharomyces cerevisiae*. *RNA* **5**, 221-34.
- Staley, J. P. and Guthrie, C.** (1998). Mechanical devices of the spliceosome: motors, clocks, springs, and things. *Cell* **92**, 315-26.
- Staley, J. P. and Guthrie, C.** (1999). An RNA switch at the 5' splice site requires ATP and the DEAD box protein Prp28p. *Mol. Cell* **3**, 55-64.
- Stark, H. et al.** (2000). Large-Scale Movement of Elongation Factor G and Extensive Conformational Change of the Ribosome during Translocation. *Cell* **100**, 301-09.
- Stark, H. et al.** (2000). Large-scale movement of elongation factor G and extensive conformational change of the ribosome during translocation. *Cell* **100**, 301-9.
- Stevens, S. W. and Abelson, J.** (1999). Purification of the yeast U4/U6.U5 small nuclear ribonucleoprotein particle and identification of its proteins. *Proc. Natl. Acad. Sci. U. S. A.* **96**, 7226-31.
- Stevens, S. W. et al.** (2001). Biochemical and genetic analyses of the U5, U6, and U4/U6 x U5 small nuclear ribonucleoproteins from *Saccharomyces cerevisiae*. *RNA* **7**, 1543-53.
- Stevens, S. W. et al.** (2002). Composition and Functional Characterization of the Yeast Spliceosomal Penta-snRNP. *Mol. Cell* **9**, 31-44.
- Sun, J. S. and Manley, J. L.** (1995). A novel U2-U6 snRNA structure is necessary for mammalian mRNA splicing. *Genes Dev.* **9**, 843-54.
- Tan, E. M. and Kunkel, H. G.** (1966). Characteristics of a soluble nuclear antigen precipitating with sera of patients with systemic lupus erythematosus. *J. Immunol.* **96**, 464-71.
- Taylor, D. J. et al.** (2007). Structures of modified eEF2 80S ribosome complexes reveal the role of GTP hydrolysis in translocation. *EMBO J.* **26**, 2421-31.
- Teigelkamp, S. et al.** (1998). The 20kD protein of human [U4/U6.U5] tri-snRNPs is a novel cyclophilin that forms a complex with the U4/U6-specific 60kD and 90kD proteins. *RNA* **4**, 127-41.

- Teigelkamp, S. et al.** (1997). The human U5 snRNP-specific 100-kD protein is an RS domain-containing, putative RNA helicase with significant homology to the yeast splicing factor Prp28p. *RNA* **3**, 1313-26.
- Thuman-Commike, P. A.** (2001). Single particle macromolecular structure determination via electron microscopy. *FEBS Lett.* **505**, 199-205.
- van Heel, M. and Frank, J.** (1981). Use of multivariate statistics in analysing the images of biological macromolecules. *Ultramicroscopy* **6**, 187-94.
- van Heel, M. et al.** (1996). A New Generation of the IMAGIC Image Processing System. *J. Struct. Biol.* **116**, 17-24.
- van Heel, M. and Stoffler-Meilicke, M.** (1985). Characteristic views of *E. coli* and *B. Stearothermophilus* 30S ribosomal subunits in the electron microscope. *EMBO J.* **4**, 2389-95.
- van Nues, R. W. and Beggs, J. D.** (2001). Functional Contacts With a Range of Splicing Proteins Suggest a Central Role for Brr2p in the Dynamic Control of the Order of Events in Spliceosomes of *Saccharomyces cerevisiae*. *Genetics* **157**, 1451-67.
- Vidal, V. P., Verdone, L., Mayes, A. E. and Beggs, J. D.** (1999). Characterization of U6 snRNA-protein interactions. *RNA* **5**, 1470-81.
- Will, C. L. and Lührmann, R.** (2001). Spliceosomal U snRNP biogenesis, structure and function. *Curr. Opin. Cell Biol.* **13**, 290-301.
- Will, C. L. and Lührmann, R.** (2006). Spliceosome structure and function. In *The RNA World*, (ed. R. F. Gesteland T. R. Cech and J. F. Atkins), pp. 369-400. Cold Spring Harbor, New York: Cold Spring Harbor Laboratory Press.
- Will, C. L. et al.** (2002). Characterization of novel SF3b and 17S U2 snRNP proteins, including a human Prp5p homologue and an SF3b DEAD-box protein. *EMBO J.* **21**, 4978-88.
- Xu, Y., Petersen-Bjorn, S. and Friesen, J. D.** (1990). The PRP4 (RNA4) protein of *Saccharomyces cerevisiae* is associated with the 5' portion of the U4 small nuclear RNA. *Mol. Cell Biol.* **10**, 1217-25.
- Yarbrough, D. et al.** (2001). Refined crystal structure of DsRed, a red fluorescent protein from coral, at 2.0-Å resolution. *Proceedings of the National Academy of Sciences* **98**, 462-67.
- Zhang, M. Q.** (1998). Statistical features of human exons and their flanking regions. *Hum. Mol. Genet.* **7**, 919-32.
- Zhou, Z., Licklider, L. J., Gygi, S. P. and Reed, R.** (2002). Comprehensive proteomic analysis of the human spliceosome. *Nature* **419**, 182-5.

6 Appendix

List of Abbreviations

2D	two-dimensional
3D	three-dimensional
3' SS	3' splice site
5' SS	5' splice site
°C	degree Celsius
A	adenosine
Å	Ångström
AA	acrylamide
ABS	antigene binding site
ADP	adenosine-5'-diphosphate
Amp ^r	Ampicillin resistance
APS	ammonium peroxy sulfate
ATG	Start codon
ATP	adenosine-5'-triphosphate
BAA	bis-acrylamide
bp	base pair
C	cytosine
<i>C. albicans</i>	<i>Candida albicans</i>
CBP	calmodulin binding peptide
Ci	Curie
CMCT	1-cyclohexyl-3-(2-morpholinoethyl) carbodiimide metho- <i>p</i> -toluene sulfonate
Co-IP	co-immunoprecipitation
Da	Dalton
DMS	dimethylsulfate
DMSO	dimethylsulfoxide
DNA	deoxyribonucleic acid
dNTPs	deoxynucleotide-5'-triphosphates
DTT	1,4-dithiothreitol
<i>E. coli</i>	<i>Escherichia coli</i>
EDTA	ethylenediamine-N, N, N', N'-tetraacetic acid
ELISA	Enzyme-linked immunosorbent assay
EM	electron microscopy

Fc-portion	C-terminal constant domains CH2 and CH3 of the heavy chains of the antibody
fmole	femtomole
G	guanosine
GDP	guanosine-5'-diphosphate
GFP	green fluorescent protein
GTP	guanosine-5'-triphosphate
h	hour
HIS	Histidine
HRP	horseradish peroxidase
IgG	immunoglobulin G
Kan ^r	Kanamycin resistance
kb	kilo base
kDa	kilo dalton
<i>K. lactis</i>	<i>Kluyveromyces lactis</i>
kV	kilo volt
L	liter
LB	Luria Bertani
Lsm	Like-Sm
μ	micro
μl	microliter
μm	micrometer
μM	micromolar
μmol	micromol
M	molar
m ₃ G	2,2,7-trimethylguanosine
min	minute
ml	milliliter
mM	millimolar
mRNA	messenger RNA
MS	mass spectrometry
MSA	multivariate statistical analysis
n	nano
nm	nanometer
nM	nanomolar
NMR	nuclear magnetic resonance spectroscopy
Nmol	nanomol
NP-40	Nonidet P-40

nr	non-redundant
ns	nucleotides
NTPs	nucleotide-5'-triphosphates
OD	optical density
ORF	open reading frame
PAA	Poly-acrylamide
PAGE	polyacrylamide gel electrophoresis
PAP	peroxidase-antiperoxidase complex
PBS	phosphate-buffered saline
PCI	phenol-chloroform-isoamyl alcohol
PCR	polymerase chain reaction
PCV	packed cell volume
PEG	polyethylene glycol
pmole	picomole
poly (A)	poly-adenine
poly (U)	poly-uridine
pre-mRNA	pre-messenger RNA
ProtA	<i>Staphylococcus aureus</i> protein A
ProtA-gold	colloidal gold coated with protein A
Prp	pre-mRNA processing
RNA	ribonucleic acid
RNP	ribonucleoprotein
RRM	RNA recognition motif
RT	room temperature
RT-mix	reverse transcriptase mix
S	second
S	Svedberg
<i>S. cerevisiae</i>	<i>Saccharomyces cerevisiae</i>
SC-HIS	synthetic complete-medium lacking histidine
SC-TRP	synthetic complete-medium lacking tryptohane
SC-URA	synthetic complete-medium lacking uracil
SDS	sodium dodecyl sulfate
Sm	Smith (Stefanie); systemic lupus erythematosus patient in which Sm proteins were first discovered as antigens
snoRNA	small nucleolar ribonucleic acid
snRNA	small nuclear ribonucleic acid
snoRNP	small nucleolar ribonucleoprotein
snRNP	small nuclear ribonucleoprotein

SNR	signal-to-noise ratio
<i>S. pombe</i>	<i>Schizosaccharomyces pombe</i>
T	thymidine
TAP	tandem affinity purification
TBE	Tris-borate-EDTA buffer
TBS	Tris-buffered saline
TE	Tris-EDTA buffer
TEMED	N, N, N', N'-tetramethylethylenediamine
TEV protease	<i>tobacco etch virus</i> protease
TMB	3,3',5,5'-tetramethylbenzidine
TPR	tetratricopeptide repeat
TRP	tryptophane
U	uridine
URA	uracil
U _{sn} RNA	uridine-rich small nuclear ribonucleic acid
U _{sn} RNP	uridine-rich small nuclear ribonucleoprotein
UTR	untranslated region
UV	ultra violet
YFP	yellow fluorescent protein
YPD	yeast extract, peptone, dextrose
YPG	yeast extract, peptone, galactose

Publications

Parts of this work will be published in:

Häcker, I., Sander, B., Golas, M., Wolf, E., Karagöz, E., Kastner, B., Stark, H., Fabrizio, P., Lührmann, R. (2008) Localization of Prp8, Brr2, Snu114 and U4/U6 proteins in the yeast tri-snRNP by electron microscopy. *Nature Structural and Molecular Biology*, in press.

Danksagung

Diese Gelegenheit möchte ich nutzen, um einigen Personen zu danken, ohne die diese Arbeit nicht möglich oder die Freude an der Arbeit sehr viel geringer gewesen wäre:

Prof. Dr. Reinhard Lührmann danke ich für dieses interessante Projekt, seine Diskussionsbereitschaft und Unterstützung, und dafür, dass er sich immer Zeit für meine Fragen und Probleme nahm. Darüber hinaus danke ich ihm für die Möglichkeit, meine Arbeit mit einem Vortrag bei der “Eucaryotic mRNA Processing” Konferenz in Cold Spring Harbor, USA vorzustellen.

Ein riesiges Dankeschön geht an **Patrizia** für die tolle Betreuung. Sie hatte immer Zeit für Fragen und Diskussionen, ganz egal wieviel sie selbst zu tun hatte. Vielen Dank für die vielen guten Tips und die Hilfe rund um meine Doktorarbeit und für eine tolle und interessante Zeit!

Reinhard Rauhut danke ich für seine wertvollen Tips, die immer prompte Lösung meiner Alltagsprobleme mit meinem Mac und viele kleine Späße am Rande.

Jochen, Nadine, Michael, Elmar, Ramazan, Nikolas und **Julia**, möchte ich für ihre Unterstützung und Aufmunterung in den diversen Downs dieser Arbeit danken und dafür, dass sie immer ein offenes Ohr für mich hatten.

Nadine, vielen Dank für die tolle Zeit in CSHL 2007, in NYC und zusammen in Labor 118!

Gabi danke ich für ihren unermüdlichen Einsatz und ihre Hilfsbereitschaft, und für viele schöne Gespräche.

Ein großes Dankeschön geht an **Uschi** und **Gertrud**, unseren guten Seelen, die das Labor vor dem Chaos bewahren, und mir immer ein Plätzchen in ihren Autoklaven einräumten.

Allen Mitarbeitern der Abteilung danke ich für die angenehme Atmosphäre im Labor und ihre Hilfsbereitschaft.

Dem **Stipendien-Fonds** des Verbandes der Chemischen Industrie danke ich für die finanzielle Unterstützung des Projektes.

Mein ganz besonderer Dank gilt meiner **Familie** und **Marc**, die mich während der ganzen Zeit unterstützt und ermutigt haben. Besonders danke ich Marc für eine wunderschöne Zeit und seine Liebe.

Erklärung/Affidavit

Hiermit erkläre ich an Eides Statt, dass die Dissertation mit dem Titel “Electron microscopic localization of tagged proteins in the yeast *S. cerevisiae* spliceosomal U4/U6.U5 tri-snRNP” selbständig und ohne unerlaubte Hilfe angefertigt wurde.

I declare that my Doctoral Thesis ‘Electron microscopic localization of tagged proteins in the yeast *S. cerevisiae* spliceosomal U4/U6.U5 tri-snRNP’ has been written independently and with no other sources and aids than quoted.

Irina Häcker

Göttingen, 26.05.2008

Curriculum Vitae

Irina Häcker

Diplom-Biochemikerin

geboren am 25.10.1978 in Stuttgart

Staatsangehörigkeit: deutsch

Studium

- Seit 04/2005 **Promotionsstudium am Max-Planck-Institut für Biophysikalische Chemie**, Abteilung Zelluläre Biochemie unter der Leitung von Prof. Dr. Reinhard Lührmann
- 11/2003 – 06/2004 **Diplomarbeit im Fach Biochemie** unter der Leitung von Prof. Dr. Dr. h.c. Mathias Sprinzl; Thema: *Wechselwirkung von Transkriptionsfaktoren mit RNA*
- 10/1999 – 11/2003 **Studium der Biochemie, Universität Bayreuth**
Vertiefungsfächer: Biochemie, Genetik, Biophysikalische Chemie, Bioorganische Chemie; Abschluss: Diplom-Biochemikerin

Stipendien

- 09/2005 – 08/2007 Kekulé-Stipendium der Stiftung Stipendien-Fonds des Verbandes der Chemischen Industrie

Präsentationen

- 08/2007 “Eucaryotic mRNA Processing”, Cold Spring Harbor, USA; Präsentation eines Vortrages: “*Structural analysis of the yeast U4/U6.U5 tri-snRNP spliceosomal particles by electron microscopic localization of genetically tagged proteins*”
- 09/2007 “Horizons in Molecular Biology” 4th Intern. PhD Student Symposium, Göttingen; Präsentation eines Posters: “*Structural analysis of the yeast U4/U6.U5 tri-snRNP spliceosomal particles by electron microscopic localization of genetically tagged proteins*”

Publikationen

Häcker et al. (2008) Localization of Prp8, Brr2, Snu114 and U4/U6 proteins in the yeast tri-snRNP by electron microscopy. *Nature Structural and Molecular Biology*, in press.

Praktische Tätigkeiten vor und nach dem Studium

- 09/2004 – 01/2005 Berufsfindungsphase und Bewerbung
- 08/2004 – 09/2004 Aushilfskraft bei der Firma Linz GmbH, Pegnitz
- 03/1999 – 07/1999 Aushilfskraft bei der Firma Robert Bosch GmbH, Stuttgart im Bereich
Forschung, anorganische Chemie
- 11/1998 – 02/1999 Praktikum bei der Firma Robert Bosch GmbH, Stuttgart im Bereich
Forschung, anorganische Chemie

Schule

- 06/1998 Abitur
- 1989 – 1998 Allgemeinbildendes Gymnasium, Gerlingen
- 1985 – 1989 Grundschule in Gerlingen